WIRELESS NEUROPHYSIOLOGY FOR THE STUDY OF BEHAVIOR IN HEALTH AND DISEASE

A Dissertation

Presented to the Faculty of the Graduate School

of Cornell University

in Partial Fulfillment of the Requirements for the Degree of

Doctor of Philosophy

By

Alycia Susan Gailey

May 2014

WIRELESS NEUROPHYSIOLOGY FOR THE STUDY OF BEHAVIOR IN HEALTH AND DISEASE

Alycia Gailey
Cornell University 2014

The objective of this study was the development of a simple but versatile wireless voltammetry device that can wirelessly record the release of oxidizable neurotransmitters in the central nervous system of freely moving research animals and to demonstrate the utility of the device in freely behaving rats. The rationale behind this approach is in allowing freedom of movement of small animal subjects during electrochemical recording of neurotransmitter release. Neurotransmitters play a vital role in signaling within the central nervous system. A variety of neurological diseases are associated with neurotransmitter abnormalities. Parkinson's disease is an example of such a disease, characterized by dopamine depletion in the basal ganglia structure due to a death of dopaminergic neurons in the substantia nigra. With the use of the wireless voltammetry device presented here, the motor abnormalities associated with Parkinson's disease can be examined in animal models during recording experiments without the mess of wires.

Chapter 1 gives an introduction to dopamine and its role in a variety of brain functions from motor control to the feeling of pleasure. Chapter 2 demonstrates the utility of the wireless device in the recording of dopamine release *in vitro*. By comparing results of the conventional wired setup to results of the wireless setup, the reliability of the wireless device in detecting dopamine release is established. Chapter 3 presents the

use of the wireless device in recording dopamine release in a live rat. In these experiments, the circuit board and battery were placed inside of a pouch that was secured onto the back of a rat with a harness. Chapter 4 presents a discussion of implications for a broad array of future work regarding the role of wireless voltammetry in studying the neurobiological underpinnings of observable behavior.

Chapter 5 presents an electronics curriculum for junior and senior level high school students in the local school district.

BIOGRAPHICAL SKETCH

The author received a Bachelor of Science in electrical engineering from the University of Massachusetts Amherst in 2006 before enrolling in the Cornell PhD program in the same year. The author was later awarded a Master's degree in biomedical engineering from Cornell University in 2009. Primary research interests include the role of neurochemical and neuroelectrical signaling in observable behavior, both in normal and diseased subjects. Previous research projects include the study of attenuation statistics of X-band radar beams in 2005; and the study of clear air refractive index in 2006. During the PhD program, the author worked on the design and implementation of a wireless voltammetry device that can detect the release of oxidizable neurotransmitters in the brain of research animals on subsecond time scales.

Dedicated to my loving and supportive parents

Ronald and Susan Gailey

ACKNOWLEDGMENTS

When I first began the wireless voltammetry project, I did not know where to begin. I had hardly any understanding of wireless technology despite my electrical engineering background. The help and patience of Prof. Manfred Lindau, Khajak Berbarian and Brian N Kim was what enabled me to get started. I would like to thank Khajak Berbarian for teaching me what I know about voltammetry and for teaching me the surgical procedure for implantation of the electrodes in the live rat. I would like to thank Brian N Kim for helping us get Bluetooth device to work. Most of all, I would like to thank Prof. Lindau for being a great advisor and for spending hours sitting next to me at the computer when I needed to troubleshoot.

I also want to send my gratitude to: Mark Wightman for allowing me to test the wireless device on the rats in his laboratory; to Beth Butcher for her hours spent working with me in collecting some of my most important data demonstrating the utility of the wireless recording device. Dr. Paul Phillips for being so hospitable and allowing me to visit his laboratory to learn their carbon fiber electrode fabrication techniques. Christina Akers for teaching me how to fabricate the chronically implantable *in vivo* recording electrodes. Dr. Michael G. Kaplitt at Cornell Weill Medical College for allowing me to shadow him and watch him perform neurosurgeries on patients. Alyssa Apsel for giving me helpful advice regarding my circuit design despite her busy schedule. Dr. Jonathan Rubin for lending me his expertise on computational modeling of the basal ganglia network. Prof. Christiane Linster for always being there in case I wanted help with something or needed someone to talk to. John Guckenheimer for being on my committee. All of my colleagues for making my work environment so friendly and memorable.

TABLE OF CONTENTS

LIST OF FIGURES

LIST OF TABLES

LIST OF ABBREVIATIONS

AMP----------adenine monophosphate
ATP----------adenine triphosphate
CFE----------carbon fiber electrode
D1-5----------dopamine receptors 1-5
DA----------dopamine
DARPP-32----------dopamine and cyclic AMP-regulated phosphoprotein, 32 kDa
DBS----------deep brain stimulation
ERK----------extracellular signal-regulated kinase
FSCV----------fast scan cyclic voltammetry
GABA----------gamma aminobutyric acid
GPe----------external segment of the globus pallidus
GPi----------internal segment of the globus pallidus
GTP----------guanosine triphosphate
IPSP----------inhibitory post synaptic potential
L-DOPA----------levodopa
MPTP----------1-methyl-4-phenyl-1,2,3,6-tetrahydropyridine
NMDA----------N-methyl-D-aspartate
PD----------Parkinson's Disease
PET----------positron emission tomography
PKA----------protein kinase A
PP1----------protein phosphatase 1
SNc----------substantia nigra pars compacta
SNr----------substantia nigra pars reticulata
STN----------subthalamic nucleus
PD----------Parkinson's Disease
RAT----------Real-Time Telemetry system
wFSCV----------wireless fast scan cyclic voltammetry

Chapter 1
Introduction

1.1 What is dopamine?

Dopamine is an organic catecholamine compound that plays a major role in chemical signaling in the central nervous system. Dopamine is well known for its role in reward-seeking and motivated behaviors (Ikemoto and Panksepp, 1999). Dopamine release in the nucleus accumbens is responsible for feelings of pleasure during eating (Evans and Eikelboom, 1987; Hernandez and Hoebel, 1988; Volkow et al., 2003), sexual activity (Paredes and Ågmo, 2004), amphetamine exposure (Badiani et al., 1998; Drevets et al., 2001; Butcher et al., 1988) and other behaviors that induce pleasure. Dopamine has other functions as well, one of which is facilitation of movement (Kandel et al., 2000). As shown in Figure 1.1, the dopamine molecule consists of a benzene ring, two hydroxyl groups and an amine group $CH_2CH_2NH_2$.

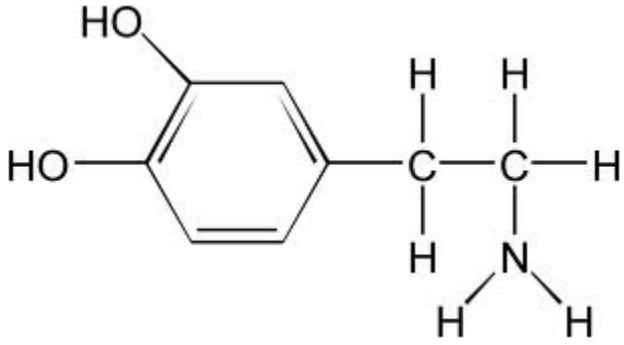

Figure 1.1 Dopamine molecular structure

1.2 Dopamine release and reuptake

Dopamine is synthesized inside the cells. It starts out as the amino acid L-tyrosine, and is converted to L-DOPA (3,4-dihydroxy-l-phenylalanine) by an enzyme called tyrosine hydroxylase. Next, DOPA decarboxylase cleaves the carboxyl group to yield dopamine (Siegel et al., 1999) as illustrated in Figure 1.2.

After dopamine is manufactured, it is transported into spherical organelles called vesicles. Each vesicle has its own lipid bilayer with specific transporters that span the vesicle membrane 12 times and catalyze the uptake of charged neurotransmitter molecules such as DA in exchange for protons (Kandel et al., 2000). Because DA uptake is driven by the proton gradient, hydrolysis of ATP is necessary to maintain the pH gradient across the vesicular membrane.

The process of dopamine release is stimulated when the cell membrane is depolarized. When the intracellular space is changed to a more positive electrical potential relative to the extracellular space, voltage-gated calcium (Ca^{2+}) ion channels open and allow an influx of Ca^{2+} (Kandel et al., 2000). The increase in intracellular calcium ion concentration allows for increased binding of calcium ions to synaptotagmin, a synaptic vesicle membrane protein (Sutton et al., 1995; Fernandez et al., 2001). Calcium ion binding causes other proteins to undergo conformational changes, leading to the fusion of docked vesicles with the cell membrane. As illustrated in Figure 1.3, vesicle fusion with the cell membrane allows the vesicle to release dopamine into the extracellular space where it binds to dopamine receptors on the membrane of other postsynaptic neurons (Li and Chin, 2003; Katz, 1969).

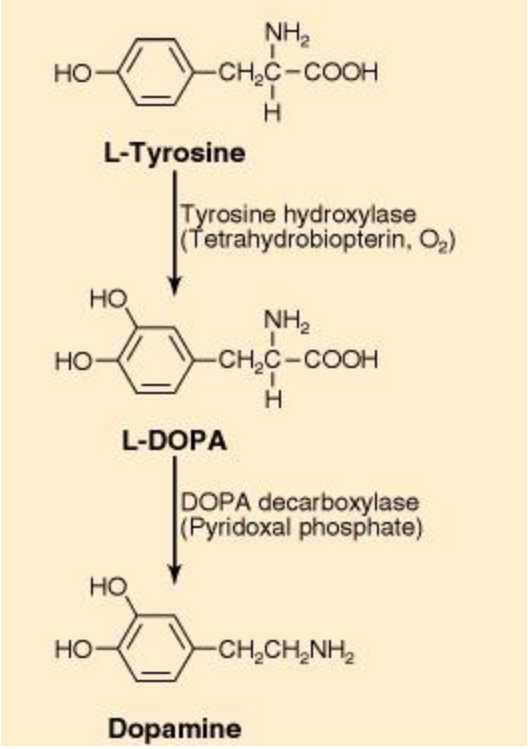

Figure 1.2 Dopamine biosynthetic pathway (Siegel GJ et al., 1999)

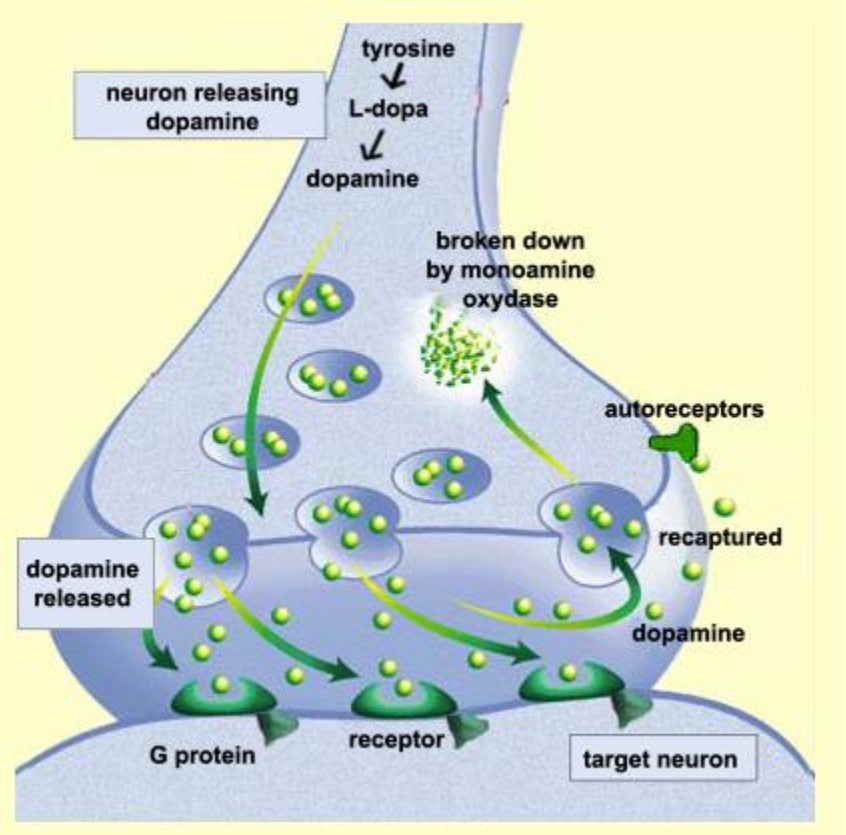

Figure 1.3 Illustration of dopamine storage in vesicles, dopamine release, dopamine binding to receptors, dopamine reuptake and dopamine degradation (http://thebrain.mcgill.ca)

After dopamine has completed its signaling task, dopamine extracellular concentration must be reduced back to baseline levels. Reduction in dopamine extracellular concentration occurs by at least two mechanisms---one of which is thermally-induced diffusion of dopamine molecules from the site of the synapse. Another mechanism is in the action of neurotransmitter transporters at the presynaptic membrane that transport dopamine back across the cell membrane into the intracellular space (Norregaard and Gether, 2001; Chen and Reith, 2000).

1.3 Dopamine receptors

The influence of a neurotransmitter on brain function depends upon which receptors the neurotransmitter binds to. Different parts of the brain have different receptors for a single neurotransmitter so that each neurotransmitter performs a different function at different parts of the brain.

A large portion of dopamine receptors in the brain play a role in reward seeking behaviors, both for inducing a feeling of pleasure and for allowing the individual to learn new forms of behavior in pursuit of a reward. For example, dopamine plays a major role in drug addiction behaviors (Hyman and Malenka, 2001; Berke and Hyman, 2000) sexual behaviors (Paredes and Ågmo, 2004), and eating (Hernandez and Hoebel, 1988; Volkow et al., 2003; Nirenberg and Waters, 2006).

Dopamine receptors are classified into subtypes: D1, D2, D3, D4 and D5. These receptor subtypes fall into two categories: D1-like receptors (D1 and D5) and D2-like receptors (D2, D3, and D4). Figure 1.4 illustrates the signaling cascade that is triggered by dopamine receptor binding. Dopamine receptor signaling involves D1-like and D2-like receptor activation of different classes of G proteins (Neve et al., 2004). D1-like receptor binding activates the GTP binding proteins, $G_{\alpha s}$ and G_{olf}, which bind to the C2 cytosolic domain of adenylate cyclase, increasing adenylate cyclase enzyme activity. Adenylate cyclase catalyzes the conversion of ATP into cyclic AMP, which then binds to protein kinase A (PKA). PKA phosphorylates a number of different signaling molecules, one of which is DARPP-32 (dopamine and cyclic AMP-regulated phosphoprotein, 32 kDa). DARPP-32 is a signaling protein that inhibits protein phosphatase 1 (PP1), preventing PP1-catalyzed dephosphorylation. Decreased PP1-catalyzed dephosphorylation of Ser573 of the sodium ion channels decreases Na^+ currents by reducing the open probability of the sodium ion channels. More importantly, D1-like receptor binding also has been found to suppress inwardly rectifying K^+ currents (Dong et al., 2004). Such suppression of hyperpolarizing K^+ currents increases membrane excitability.

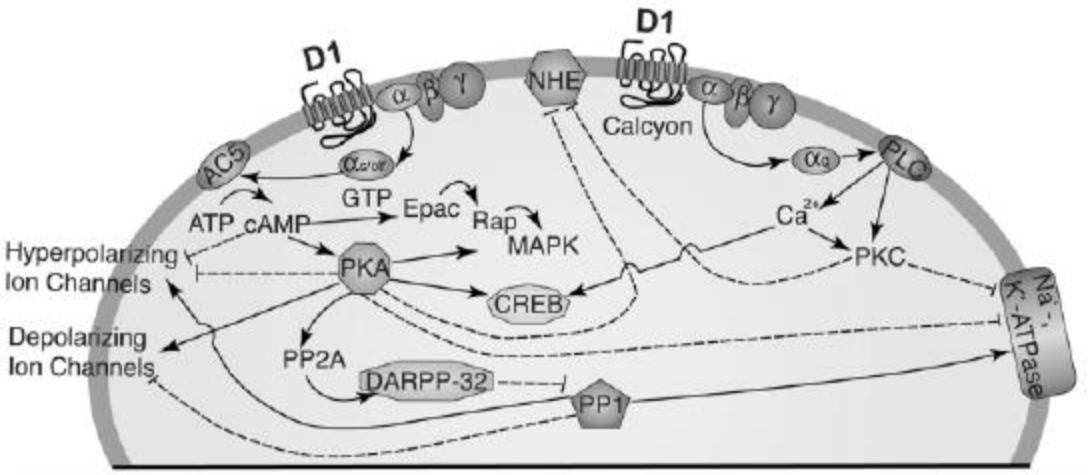

Figure 1.4 Dopamine binding to D1 receptors activates a signaling cascade that starts with activation of $G_{\alpha s}$ and G_{olf} (Neve et al., 2004). CREB = cyclic AMP response element binding protein; DARPP-32 = dopamine-related phosphoprotein, 32 kDA; MAPK = mitogen-activated protein kinase; NHE = Na^+/H^+ exchanger; PKA = protein kinase A; PKC = protein kinase C; PLC = phospholipase C; PP1 or PP2A = protein phosphatase 1 or 2A

D2-like receptor binding has the opposite effect of D1-like receptor binding. As illustrated in Figure 1.5, D2-like receptors activate $G\alpha_{i/o}$. $G\alpha_i$ inhibits adenylate cyclase activity, decreasing phosphorylation of PKA substrates such as DARPP-32. Inhibition of adenlyate cyclase explains why D2-like receptor binding yields many of the opposite effects from D1-like receptor binding. While K^+ hyperpolarizing currents are reduced in the case of D1-like receptor binding, K^+ currents are increased in the case of D2-like receptor binding (Einhorn et al., 1991).

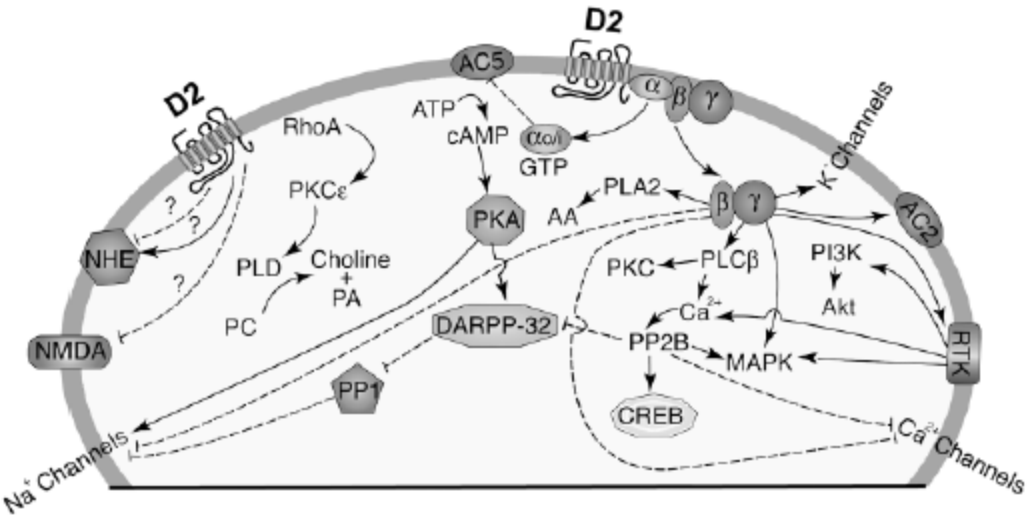

Figure 1.5 Dopamine binding to D2 receptors activates multiple signaling cascades that starts with activation of the $G\alpha_{i/o}$ and $G_{\beta\gamma}$ classes of G proteins (Neve et al., 2004). AA = arachidonic acid; AC2 or AC5 = adenylate cyclase type 2 or 5; CREB = cyclic AMP response element-binding protein; DARPP-32 = dopamine- and cyclic AMP-regulated phosphoprotein, 32 kDA; MAPK = mitogen-activated protein kinase; NHE = Na^+/H^+ exchanger; PA = phosphatidic acid; PC = phosphatidylcholine; PI3K = phosphatidylinositol 3-kinase; PKA = protein kinase A; PKC = protein kinase C; PLA2 = phospholipase A2; PLC = phospholipase C; PLD = phospholipase D; PP1 or PP2A = protein phosphatase 1 or 2A; RTK = receptor tyrosine kinase

Figure 1.6 shows the effects of D1 versus D2 receptor binding on various ionic currents. D1 receptors have been shown to inhibit Na^+ currents in striatal neurons while D2 receptors may inhibit Na^+ currents in some striatal neurons and excite Na^+ currents in other striatal neurons (Surmeier et al., 1992). More specifically, D1 receptor binding increases the amount of depolarization necessary to open sodium ion channels. Conversely, D2 receptor binding reduces the threshold voltage for the opening of sodium ion channels.

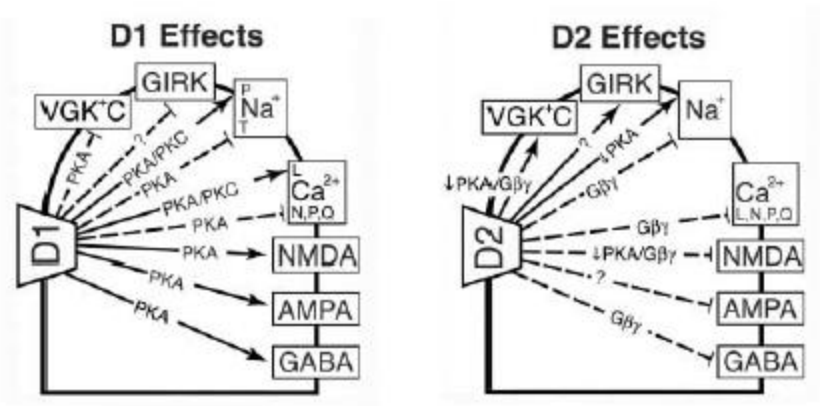

Figure 1.6 Effects of D1 (left) and D2 (right) receptor signaling on membrane currents (Neve et al., 2004). Stimulatory effects are solid lines, inhibitory effects are dashed lines. VGK^+C = voltage-gated K^+ channels; GIRK = G-protein coupled inwardly-rectifying potassium channel; PKA = protein kinase A; PKC = protein kinase C; NMDA = N-methyl-D-aspartate receptors; AMPA = α-amino-3-hydroxy-5-methyl-4-isoxazolepropionic acid receptors; GABA = γ-aminobutyric acid receptors

(Trantham-Davidson et al., 2008) found that while D1 receptor binding increases prefrontal cortex interneuron excitability, the increase in excitability was not found to be dependent on DARPP-32 activity. DARPP-32 knockout mice were found in the study to show the same DA-induced increases in membrane excitability as wild type. Therefore, other chemical signaling pathways may be underlying the increased neuronal excitability due to D1 receptor binding.

However, (Schiffman et al., 1995) found in whole-cell recordings of rat striatal neurons that only peak Na^+ current is reduced as a result of D1 receptor binding. The steady-state voltage dependence of activation and inactivation of sodium ion channels was found to be unchanged. In voltage clamp studies of nucleus accumbens neurons, (Maurice et al., 2001) observed that D1 and D5 receptor binding inhibits transient, fast inactivating Na^+ currents and has no effect on persistent, slow-inactivating Na^+ currents.

Inhibition of transient Na^+ currents may make the neuron more selectively responsive to larger excitatory signals and prevent neuronal firing in response to smaller stray signals.

D1 receptor binding in the dorsal striatum increases the striatal inhibition of the internal globus pallidus (GPi) by increasing the frequency of GABA-induced IPSPs sent from the striatum to the globus pallidus. Conversely, D2 receptor binding reduces the frequency of GABA-induced IPSPs sent from the striatum to the external globus pallidus (Stanford and Cooper, 2001).

Some differences among the dopamine receptor subtypes within the same category have been discussed (Neve et al., 2004). For instance, D2 and D4 receptor binding both lead to increased adenylate cyclase 2 activity whereas D3 receptor binding has little or no effect on adenylate cyclase 2. Adenylate cyclase 2 catalyzes dephosphorylation of ATP into cAMP. Therefore, D3 receptor binding may yield less cAMP synthesis, and hence less PKA activation than D2 or D4 receptor binding. Reduced PKA activity means lower open probability for sodium ion channels and less DARPP-32 activity. D2 receptors differ from D3 and D4 receptors in that unlike D2 receptors, D3 and D4 receptors activate ERK (extracellular signal-regulated kinase), which is necessary for NMDA receptor-dependent long-term potentiation (Kanterewicz et al., 2000).

The consequences of DA release are highly complex, and methods to achieve a better understanding of the molecular and cellular mechanisms are needed.

1.4 Parkinson's Disease and the Basal Ganglia

The basal ganglia are a group of structures within the brain that are important for regulating movement. Figure 1.7 illustrates the network of excitatory and inhibitory synaptic connections within the basal ganglia. The cortex projects to the substantia nigra and striatum. The substantia nigra is a group of dopamine-rich neurons that projects to the striatum. Striatal neurons with D1 receptors project primarily to the GPi (internal globus pallidus), and striatal neurons with D2 receptors project primarily to the GPe (external globus pallidus) (Kandel et al., 2000). There are two signaling pathways from the striatum to the thalamus – the direct and indirect signaling pathways, as discussed in (Kandel et al., 2000; Smith et al., 1998). In the direct signaling pathway, the striatum sends inhibitory projections to the GPi, rendering the GPi less active and less able to inhibit the thalamus. As a result, the thalamus becomes disinhibited, and relays more sensorimotor signals to the cortex. Therefore, the direct signaling pathway facilitates movement by disinhibiting the thalamus. In the indirect signaling pathway, the striatum sends inhibitory projections to the GPe, which becomes less active and less able to inhibit the STN. The STN becomes more active and more able to excite the GPi. As a result, the GPi becomes more active and more able to inhibit the thalamus. Increased thalamic inhibition inhibits the relay of sensorimotor inputs through the thalamus to the cortex. In this way, the indirect signaling pathway inhibits movement.

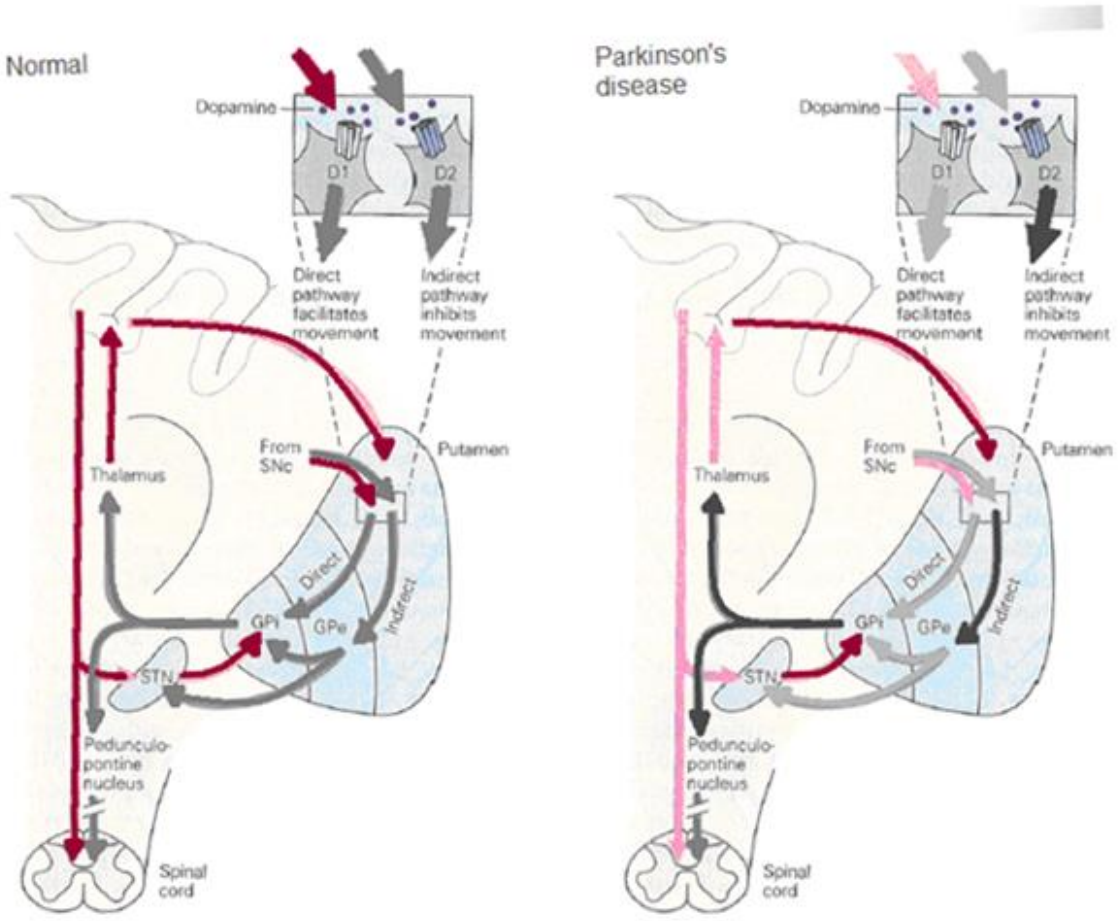

Figure 1.7 An illustration of synaptic connections among basal ganglia structures from (Kandel et al., 2000). Red lines represent excitatory connections, gray lines inhibitory connections. Lighter red means weaker excitation, light gray means weaker inhibition, and darker gray means stronger inhibition. D1 and D2 = D1 and D2 dopamine receptors; GPi = internal segment of the globus pallidus; GPe = external segment of the globus pallidus; STN = subthalamic nucleus; SNc = substantia nigra pars compacta

In a normal brain, there is a balance between the direct and indirect signaling pathways where the direct signaling pathway facilitates desired movements and the indirect signaling pathway inhibits undesired movements. Dopamine binding to D1 receptors strengthens striatal inhibition of the GPi whereas dopamine binding to D2 receptors reduces striatal inhibition of the GPe. In other words, when nigrostriatal signaling increases extracellular dopamine concentration in the striatum, the balance between the

direct and indirect signaling pathways is shifted in favor of the direct signaling pathway, thus facilitating movement (Kandel et al., 2000).

In the brain of an individual with Parkinson's disease (PD), dopaminergic neurons in the SNc have died off, leading to a dopamine depletion in the dorsal striatum. As a result, the direct signaling pathway is underactive due to reduced D1 receptor binding and the indirect signaling pathway is overactive due to reduced D2 receptor binding. The thalamus receives chronically increased inhibition, causing difficulty in relaying sensorimotor inputs to the cortex. Movement becomes more difficult, and the patient experiences bradykinesias (slowness of movement) and akinesias (difficulty initiating movements) (Kandel et al., 2000).

The oldest and most effective treatment for PD is levodopa (L-dopa) treatment. Levodopa is a dopamine precursor (Figure 1.2), and levodopa medication is able to cross the blood-brain barrier. Levodopa is particularly effective at early and intermediate stages of PD, but at later stages, as more and more levodopa is necessary to make up for the lack of dopamine availability, levodopa side effects appear. The signature side effect of levodopa treatment is excessive involuntary movements called dyskinesias. The prevalence of these dyskinesias with respect to time since diagnosis and time since starting levodopa treatment have been reviewed (Fabbrini et al., 2007). It was found that after 4-6 years of levodopa treatment, just under 40% of patients developed dyskinesias (Ahlskog and Muenter, 2001). It is likely that dyskinesias are a result of overactivation of the direct signaling pathway and/or underactivation of the indirect signaling pathway. A signaling pathway imbalance that is in favor of the direct

signaling pathway may interfere with suppression of undesired movements, explaining why levodopa treated PD patients often exhibit excessive unwanted movements.

The progression of PD is likely what causes an individual to be susceptible to levodopa-induced dyskinesias. In patients with PD only on one side, dyskinesias were more likely to occur on the affected side in response to levodopa treatment and normal healthy subjects did not seem prone to developing levodopa-induced dyskinesias (Mones et al., 1971). An explanation for this observation is in failure of dopamine reuptake. Death of dopaminergic neurons in the SNc not only reduces the supply of dopamine, but also reduces the number of cells available for performing dopamine reuptake. Without dopamine reuptake, levodopa can cause a spike in extracellular dopamine concentration that does not occur in a levodopa-treated healthy subject with an intact nigrostriatum.

If levodopa dosage is reduced, then PD symptoms can return. Continuous levodopa treatment, however, has been shown to provide a longer term increase in extracellular dopamine concentration to normal levels without unwanted spikes to abnormally high levels. Standard intermittent levodopa treatment, when administered to Parkinsonian rats, causes a spike in extracellular dopamine concentration to abnormally high levels for a couple of hours after administration (Engbar et al., 1989). Continuous levodopa treatment, however, did not cause such a spike. Levodopa rendered D1 agonists less effective when administered simultaneously, indicating that levodopa may have higher affinity for D1 receptors than D2 receptors (Engbar et al., 1989). An increased affinity

for D1 receptors would mean that overactivation of the direct signaling pathway is a more likely explanation for levodopa-induced dyskinesias than underactivation of the indirect signaling pathway.

In advanced PD when chemical treatments are insufficient for controlling PD symptoms, a stimulating electrode is often inserted into one of the basal ganglia structures---most commonly the STN. Stimulating square pulses at ~180 Hz frequency are continuously applied to the electrode. This deep brain stimulation (DBS) treatment has been surprisingly effective in controlling hypokinetic PD symptoms and hand tremors (Benabid, 2003). However, despite how effective DBS has been in the treatment of PD, the mechanisms of action are incompletely understood (Benabid et al., 2009). What is known is that DBS of a structure within the basal ganglia seems to yield similar results as ablation of that same structure (Benabid et al., 1987). A common target of DBS is the STN because the STN and GPe is where much of the abnormal oscillatory activity takes place. Some treatments have involved ablation of the STN, but such treatment is irreversible. DBS, on the other hand, can not only be turned on and off, but also be adjusted.

In addition to levodopa treatment, other pharmacological treatments for PD include dopamine agonists, anticholinergics, catechol methyltransferase (COMT) inhibitors, monoamine oxidase inhibitors, adenosine receptor A2a antagonists and eldepryl as reviewed in (Scapira, 2005). Dopamine agonists are somewhat less effective than levodopa, and they often show the same side effects as levodopa treatment.

Anticholinergics work by reducing acetylcholine levels and thereby increasing the dopamine to acetylcholine ratio. This therapy reduces hand tremors and muscle stiffness. COMT inhibitors enhance the efficacy of levodopa by reducing O-methylation in the gut, thereby increasing levodopa absorption and prolonging levodopa half-life.

Because PD onset has been associated with mitochondrial damage, oxidative stress, excitotoxicity and inflammatory processes, neuroprotective agents have been under investigation (Schapira, 2005). Therapeutic neuroprotective agents include multiple varieties such as pro-mitochondrial, anti-oxidant, anti-excitotoxic, anti-apoptotic, and anti-inflammatory. Dopamine agonists also have been found to be neuroprotective against certain toxicities as discussed in (Schapira and Olanow, 2003).

Various pharmacological agents that combat the dyskinesias caused by levodopa and dopamine agonists have been reviewed in (Fabbrini et al., 2007). One example is amantadine, which blocks NMDA receptors in the direct signaling pathway, reducing glutamatergic drive to the direct signaling pathway without reducing antiparkinsonian benefits.

Clearly, many efforts are being made to find improved treatments of PD with fewer side effects. To achieve this goal, a more precise knowledge of the relationship between DA levels and behavioral outcome will be of great importance.

1.5 Methods of Dopamine Detection in the Study of Parkinson's Disease

Behavioral neuroscientists investigate the chemical and electrical signaling abnormalities within the basal ganglia structures, and how these abnormalities are correlated with alterations in outward observable behavior. Some questions include: how much dopamine depletion is necessary for symptoms of PD to manifest? (Hornykewicz, 1968) What abnormalities in motor signaling cause hand tremors? (Terman and Rubin, 2004; Hadipour-Niktarash and Shahidi, 2006; Deuschl et al., 2006) Why does levodopa treatment cause dyskinesias at later stages of PD? (Fabbrini et al., 2007)? What aspects of disease progression contribute to levodopa-induced dyskinesias (Chase, 1998; Mones et al., 1971)? What changes in electrical signaling occur throughout the network when a structure is ablated versus electrically stimulated (McIntyre et al., 2004)?

Parkinson's disease involves abnormalities in both electrical and chemical signaling within the brain. Because PD involves neurotransmitter abnormalities, a major part of PD research is in the measurement of neurotransmitter release. Two such techniques are fast scan cyclic voltammetry and amperometry. Another technique, called microdialysis, measures basal neurotransmitter levels. A combination of electrophysiological and electrochemical recording techniques in conjunction with behavioral observations provide a picture of what is happening in the basal ganglia and other parts of the brain when akinesias (Pascual-Leone et al., 1994; Jenkins et al.,

1992), bradykinesias (Berardelli et al., 2001; Kühn et al., 2009) and hand tremors (Deuschl et al., 2000) first manifest. Importantly, these techniques provide clues as to how to develop better treatments (Chase, 1998; Fabbrini et al., 2007; Engbar et al., 1989).

1.5.1 Fast-Scan Cyclic Voltammetry (FSCV)

Fast-scan cyclic voltammetry (FSCV) detects the release of oxidizable chemicals both in vitro and in vivo. (Phillips and Wightman, 2003) provide an introductory paper on the basic theory behind voltammetry.

FSCV takes advantage of the redox reactions that can occur at an electrode in solution with an applied voltage. When the applied voltage at the electrode is positive relative to the surrounding solution, and the applied voltage exceeds a chemical's redox potential, then these oxidizable chemicals near the electrode will lose electrons, causing electrons to flow into the electrode. When the applied voltage at the electrode becomes more negative again (or less positive), the same molecules that have lost their electrons may be reduced, gaining their electrons back, thereby causing a net flow of electrons out of the electrode.

In FSCV experiments, a triangle shaped pulse is applied to a carbon fiber electrode (CFE) relative to the surrounding solution. Figure 1.8 shows an illustration of a carbon fiber electrode that is typically used for in vitro experiments. The electrode consists of a

5-30 µm diameter carbon fiber inside a 0.8 mm glass capillary tube. About 100 µm of carbon fiber protrudes from the pointed tip. If too much carbon fiber protrudes, then there may be too much noise in the recordings. If not enough carbon fiber protrudes, then the electrode may become less sensitive to smaller dopamine concentrations. To connect the CFE to the voltammetry circuit, a conductive wire is inserted into the opposite end of the glass capillary tube from the carbon fiber tip. To establish an electrical connection between the wire and the carbon fiber, the CFE is backfilled with an ion solution such as potassium chloride (KCl) (John and Jones, 2007).

In addition to the CFE, a reference electrode is placed in solution at a sufficient distance from the CFE. The reference electrode often consists of a chlorinated silver wire soldered to a gold pin. The voltammetry circuit applies the triangle pulse waveform between the CFE and reference electrode as illustrated in Figure 1.9.

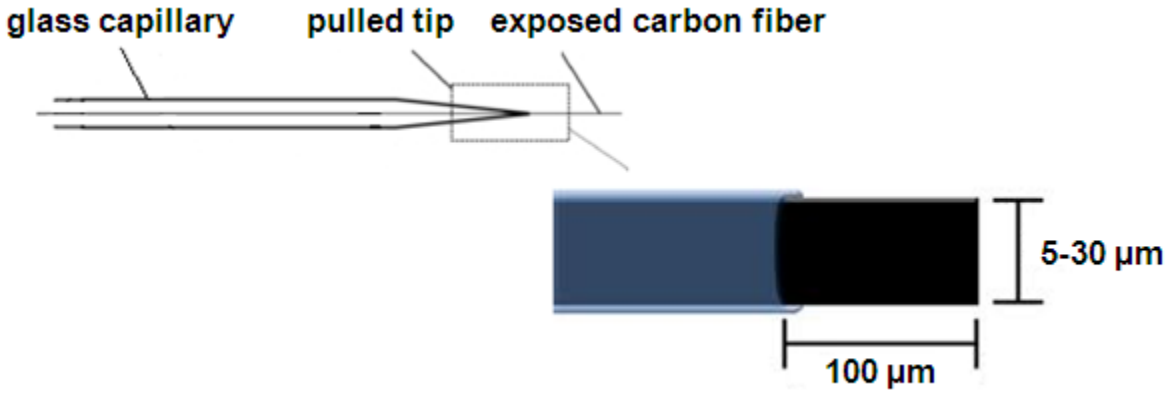

Figure 1.8: Schematic illustration of a carbon fiber electrode. A carbon fiber is inserted inside a 0.8 mm diameter glass capillary tube. The glass capillary tube is pulled so that it has a pointed tip. The carbon fiber electrode protrudes from the pointed tip by about 100 µm as illustrated in the zoomed in image.

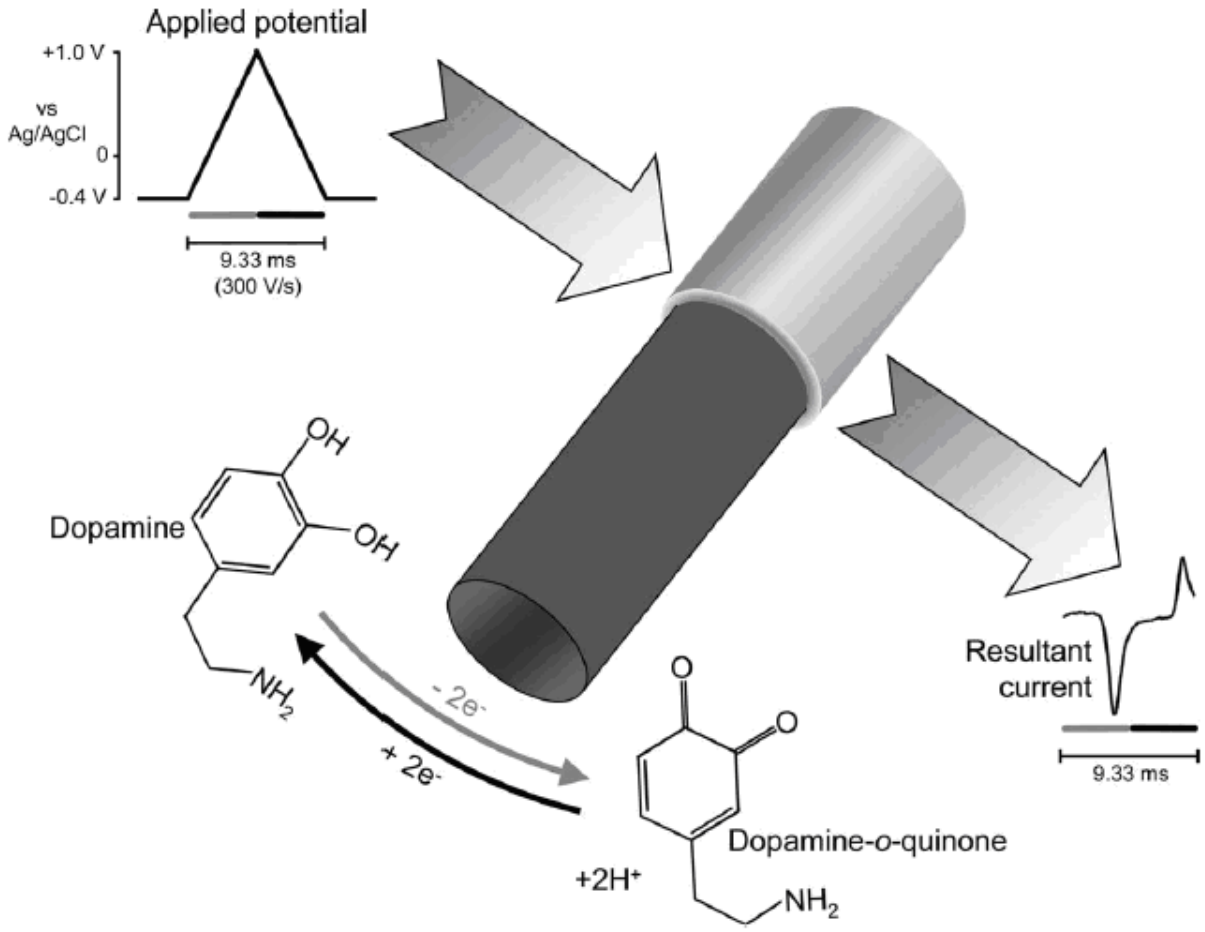

Figure 1.9: Illustration of oxidation-reduction reactions at the carbon fiber electrode in response to an applied triangle pulse from (Phillips and Wightman, 2003). On the upward phase of the pulse, dopamine oxidizes to dopamine-o-quinone. On the downward phase of the pulse, dopamine-o-quinone reduces back to dopamine. These redox reactions cause measureable current flow into the electrode. Shown in black is the conductive carbon fiber that protrudes from the end of the glass capillary tube.

A triangle pulse is applied, sweeping across a range of voltages, the voltage that shows peak oxidation current will vary from one chemical to the next, depending on the chemical's redox potential, thereby giving voltammetry chemical resolution. Ten triangle pulses are applied per second, meaning that changes in oxidizable chemical concentration can be measured ten times per second, thereby giving voltammetry a high temporal resolution.

As shown in Figure 1.9, the voltage sweep typically spans from -0.4 V to +1.0 V, although larger voltage ranges have also been used (Fig. 1.10). Dopamine oxidation current peaks at roughly +0.6 V.

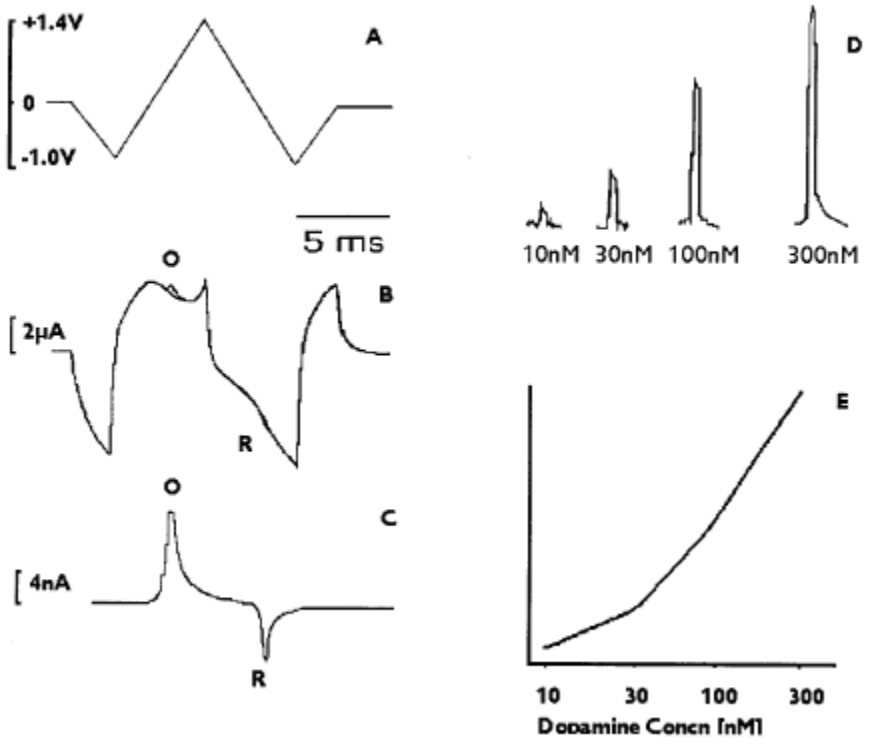

Figure 1.10: Illustration from (Kruk et al., 1998) (A) The triangle pulse waveform that is applied to the carbon fiber electrode. In this set of experiments, the voltage spans from -1.0 V to +1.4 V. (B) The total current collected at the electrode. Faintly visible near the letter O is the contribution of dopamine oxidative current. Near the letter R is the contribution of dopamine reduction current, which is hardly visible. (C) Background subtracted signal for 100 nM of DA. Oxidation and reduction current is now obvious. (D) Time courses of dopamine oxidation current measurements for different dopamine concentrations. (E) Plot that represents change in dopamine concentration versus magnitude of background subtracted oxidation signal.

Figure 1.10 illustrates the applied triangle pulse and the corresponding currents that are collected at the carbon fiber electrode for a -1.0 V to +1.4 V sweep. As shown in Figure 1.10B, most of the current collected at the CFE is not redox current. Rather, a major

component of CFE current is capacitive current. The CFE behaves like a capacitor in that as current flows into the electrode, ions accumulate at the site of the electrode tip. This accumulation of ions enables the CFE to store electric charge.

In addition to capacitive currents, any oxidizable analytes near the electrode may produce Faradaic currents. To isolate the oxidative current of the chemical of interest, current pulses are collected before and after release of the chemical. The signals collected of the chemical before release (background signals) are subtracted from the signals collected after chemical release to yield the net redox current. Provided that no other oxidizable chemicals are released at the same time, and provided that the current pulses do not undergo distortion from one pulse to the next, the background subtracted signal should only show the redox current of the chemical of interest, as shown in Figure 1.10C.

(Kruk et al., 1998) used FSCV to detect changes in dopamine concentration ranging from 10 nM to 300 nM. As shown in Figure 1.10D-E, an approximately linear relationship exists between change in dopamine concentration and magnitude of peak oxidative current.

FSCV was used to detect multiple different chemical analytes using flow injection analysis (Zachek et al., 2008). In this work, gold microelectrodes were used, but otherwise the FSCV technique was the same. In flow injection analysis, the electrode is inserted into a buffer solution. At the beginning of the recording, the electrode is only in

buffer solution. As the recording progresses, a solution of known concentration of a chemical analyte is continuously flowed into the buffer solution while the buffer solution is sucked out with a suction pump. By the end of the recording, the electrode is surrounded by the solution containing the chemical analyte at known concentration.

Current pulses collected at the beginning of the recording were subtracted from current pulses collected towards the end of the recording to yield the net redox current. This redox current was plotted with respect to applied voltage to yield a voltammogram. Figure 1.11 shows difference voltammograms that were generated for different chemical analytes. Because different types of oxidizable chemicals will see their peak oxidation current at different voltages, each type of oxidizable chemical yields a unique voltammogram, demonstrating the chemical selectivity of cyclic voltammetry.

a) Dopamine (5 μM)

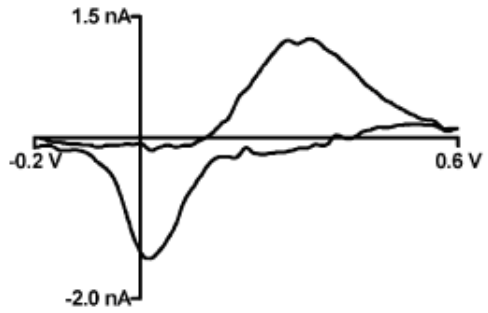

b) DOPAC (100 μM)

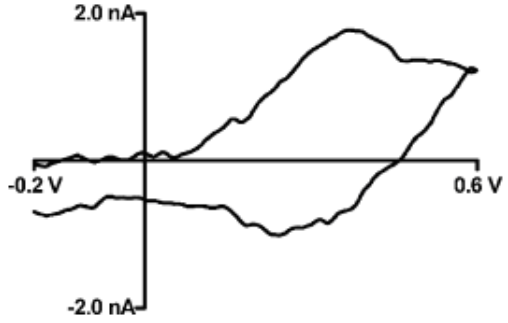

c) 3-MT (5 μM)

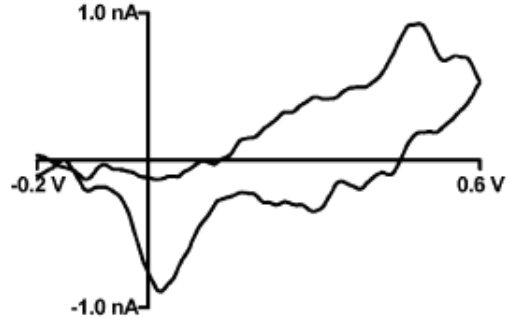

d) 5HT (5 μM)

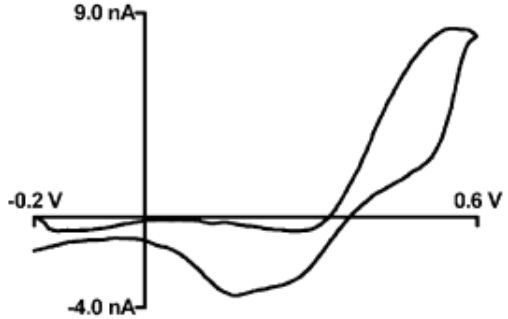

e) 5-HIAA (25 μM)

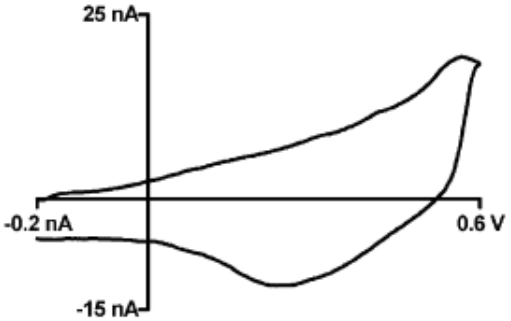

f) Δ pH (0.1 pH units)

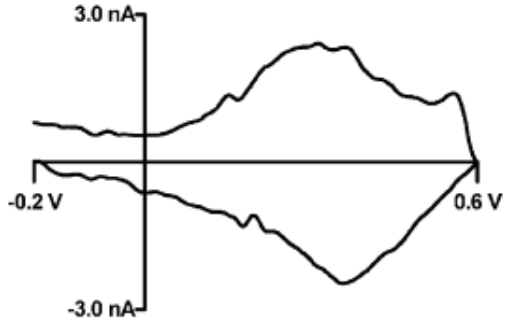

g) Norepinephrine (5 μM)

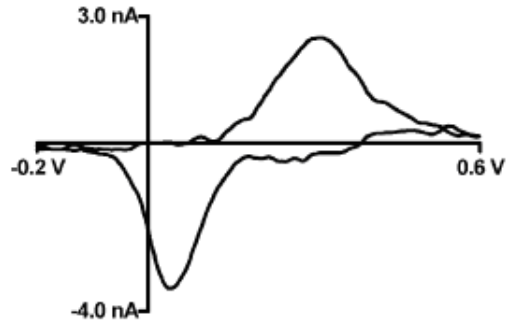

h) Epinephrine (5 μM)

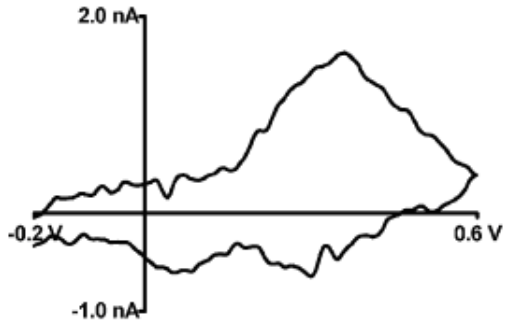

Figure 1.11: Chemical selectivity of FSCV from (Zachek et al., 2008). The isolated redox currents are plotted with respect to applied voltage to yield a voltammogram. Because different chemicals oxidize at different voltages, each type of oxidizable chemical has a unique voltammogram.

Fast scan cyclic voltammetry has its limits. For example, it can only detect changes in analyte concentration during a time period, but not the baseline analyte concentration. Chemical resolution also is limited in cases where two analytes that oxidize at similar voltages are being released. For example, norepinephrine and dopamine oxidize at similar voltages. When two oxidation peaks are close together, they may be hard or impossible to discern from each other. Another difficulty in the use of FSCV is the high background current, which reduces dynamic range. The redox signal of interest only makes up a small portion of the total current collected at the electrode.

1.5.2 Amperometry

Amperometry also takes advantage of redox reactions that occur at an electrode in response to an applied voltage. The difference is in the applied voltage. While triangle pulses are applied to the electrode in voltammetry, amperometry uses either a constant voltage or square voltage pulses. A constant voltage causes oxidizable chemicals to oxidize without reducing. If no change in analyte concentration occurs, then the oxidative current magnitude stabilizes. Molecules that are oxidized near the electrode are not allowed to reduce to their original state and are therefore only detected once. If there is a change in analyte concentration, however, then there is a corresponding change in the oxidation current.

Because the voltage is applied continuously, oxidative current can be collected continuously. This feature gives amperometry superior temporal resolution over voltammetry, where there is a limit in the number of triangle pulses per second that can be applied. Amperometry is typically used to measure release of neurotransmitters from single vesicles (Wightman et al., 1991; Chow et al., 1992). Every time a vesicle releases neurotransmitter, there is a spike. The area under the spike represents the total charge and indicates how many neurotransmitter molecules were released from a single vesicle. The time course of the amperometric spike reflects the time course of release as illustrated in Figure 1.12.

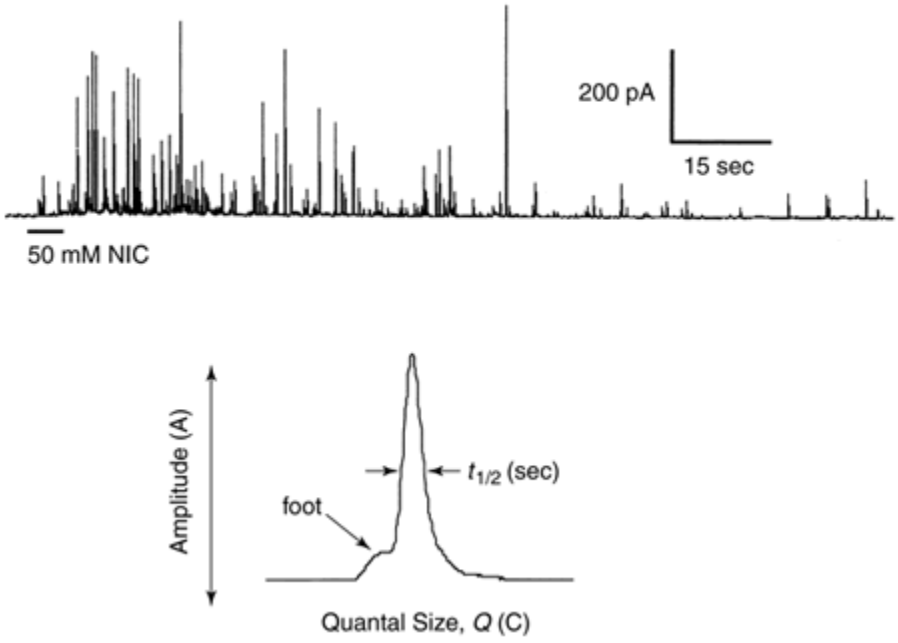

Figure 1.12: Spikes in oxidation current at the electrode from (Mundorf and Wightman, 2002). Each spike represents the release of oxidizable neurotransmitter from one or more synaptic vesicles. The bottom image shows a zoomed in view of a spike. The foot portion of the signal represents the time point at which the vesicle is starting to open up into the extracellular space. The variable $t_{1/2}$ is the half width, which represents the kinetics of vesicular release.

The disadvantage to amperometry is its lack of chemical resolution. Any oxidizable chemical present will contribute to the total oxidative current that shows up on the recording. In some cases, FSCV of the extracellular space may be necessary to confirm which analytes are present.

In some cases, molecules adsorb to the electrode and cause recordings to be lower quality with time. In pulse amperometry, the working voltage is applied to the electrode for a certain length of time, and then a pulse of a different voltage is applied that allows molecules that adhere to the electrode to be cleaned off. Data are only collected when the working voltage is applied. Pulsed amperometric detection is especially beneficial for the detection of carbohydrates (Johnson, 1986) and pharmaceutical agents (dos Santos et al., 2009).

1.5.3 Microdialysis

Another technique that is used to measure analyte concentration is microdialysis (Ungerstedt U, 1991). Microdialysis is particularly useful for measuring the concentrations of unbound analytes in extracellular fluid within any organ of the body, including blood. To perform measurements, a catheter is inserted into the tissue of interest. The catheter, or probe, mimics a capillary tube with a semipermeable membrane. Continuously flowing through the tube is an aqueous solution with ion concentrations closely resembling that of the surrounding extracellular space. The concentration gradient of the analyte across the membrane determines how much of the

analyte flows across the membrane and in what direction. The solution that leaves the probe is periodically collected for analysis. The concentration of analyte in the solution that is collected from the probe compared to the concentration of analyte in the solution going into the probe is indicative of how much analyte penetrated the semipermeable membrane and in what direction. The larger the amount of analyte that penetrates across the membrane into the probe, the larger the concentration of analyte there must be in the extracellular space.

Microdialysis has the following advantages: it can measure basal neurotransmitter concentrations whereas voltammetry and amperometry can only measure changes in neurotransmitter concentrations within the recording period; microdialysis can detect the presence of analytes that are not electroactive; microdialysis is more sensitive to lower analyte concentrations than voltammetry; microdialysis can detect the concentration of multiple analytes at the same time, which is impossible for amperometry and difficult for voltammetry. However, microdialysis has several disadvantages as discussed in (Ungerstedt, 1991). It is quite invasive because the probe tends to penetrate tissue and alter tissue morphology. The potential tissue damage caused by insertion of the probe can disrupt transmitter release and alter glucose metabolism.

The main disadvantages of microdialysis are the poor temporal and spatial resolution. Temporal resolution is limited to how often solutions are drawn from the probe, which tends to be once every few minutes. The spatial resolution is limited to the size of the probe, which is typically a few millimeters for intracerebral microdialysis.

1.5.4 Positron Emission Tomography (PET)

Positron emission tomography or PET is a medical imaging technique that produces 3D images of biological processes within the body. One example of PET application is to measure glucose concentrations in order to assess metabolic activity at different parts of the body. Another application is in the measurement of neurotransmitter concentrations in certain brain areas.

(Phelps, 2006) discusses the physics behind PET as well as the instrumentation. In PET, a radioactive tracer is injected, often into the bloodstream, where it binds to the chemical substance of interest. After a certain waiting period, the radioactive isotope accumulates in tissue where the chemical substance of interest is at highest concentration. At this point, the radioactive tracer undergoes positron decay where it emits a positron that travels a short distance before losing its kinetic energy. After losing its kinetic energy, the positron binds to an electron and emits a pair of gamma rays in opposite directions. Gamma ray pairs are detected, and complex computer analysis is performed in order to form a 3D image of the concentration of the chemical of interest.

This technique has been used to measure extracellular dopamine concentration in the brain during reward seeking behaviors such as playing a videogame (Koepp et al.,

1998), consuming amphetamines (Narendran et al., 2009; Martinez et al., 2003) and eating (Small et al., 2003).

PET scans are noninvasive, but expensive because of the need for a new supply of radioactive tracers before each use. An on-site chemical synthesis apparatus is needed to produce the radiopharmaceuticals, making it impossible for most universities and hospitals to maintain their own PET setup.

A miniaturized PET device has been specially design for rodent brain imaging (Vaska et al., 2003). Rat immobilization is unnecessary, but freedom of movement is limited because of the large size of the head mount. The spatial resolution was computed as roughly 1.28 mm. Spatial resolution of PET scanners is limited due to the distance that positrons must travel before they lose their kinetic energy. On the scale of the rat brain, 1-2 mm is quite large. However, temporal resolution is on the order of around 1 ms, sufficiently high to measure neurotransmitter release kinetics.

1.5.5 *In Vitro* and *In Vivo* Dopamine Detection

In vitro dopamine detection experiments begin with the placement of the recording electrode and reference electrode in a buffer solution with approximate physiological salt concentrations: 140 mM NaCl, 5 mM KCl, 5 mM $CaCl_2$, 1 mM $MgCl_2$ and 10 nM HEPES. These salt concentrations imitate the ion concentrations that are typically seen

in the extracellular space of the brain. Hydroxydopamine powder is dissolved in buffer solution to yield a solution of known molar concentration of dopamine. During an FSCV recording, triangle pulses are continuously applied to the recording electrode. At the beginning of the recording, the electrode is immersed in a dopamine-free buffer solution. At a certain point in the recording, another buffer solution with a known dopamine concentration starts to flow into the dish and replace the previous solution. Current signals collected before the change in solution are subtracted from current signals collected after the change in solution to yield the background-subtracted dopamine signal.

In vitro testing is useful for validation and calibration of the electrochemical measurement system. With an *in vitro* recording setup, the magnitude of peak oxidation current can be plotted with respect to the known change in dopamine concentration.

In vivo dopamine detection involves implantation of the recording electrode at a location in the brain where dopamine release is known to occur. The reference electrode is placed at another arbitrary coordinate in the brain, often contralateral to the recording electrode. As in the *in vitro* case, triangle pulses are continuously applied between the reference and recording electrode throughout the recording. Experiments of *in vivo* dopamine release may involve electrically evoked dopamine release (Garris et al., 1996; Kuhr et al., 1984), chemically evoked dopamine release (Kiyatkin et al., 1993; Giorguieff MF et al., 1978) or behaviorally evoked dopamine release (Radhakishun et al., 1988). For electrically evoked release experiments, a stimulating electrode is

implanted near axons that project from a dopamine-rich structure to the structure of interest. For example, if the recording electrode is implanted in the dorsal striatum, then a stimulating electrode would be inserted near the axons that project from the SNc to the dorsal striatum. If the recording electrode is implanted in the nucleus accumbens, then the stimulating electrode may be inserted near the ventral tegmental area, which is known to supply the nucleus accumbens with dopamine. At a certain time point in the recording, a series of stimulation pulses is applied from the stimulating electrode in order to initiate dopamine release. Current signals collected prior to stimulation are subtracted from current signals collected shortly after stimulation (Kuhr et al., 1984). The peak oxidation current in the voltammogram will reach a maximum value shortly after electrical stimulation, then decay. The decay in peak oxidation current with time reveals the kinetics of dopamine reuptake and diffusion. Since the dopamine concentration before *in* vivo stimulation is unknown, the measurement indicates only the change in DA concentration, not the absolute DA concentration.

Chemically evoked dopamine release experiments may involve exposing the animals to amphetamines or cocaine (Butcher et al., 1988), which is known to increase extracellular dopamine concentration. At a certain point in the recording, the animal is exposed to amphetamines. Behaviorally evoked dopamine release experiments typically involve exposing animals to a rewarding stimulus such as an unexpected food pellet or a mate. Current signals collected prior to introduction of the rewarding stimulus are used as the background or reference signals (Roitman et al., 2004).

Dopamine release, along with the release of other neurotransmitters, has also been measured in brain slices (Maina et al., 2012) and cell cultures (Hochstetler et al., 2000).

1.6 Previous Studies on *In Vivo* Dopamine Release and Behavior

A large number of *in vivo* studies investigate the role of dopamine release in observable behavior. These research studies can be divided into multiple categories: drug addiction studies; eating and sex; diseases such as PD; and impulsive behaviors. Rats are frequently used as animal models across all categories of dopamine related behaviors.

Dopamine plays a major role in drug addiction. Several studies have investigated the role of dopamine in cocaine self administration (Ito et al., 2000; Ito et al., 2002; Nader et al., 2008), amphetamines (Badiani et al., 1998; Drevets et al., 2001, Butcher et al., 1988), opiates (Chiara and Imperato, 1988; Chesselet et al., 1982), morphine (Acquas et al., 1991; Chesselet et al., 1981) and drug withdrawal (Rossetti et al., 1992). Many of these studies used microdialysis to measure dopamine release. Microdialysis readings are collected once every few minutes, yielding low time resolution. However, drug-induced changes in extracellular dopamine concentration tend to be on longer time scales on the order of 1-2 hours. These studies have shown that dopamine levels increase substantially in the dorsal and ventral striatum during administration of addictive substances.

Dopamine also plays an important role in governing eating behaviors (Evans and Eikelboom, 1987; Hernandez and Hoebel, 1988; Radhakishun et al., 1988; Volkow et al., 2003;). The nigrostriatal dopamine system also plays a role in gnawing and licking behaviors in rats (Antelman et al., 1975). Studies on eating-induced dopamine release in the striatum often used microdialysis or PET for dopamine measurements. In a behavioral study in which rats were exposed to amphetamines (which are known to increase striatal dopamine levels) it was found that the rats lost interest in eating as evidenced by reduced consumption of food pellets (Evans and Eikelboom, 1987). These results suggested that increases in striatal dopamine levels are a primary motivation for eating, and by increasing striatal dopamine levels artificially, amphetamines cause rats to lose interest in food.

Dopamine signaling is affected in certain diseases such as Parkinson's disease, Huntington's disease and schizophrenia. In Parkinson's disease (PD), there is a degeneration of dopaminergic neurons in the substantia nigra pars compacta (SNc), leading to dopamine depletion in the dorsal striatum (Agid et al., 1993; Anglade et al., 1997; Ehringer and Hornykiewicz, 1998; Jeon et al., 1995). Animal models of PD are used to study the correlations between dopamine depletion and observable motor deficits (Deumens et al., 2002; Winkelmüller and Nitsch, 1975). In addition, animal studies can assess both neurological and behavioral responses to pharmaceutical treatments (Akai et al., 1993; Cenci et al., 1998; Porrino et al., 1987).

In rat models of PD, 6-hydroxydopamine was injected into the SNc, leading to a death of SNc neurons (Ungerstedt, 1968). The resulting dopamine depletion caused rats to exhibit many of the signature motor deficits of PD including muscle rigidity, slowness of movement, and hunched posture (Winkelmuller and Nitsch, 1975). Generally, up to a 70%-80% drop in dopaminergic neurons is observed before behavioral deficits manifest, owing to compensatory mechanisms that counteract the effects of dopamine depletion (Hornykewicz, 1968).

Monkey models of PD were injected systemically with 1-methyl-4-phenyl-1,2,3,6-tetrahydropyridine (MPTP). MPTP can cross the blood-brain barrier and imitate the oxidative neurotoxicity that is thought to cause the onset of Parkinsonism in humans (Langston, 1983). MPTP has been a valuable tool for studying the underlying mechanisms of motor deficits of PD and dyskinesias caused by levodopa treatment (Jenner, 2003).

Diseases associated with abnormally elevated striatal dopamine levels include Huntington's disease and schizophrenia. Schizophrenia is associated with abnormally high dopamine activity in the caudate nucleus. PET studies on human volunteers showed that D2 receptor density was higher in schizophrenic patients than in control volunteers (Wong et al., 1986). Elevated dopamine levels cause psychotic symptoms associated with schizophrenia as well. For example, amphetamines have been shown to increase psychotic symptoms of schizophrenia by elevating extracellular dopamine concentration (Laruelle et al., 1996; Breier et al., 1997).

While PD is a hypokinetic disorder associated with abnormally low dopamine levels in the dorsal striatum, Huntington's disease is a hyperkinetic disorder associated with neurotoxic effects of dopamine in the dorsal striatum. The symptoms of Huntington's disease are chorea (excessive movements), cognitive impairment (dementia) and behavioral/psychiatric disturbances. (Jakel and Maragos, 2000) present a review paper on the role of dopamine toxicity in the degradation of dorsal striatal neurons in Huntington's disease. (Roze et al., 2011) present a review paper on the abnormal chemical and electrical signaling caused by dopamine neurotoxicity. Dorsal striatal degradation was found to occur in D2 receptor neurons first, then in D1 receptor neurons. Since D2 receptor neurons send inhibitory projections to the GPe (Figure 1.7), death of these neurons can lead to increased GPe activity, which leads to increased inhibition of the STN. Inhibition of the STN renders the STN less active and less able to excite the GPi. With reduced GPi excitation, the thalamus becomes disinhibited and relays more sensorimotor inputs to the cortex. Increased thalamic disinhibition due to reduced striatal inhibition of the GPe may explain the hyperkinetic symptoms of Huntington's disease such as chorea (Kim et al., 2001; Kandel et al., 2000).

Dopamine also plays a role in compulsive behaviors (Nirenberg and Waters, 2006). One example is pathological gambling (Bergh et al., 1997). Pathological gambling tendencies were high in PD patients on high doses of dopamine agonists (Driver-Dunckley E, et al., 2003).

Because dopamine plays such a major role in outward observable behavior (including motor behavior), it is important to be able to take recordings of dopamine activity from live behaving subjects in a noninvasive manner so that behavior during recording experiments is as natural as possible.

1.7 Wireless Detection of Dopamine Release

A major goal of wireless neurophysiology setups is to allow laboratory animals to behave in a more natural environment during recordings. The necessity of cables connecting animals directly to an amplifier and data acquisition system causes animals more anxiety, and may cause signal artifacts in recordings due to mechanical perturbations in the wires.

Major challenges with wireless systems lie in achieving reliability of wireless transmission and in making the device light-weight enough to mount onto an animal.

Figure 1.13 shows a block diagram of a conventional wired FSCV setup. A PCI-6052 data acquisition board imports signals into a desktop computer and export signals out of the desktop computer. The PCI-6052 provides 16 bits of resolution, and can deliver signals at a transmission rate as high as 333 kilosamples per second. The triangle pulse waveform is applied to an amplifier box, which sends the amplified triangle pulse waveform to the voltammetry circuit. The voltammetry circuit operates so that the triangle pulse waveform is applied between the recording electrode and reference

electrode. The resulting current is run through a current-to-voltage converter, and digitized via the PCI-6052.

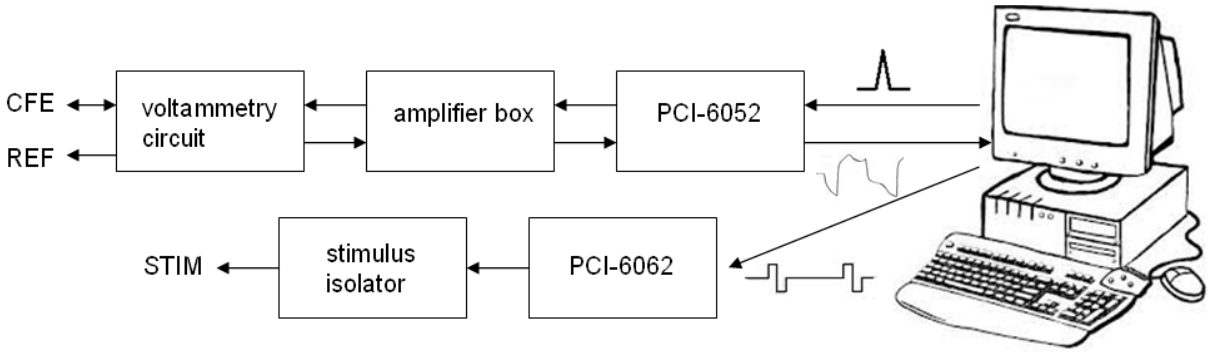

Figure 1.13: A conventional fast-scan cyclic voltammetry setup includes a desktop computer, a PCI-6062 data acquisition box for stimulation signals, an amplifier box, a stimulus isolator, a PCI-6052 data acquisition box for volammetric signals, and a voltammetry circuit that is interfaced with a carbon fiber electrode (CFE) and reference electrode (REF).

In vivo FSCV setups often include features that allow investigators to electrically stimulate the brain and evoke neurotransmitter release. In this part of the setup, as illustrated in Figure 1.13, the computer generates a stimulation square pulse train via the PCI-6062 data acquisition box, which has only 12 bits of resolution compared to 16 bits of resolution in the PCI-6052. The bipolar square pulse train is sent into a stimulus isolator, which outputs a user-defined amount of current per mV input. The output of the stimulus isolator is connected through a special cable to a stimulation electrode. The stimulating electrode is implanted into a part of the brain that is near the axons of presynaptic neurons that supply neurotransmitters to the postsynaptic neurons. When these axons get electrically stimulated, neurotransmitter release occurs, and the recording electrode is able to detect this release.

Attempts at wireless voltammetry emerged in the 1980s when infrared transmission systems started to be implemented in place of FM telemetry systems. The use of infrared signals prevented radio wave interference and allowed signals to bounce off of walls and ceilings. A bidirectional infrared transmission system for cyclic voltammetry was developed using a polarograph (Annovazzi-Lodi and Donati, 1988). The polarograph is an older form of instrumentation used to supply a user-defined voltage waveform to a specimen and plot the resulting current with respect to the applied voltage. In cyclic voltammetry applications the polarograph generated the triangle pulse waveform and input the signal into a V/F converter that converts the waveform to an infrared signal (Annovazzi-Lodi and Donati, 1988). The infrared signal was sent to an array of photodiodes on the remote device. After current signals were collected at the recording electrode, they were converted to infrared signals and transmitted back to the polarograph via the LED array. The remote device measured 28 mm X 26 mm X 8 mm, and was mounted onto a rat.

Later, (De Simoni et al., 1990) developed a similar infrared voltammetry system that had a longer operating range, was more light weight (16 grams), and operated on a power supply of ± 3 V. Battery life was up to 20 hours. A major concern for this system is the susceptibility of infrared signals to interference from sources such as ambient light (Moreira et al., 1996).

(Crespi et al., 2004) implemented an infrared transmission system that could be used for voltammetry and amperometry applications. Wireless transmission was only in one

channel to avoid interference between the input and output channels. The device weighed 5-6 grams with spatial dimensions of 1.0 cm X 1.2 cm X 0.5 cm.

Garris et al., (2004) presented a proof of principle paper on a wireless FSCV system that uses Bluetooth technology. For *in vitro* testing, a flow injection setup was used. For *in vivo* testing, a carbon fiber electrode was implanted into the caudate-putamen of an anesthetized rat. Dopamine release was evoked with electrical stimulation. Device dimensions were 3.3 cm X 1.7 cm X 0.25 cm. Operating distance was 9 meters. Overall, the device showed promise for *in vivo* voltammetric measurements of neurotransmitter release on freely moving rats. A limitation of the technology was that wireless transmission was unidirectional. Signals could be transmitted from the remote device to the computer base station, but no signals could be transmitted from the computer to the remote device. Instead of the user sending the triangle pulse waveform to the remote device, the triangle pulse waveform had to be generated on a microprocessor chip at the remote device. This setup denies the user the flexibility to change to a different applied pulse during the course of an experiment. In other words, if the user wants to change the duration or peak voltage of the applied waveform, the experiment must be stopped, and the wireless device must be removed from the rat so the microcontroller can be reprogrammed. If the user lacks the skills required to reprogram a microcontroller, then the device may not be as useful to a user who wants to use a variety of applied waveforms from one experiment to the next.

1.7.1 Recent Wireless Voltammetry Systems

Some of the most recent wireless voltammetry systems include the Real-Time Telemetry (RAT) system (Garris et al., 2007), the Wireless Instantaneous Neurotransmitter Concentration System (WINCS) (Bledsoe et al., 2009; Agnesi et al., 2009; Griessenauer et al., 2010; Shon et al., 2010) and wireless voltammetry systems consisting of integrated circuits (Roham et al., 2008; Roham et al., 2009; Roham et al., 2010).

Figure 1.14 shows the block diagram of the RAT system presented in (Garris et al., 2007). Wireless voltammetry setups today typically consist of a home base unit and a remote device. The home base unit consists of a computer and wireless transceiver. The remote unit consists of a wireless transceiver and the voltammetry circuit that interfaces with the electrodes. Often there is a microprocessor chip that generates the triangle pulse waveform and sends the output of the voltammetry circuit to the wireless transceiver.

The RAT system combines wireless technology and electrochemistry techniques for a variety of possible applications including wireless electrophysiology, wireless voltammetry and wireless electrical stimulation. A wireless voltammetry system was implemented for continuous monitoring of neurotransmitter release in freely moving rats (Garris et al., 2007). Bluetooth is a suitable wireless technology for its small size, low power requirements, and convenient integration with computer systems. Voltammetry

is the electrochemical technique of choice for its high chemical resolution and high time resolution.

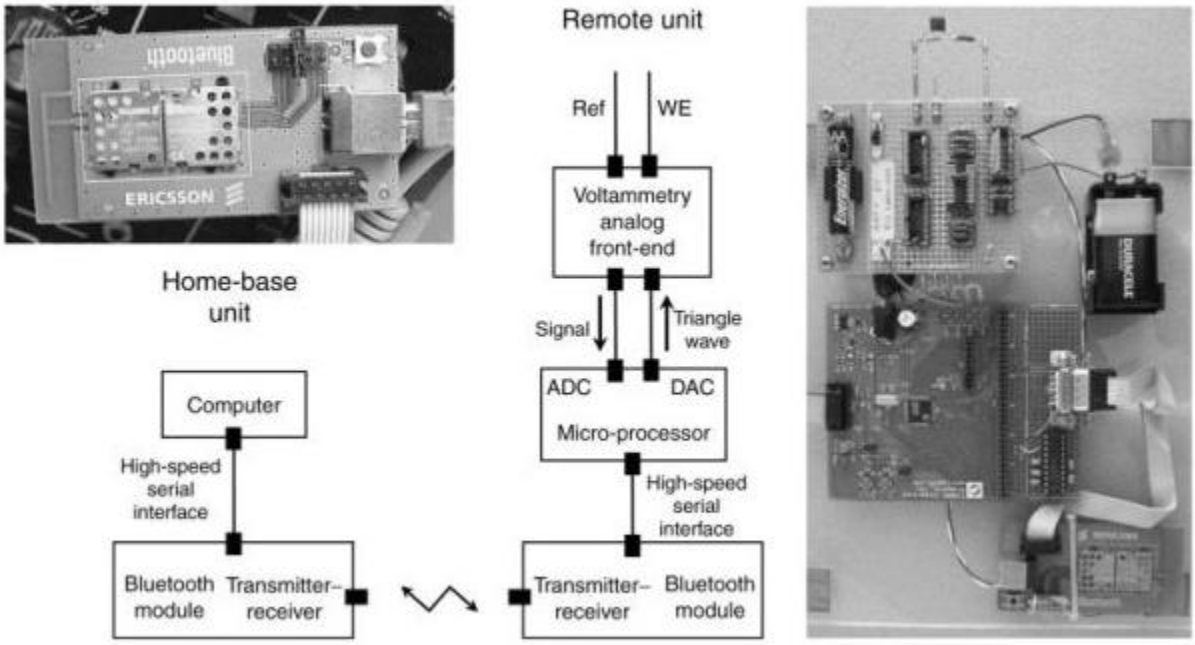

Figure 1.14: A block diagram of the RAT system presented in (Garris et al., 2007). A working electrode (WE) and reference electrode (Ref) are implanted into a rat's brain. The remote device on the rat consists of a voltammetry circuit, microprocessor chip and a Bluetooth transceiver, plus a battery and stimulator which are not shown. Wireless data signals are communicated to the based station shown at the left, which consists of a computer and Bluetooth transceiver.

The device was tested using urethane-anesthetized rats. Dopamine readings with the RAT system were compared to those of the hardwired system. In addition, the electrical stimulator on the circuit was tested for its effectiveness in evoking dopamine release, and then compared to an external electrical stimulator. Both the on-board stimulator and external stimulator yielded similar dopamine release magnitude and kinetics. The hardwired transmission of data and wireless transmission of data yielded similar dopamine release curves.

The RAT system presented in (Garris et al., 2007) showed promise for *in vivo* voltammetric recordings in freely moving rats, but it was only tested on anesthetized rats. In addition, wireless transmission was still unidirectional. The triangle pulse waveform was generated on a microcontroller chip on the board, making it difficult for a user to change the applied waveform without microcontroller programming experience.

Kagohashi et al., (2008) reported on a wireless voltammetry system that was used on unanesthetized ambulatory rats. Radio transmission was also unidirectional, from remote device to the home base unit. The triangle pulse waveform was generated on the chip by the CPU. A potentiostat received information from the CPU about the triangle pulse waveform, and then applied the triangle pulse waveform across the working electrode and reference electrode. The system used a 7.2 V battery and it weighed around 90 grams so that it could be used with small animals. The dopamine release detection limit was around 270 nM. *In vitro* experiments were performed on dopamine concentrations ranging from 0.1 μM to 0.5 μM. There was a linear relationship between the magnitude of dopamine release and the detected dopamine current. Results obtained with the wireless device were comparable to those obtained with the conventional wired setup.

The WINCS device was modeled after RAT instrumentation specifically for use during rat neurosurgeries. When electrodes are implanted into an animal, voltammetry recordings are taken during the surgery to ensure placement of electrodes at the correct

stereotaxic coordinates. (Bledsoe et al., 2009) reported on an electrochemical device that can wirelessly detect neurotransmitter release during surgeries. It operates at 3.7 V power supply, making it safer than other higher power voltammetry circuits. The dimensions are 3.3 cm X 6.5 cm.

WINCS custom software has a user interface that allows the user to modify the applied triangle waveform, start/stop data acquisition, control the sampling rate, and process the received data. The user can modify the amplitude and offset of the applied voltage in 10 mV increments, and modify the triangle waveform slope to anywhere from 100 V/s to 1000 V/s. The user may also apply and N-shaped waveform that is specially used for serotonin detection. Low pass filtering is done in software with a series of built-in low pass filters to choose from including Chebyshev and Butterworth filters. Displays include current versus time in one plot and background subtracted current versus applied voltage in another plot. Sampling frequency varies from 50 kHz to 100 kHz. (Agnesi et al., 2010) reported on an extended use of WINCS for amperometric detection of neurotransmitter release.

WINCS gives the user much more flexibility than the RAT system, but as with the RAT system, WINCS was only demonstrated to work on anesthetized rats. The system is designed for use during rat neurosurgeries, but has not been adapted for use on awake and freely moving rats. Furthermore, all measurements were of electrically evoked neurotransmitter release, which does not occur in a natural behavioral setting.

Roham et al., (2008) implemented a wireless voltammetry integrated circuit (IC) with much lower weight and lower power consumption (1 mW consumption at 2.6 V power supply). The remote device that is mounted onto a rat occupies an area of 5 mm^2. The circuit has four channels. Flow injection technique was used to test the device. The voltage scan rate was 300 V/s, with 3.3 scans performed per second. Dopamine sensitivity was found to be 7.7 nA per μM of dopamine with a detection limit of 16.7 nM of dopamine. For *in vivo* testing, a carbon fiber electrode was implanted into the caudate-putamen of a live rat, and electrically evoked dopamine release was detected. An *in vivo* dopamine voltammogram was successfully generated in (Roham et al., 2008) and (Roham et al., 2009). An additional feature allowed for electrophysiological recording at the same time as electrochemical recording using a time-share integrated circuit (Roham et al., 2009).

The system was further developed to accommodate ambulatory subjects (Roham et al., 2010). In other words, *in vivo* measurements were performed on awake moving rats rather than on anesthetized rats. The device was miniaturized to 2.3 grams including the battery, and operates on a 3-V power supply. Recordings of dopamine release were taken from the forebrain of rats on amphetamine. Very large scale integration (VLSI) design and CMOS technology were used to improve the signal-to-noise ratio, reduce power consumption and reduce the dimensions and weight of the device. The triangle pulse waveform was programmed into the chip during power up. An inductor was used for wireless transmission at a frequency of 433 MHz. The RC low pass

filtering circuit has a feedback resistor value of 22 kΩ and a capacitor value of 10 nF, yielding a cutoff frequency of 723 Hz.

(Roham et al., 2010) and (Kagohashi et al., 2008) were among the first to report on a wireless FSCV device that enabled wireless electrochemical detection of neurotransmitter release from awake and freely moving rats.

1.7.3 Summary and Future Directions

The WINCS device provides much flexibility for the user that the VLSI circuit presented in (Roham et al., 2010) does not. While the VLSI circuit has a microcontroller that must be programmed with a triangle waveform of predetermined amplitude, offset and slope, the WINCS custom software allows the user to not only control the basic characteristics of the triangle pulse waveform, but also what type of waveform is applied. However, the WINCS device is primarily for use on anesthetized rats undergoing neurosurgery, and has not been tested on live ambulatory rats. The VLSI circuit is much smaller and therefore better for use on live moving rats.

It is difficult to find a wireless voltammetry system that has the flexibility of WINCS while also being usable on live moving rats. *We present an inexpensive Bluetooth wireless FSCV system that works on live awake ambulatory rats while also allowing the user to control the applied voltage waveform during an experiment. Unlike in most previous work, we use a differential amplifier circuit to subtract a capacitance compensation*

signal rather than the applied pulse. Capacitance compensation makes the output signal smaller, and increases the dynamic range of the wirelessly transmitted signal.

CHAPTER 2

In Vitro Wireless Voltammetric Detection of DA Release

Acquisition of neurophysiological data from live, freely behaving research animals requires wireless recording technology that avoids the restrictions associated with wired recording setups. One example is the voltammetric recording of neurotransmitter release to understand its link to observable animal behavior. We present here a wireless fast-scan cyclic voltammetry device designed to be carried by a laboratory rat in a backpack and connected to an implanted carbon fiber electrode. Using standard Bluetooth technology the computer wirelessly sends a triangle waveform to the remote device, which initiates redox reactions at the working electrode while the measured redox currents are converted to a voltage, capacitance compensated and wirelessly sent back to the computer base station for analysis. The device weighs 35 grams including the battery, and in vitro dopamine detection is demonstrated down to 250 nM concentration. Recordings of transient DA release in a dish of buffer solution are comparable to recordings from a conventional wired voltammetry setup using the same electrode immersed in the same buffer solution. The bidirectional communication allows adjustment of the voltage waveform according to experimental conditions, making the device highly flexible and also useful for applications requiring changes from one stimulation signal to the next during the course of a single experiment.

2.1 Introduction to Wireless Voltammetry

Electrochemical measurements of neurotransmitter release have been an important tool to achieve a better understanding of the role of neurotransmitters in brain function and

observable animal behavior. Release of oxidizable neurotransmitters such as dopamine can be recorded with high time resolution by fast scan cyclic voltammetry (FSCV) using an implanted carbon fiber working electrode (CFE) and a reference electrode (Millar et al., 1985). In a conventional set-up, a wired connection is made to the electrodes to apply a voltage ramp and to measure the resulting current, which displays small changes in response to DA concentration changes around the CFE (Garris et al., 1997). However, the wired connection limits the animal's behavioral freedom and may even alter the observable behavior.

Previous designs that used an infrared transmission system (Crespi et al., 2004), a Bluetooth transceiver (Bledsoe et al., 2009; Garris et al., 2004), or an integrated circuit using RF transmission (Roham et al., 2010; Roham et al., 2008) were capable of fast scan cyclic voltammetry by generating the voltage in the remote device. These technologies were all demonstrated using in vitro tests and in vivo measurements of dopamine or serotonin (Griessenauer et al., 2010) release in anaesthetized rats. A wireless voltammetry device using a Bluetooth radio was recently tested on awake behaving rats (Kagohashi et al., 2008). However, it was rather heavy for a rat (90 grams) and was susceptible to noise generated by the animals' movements during recordings. A much more light weight integrated circuit device was later developed, which also has been shown to record from awake ambulatory rats (Roham et al., 2010). However, this wireless device only had unidirectional communication. The user cannot easily modify the applied voltage signal during the course of an experiment.

Our objective was to create a simple wireless voltammetry device that can measure neurotransmitter release from live awake rats and allow the investigator to alter the stimulation signal during the course of an experiment without the need to reprogram a microcontroller. Here we present a bidirectional wireless voltammetry device using Bluetooth transmission that weighs 12.6 g and operates on a single rechargeable 3.7 V battery bringing the total weight to 35 g. The voltage ramp signal is transmitted wirelessly from the base station to the remote device while the current is simultaneously recorded. The voltage signal may be modified to generate arbitrary waveforms, making the device highly flexible and extending potential applications beyond FSCV.

2.2 METHODS

2.2.1 Fast Scan Cyclic Voltammetry

Fast-scan cyclic voltammetry (FSCV) is the method of choice for detection of dopamine release in vivo because of its high time resolution and chemical resolution (Phillips and Wightman, 2003) as illustrated in Figure 2.1. Typically, triangular voltage ramps from -450 mV to +1000 mV and back to -450 mV are applied to a CFE at a scan rate of ~300 V/s. The duration of one cycle is 10 ms. Ramps are applied at a frequency of 10 Hz, leaving 90 ms between pulses where the voltage is held at -450 mV. The upwards ramp causes oxidation reactions while the downwards ramp causes reduction reactions. The resulting current is recorded continuously. Each triangle pulse results in a current signal that is the sum of a background current that is produced in the absence of

dopamine and the Faradaic current due to electron transfer from oxidation/reduction reactions. The Faradaic current is obtained by subtraction of a background current signal and is converted to a difference voltammogram when plotted with respect to applied voltage.

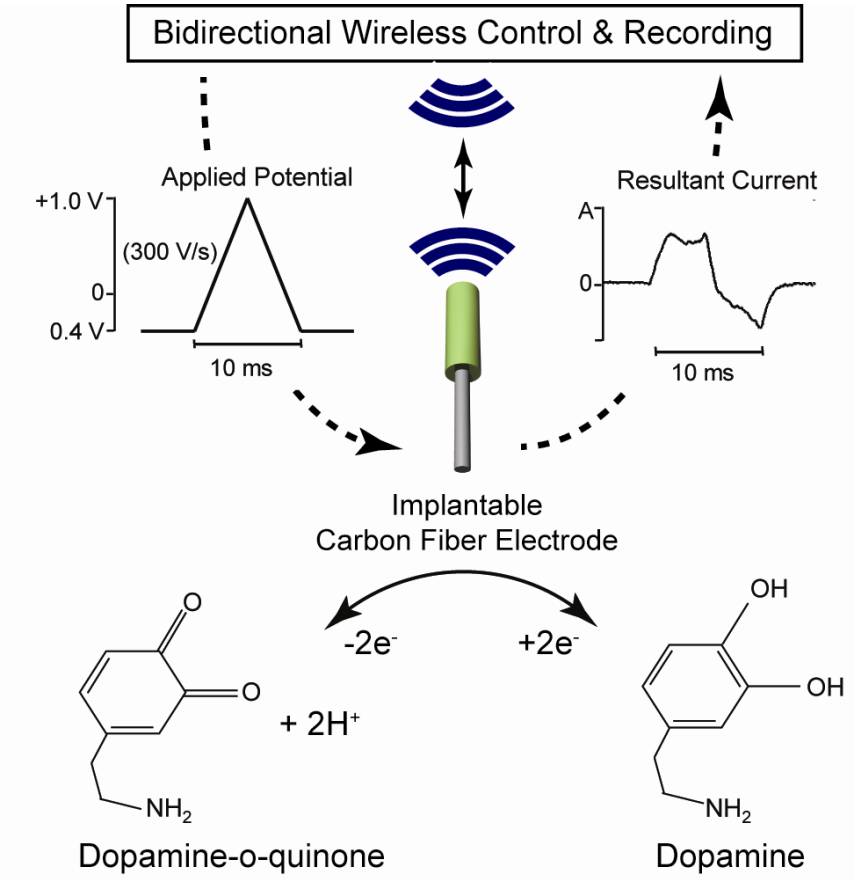

Figure 2.1: Diagram illustrating redox reactions at the carbon fiber microelectrode. A triangle pulse, shown on the upper left, is applied to the microelectrode, causing oxidizable neurotransmitters such as dopamine to lose electrons during the upwards ramp and gain electrons during the downwards ramp. The gaining and losing of electrons causes current flow into the electrode as shown in the resultant current plot at the upper right. The triangle pulses are wirelessly transmitted to the remote device while the resultant current is wirelessly transmitted from the remote device to the computer base station.

2.2.2 The Wireless Device Hardware

To perform FSCV recordings from freely moving animals, we developed a wireless voltammetry printed circuit board shown in Figure 2.2. The remote device consists of two parts: the Bluetooth circuit that communicates wirelessly with the computer base station, shown in Figure 2.2a, and the voltammetry circuit. The voltammetry circuit includes: a current-to-voltage converter for application of the voltage ramp and measurement of the CFE current; a capacitance compensation circuit; a differential amplifier for subtracting the capacitance compensation signal; an amplifier circuit for the triangle pulses and an attenuator for the capacitance compensated signal. The Bluetooth portion of the remote device includes a Free2move F2M03MLA Bluetooth transceiver with D/A and A/D converters. The wireless device (Figure 2.2b) connected to a rechargeable 3.7 V Tenergy battery measures 4.61 cm x 6.72 cm, and weighs 35 grams including the battery.

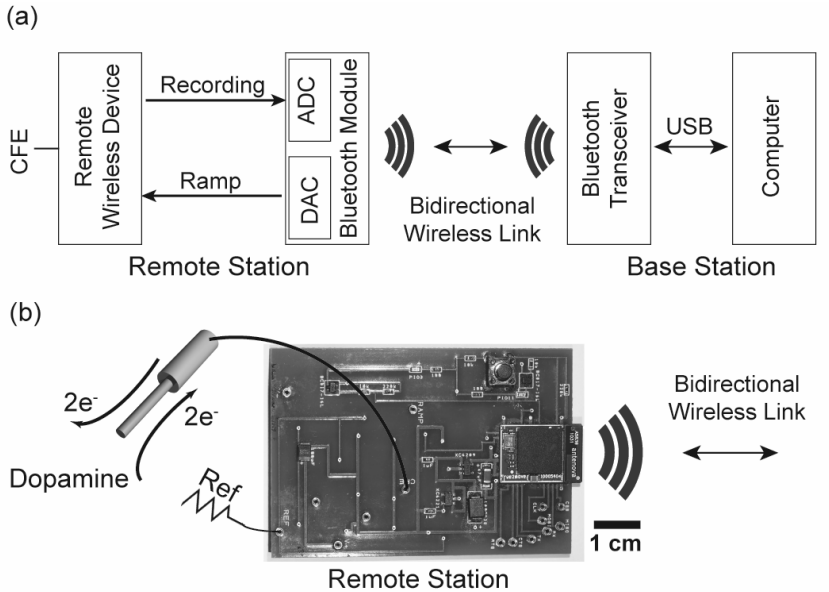

Figure 2.2: (a) A block diagram illustrating wireless transmission between the remote device and the computer base station. (b) Photograph of the wireless voltammetry circuit. CFE is the carbon fiber electrode, which is inserted into a dish filled with buffer solution. REF is the reference electrode that is placed a distance away from the CFE in

the same dish. The Bluetooth chip is located on the right. A yellow LED, located above the Bluetooth chip, flashes when the device is active, transmitting signals.

The digital triangle pulse waveform data is sent via Bluetooth from the computer base station to the Bluetooth transceiver on the remote device. The D/A converter generates an analog voltage ramp with a maximum amplitude of ~500 mV. This voltage ramp is amplified with an inverted operational amplifier circuit, and filtered to smooth the D/A staircase output by an LMV751 amplifier with a 15 kΩ/22 nF RC feedback circuit (Figure 2.3a, top) that yields a 482 Hz cutoff frequency. The triangle pulses are applied to the CFE via the non-inverting input of an LMV751, and the resultant CFE current is converted to a voltage with Rf=3 MΩ / CCFE=100pF RC feedback (Figure 2.3a) to obtain a current-to-voltage converter gain of 3 mV/nA and a 530 Hz cutoff frequency low pass filter. The LMV751 was chosen because of its low noise and low power consumption. The 530 Hz low pass filter reduces noise without attenuating the dopamine signal.

Because most of the CFE current is a capacitive background current, capacitance compensation is performed by subtracting the current collected in an RC series circuit (Figure 2.3a, red box) with a second LMV751. The capacitive background current of a CFE for in vivo recordings is mainly generated by the double layer capacitance that is created at the electrode/electrolyte interface. The double layer capacitance (CD) of such an electrode is approximately:

$$C_D = \varepsilon_0 \frac{A}{d} \qquad (1)$$

where A is the electrode area, d the Debye length (~1 nm for physiological saline), ε0 the permittivity of vacuum (8.85 pF/m), and ε the relative dielectric constant of water (~80). For a carbon fiber with 5 μm diameter that protrudes ~100 μm from the glass tip, C_D is ~1.1 nF. A suitable approximation of the background current was obtained by using a capacitance C_c=1 nF in series with a resistance R_c=100 kΩ (Fig. 3a).

To avoid extra noise introduced by the capacitance compensation, the RC low pass filter of the current-voltage converter was set to R_f=3 MΩ / C_{Comp}=300 nF (Fig. 3a), reducing the cutoff frequency to 177 Hz. The capacitive current is subtracted from the CFE current at the INA132 differential amplifier, reducing the amplitude of the CFE current output signal. Because the amplitude of the differential amplifier output still exceeds the ADC range, a Π type attenuator, with an attenuation factor of 2.5, is inserted between the differential amplifier and the Bluetooth ADC.

The total power consumption of the device is ~165 mW. It is operated from a 3.7 V Tenergy lithium battery that is contained in a custom-made Lomir backpack together with the remote device circuit board. Both sides of the printed circuit board are used with the Bluetooth circuit facing up while the analog voltammetry circuit faces towards the animal. The Bluetooth circuit also includes a voltage regulator (Bluetooth requires 3-3.6 V power supply), a push button for initiating a wireless connection, an LED that indicates whether the device is actively transmitting signals, and connectors for the RS232 connector board. The RS232 connector board is used to connect the circuit to a

desktop computer hyperterminal and establish parity between the remote device and the computer prior to the experiments. For more details on the hardware, see appendix.

2.2.3 The Software Setup

Igor Pro (Wavemetrics) software was written for both data acquisition and data analysis. In our experiments, this software sends a waveform, consisting of a series of triangle pulses, to the remote device via a Bluetooth USB dongle, while it records the data from the remote device. Bluetooth data transmission is performed in headset mode to enable bidirectional transmission.

The user may define the duration of each triangle pulse, time between triangle pulses, total duration of the waveform, sampling frequency (usually 44,100 samples/s), holding voltage between pulses and peak voltage. The waveform is converted to a sound file that can be played with Windows Media Player or any software that can play sound files. We used Igor software to play the triangle pulse waveform and record the resultant current simultaneously. The waveform was applied continuously throughout the experiment. The triangle pulse waveform was 20 minutes long, and was restarted each time it ended. Waveform amplitude and offset are adjusted in software to yield the desired parameters of the applied waveform at the CFE. The offset of the waveform in software determines the holding potential at the CFE. Calibration measurements were performed to determine how the counts of the digital representation of the signal in software correspond to voltage applied to the CFE on the remote device.

After wireless transmission from remote device to computer, the recorded data may be filtered digitally. We applied a Kaiser-Bessel filter with 1 or 2 kHz cutoff frequency. For background current subtraction the user enters the sampling frequency, the time in the recording that is defined as background, the number of background signals to average, and whether to use filtered or unfiltered data. The averaged background signal is then subtracted from running averages of a user-defined number of signal pulses for the neurotransmitter signal. Background subtracted currents are finally plotted with respect to the applied voltage to obtain the difference voltammograms. For more details on data analysis, see appendix.

2.2.4 *In vitro* dopamine recording

For in vitro testing, a simple flow system was used. A petri dish was filled with buffer solution containing 140 mM NaCl, 5 mM KCl, 5 mM CaCl2, 1 mM MgCl2, and 10 mM HEPES/NaOH pH 7.3. Dopamine solutions were made fresh by dissolving dopamine hydrochloride powder in buffer solution at concentrations varying from 200 nM to 5 □M. At the start of the recording, a solution of known DA concentration was flowed through the dish to replace buffer solution. After two minutes of recording, DA-free buffer solution was flowed into the dish to replace the DA solution. Experiments were done with the wireless voltammetry board inside a Faraday cage. The Bluetooth USB dongle was connected to the computer via a USB extension cable such that both, the USB dongle and the remote device were located inside the Faraday cage.

2.2.5 *In Vitro* Recording Procedure

To generate a time-dependent DA concentration change, a small volume of concentrated 20 µM DA solution was manually injected into the dish containing DA-free buffer solution during the recording using an Eppendorf pipette. After DA is applied near the electrode tip, it diffuses away within a few seconds, generating a transient DA signal. For comparison, these experiments were repeated with the wired setup using the same electrode. The buffer solution in the dish was replaced when the recording setup was switched.

2.3 Results

Figure 2.3a shows the voltammetry circuit schematic. Outlined in red is the capacitance compensation circuit, which acts as a dummy electrode. Current collected from the compensation circuit is subtracted from current collected at the CFE in order to reduce signal magnitude and increase dynamic range. The numerical labels indicate points in the circuit that were probed. Figure 2.3b shows measurements from the different test points of the voltammetry circuit. The upper left shows the digital triangle pulse data before wireless transmission. The digital representation of the triangle pulse waveform is in 16 bit signed integer format. To obtain a -450 mV holding potential and a +1300 mV peak relative to Vref at the remote device, the digital triangle pulse waveform spans a range from ~8000 to ~24000 counts (Figure A.1). The triangle pulse applied to the CFE after wireless transmission to the remote device, amplification and on-chip low pass filtering at 530 Hz cutoff frequency, is shown in the upper right plot of Figure 2.3b. The noise level is approximately 3 mV, yielding an SNR of ~600. The middle left plot of

Figure 2.3b shows the current signal at the CFE current-to-voltage converter output. This signal consists of the sum of the applied triangle pulse and the CFE current. When the CFE was disconnected, the CFE current-to-voltage converter output had a noise level of around 4 mV. When the CFE was connected, the noise level increased to 9 mV. The middle right shows the signal at the capacitance compensation current-to-voltage converter output. The current-to-voltage converter for the capacitance compensation has a lower cutoff frequency for the low pass filter at 172 Hz because, in contrast to the dopamine signal recorded by the CFE, the high frequency components do not need to be resolved in the compensation signal. With the reduced cutoff frequency, the peak-to-peak noise at the capacitance compensation output is ~5 mV.

Typically, wireless voltammetry devices use pulse compensation (Bledsoe et al., 2009; Garris et al., 2004; Kagohashi et al., 2008) where the triangle pulse is subtracted from the CFE signal. The lower left plot of Fig. 3b shows the pulse compensated signal, which was computed by subtracting the triangle pulse from the CFE signal in software. The signal magnitude is reduced from 1350 nA to 800 nA peak-to-peak. The peak-to-peak noise in current units is ~2.7 nA.

A unique feature of the device presented here, is that is utilizes capacitance compensation rather than pulse compensation. Our capacitance compensated signal is shown in the lower right of Figure 2.4b. By subtracting the capacitance compensation signal shown in the middle right, the signal magnitude is reduced to less than half, down

to 290 mV, thus increasing dynamic range. The capacitance compensated signal is digitized by the Bluetooth chip for transmission to the computer.

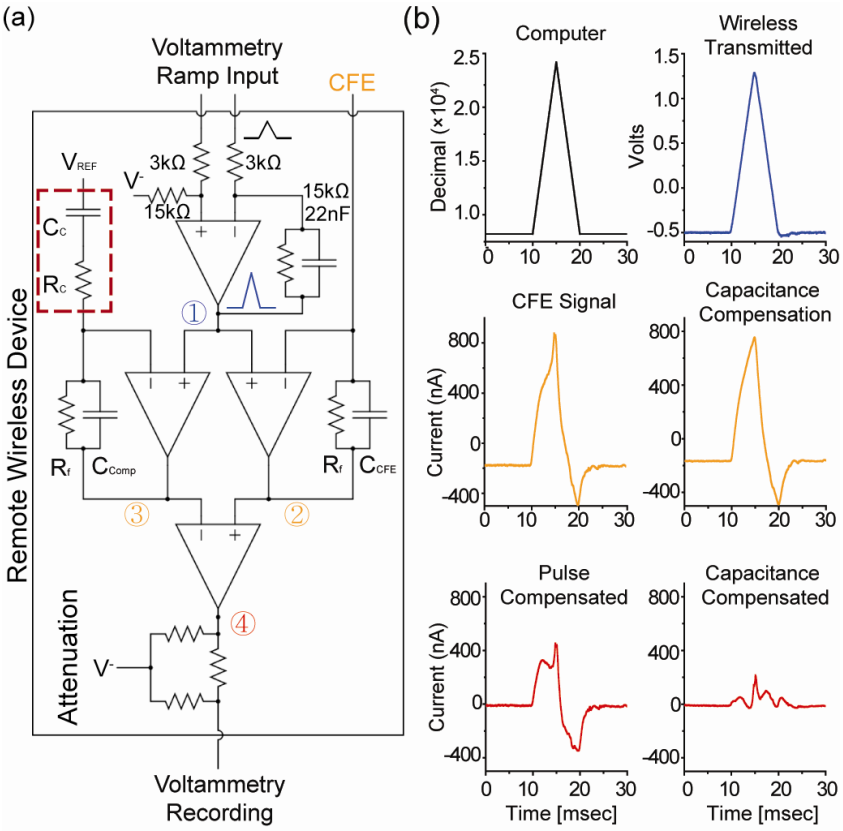

Figure 2.3: (a) The voltammetry circuit diagram. The numerical labels 1-4 are test points in the circuit that were probed. Point #1 represents the triangle pulse waveform that is applied to the CFE and the compensation circuit after wireless transmission and amplification. Point #2 is the CFE signal after conversion to a voltage. Point #3 is the capacitance compensation signal after conversion to a voltage. Point #4 is the differential signal. (b) The signal recorded from different parts of the remote device voltammetry circuit. The upper left plot shows the digital signal prior to wireless transmission. The upper right plot shows the triangle pulse after it is wirelessly transmitted to the remote device and amplified with the ramp amplifier circuit probed at position #1 of the circuit diagram . The middle left plot shows the CFE current signal, probed in position #2. The middle right plot shows the capacitance compensation current from the RC series circuit, probed in position #3. The lower left plot shows what the signal looks like when it is pulse compensated by subtraction of the triangle pulse. The lower right plot shows the capacitance compensated signal at the output of the differential amplifier, probed in position #4.

Figure 2.4 shows DA voltammograms generated from wirelessly transmitted data. Each set of plots shows the background current pulse before DA application (in black)

superimposed over the current pulse measured in the presence of DA (in red). The shape of these voltammograms differs from that typically reported due to the capacitance compensation, which reduces the amplitude of the background current. Shown in purple is the background-subtracted signal plotted with respect to applied voltage. Figure 2.4a shows a 2 μM DA voltammogram generated from unfiltered data. Figure 2.4b shows the same 2 μM DA voltammogram after digital filtering using a Kaiser-Bessel low pass filter with 1 kHz cutoff frequency. These voltammograms show the oxidation and reduction peaks characteristic of DA detection. Figure 2.4c shows DA voltammograms for various DA concentrations generated from digitally filtered data.

The relationship between DA concentration and magnitude of the peak oxidation current is roughly linear as illustrated in Figure 2.5. Magnitude of the oxidation peak was quantified by determining the mean current around the peak of the background-subtracted signal (680 to 830 mV) as indicated by the vertical dotted lines in Figure 2.4c. DA sensitivity is about 4.7 nA per μM of DA concentration for concentrations up to 2 μM. This factor depends specifically on the CFE surface area.

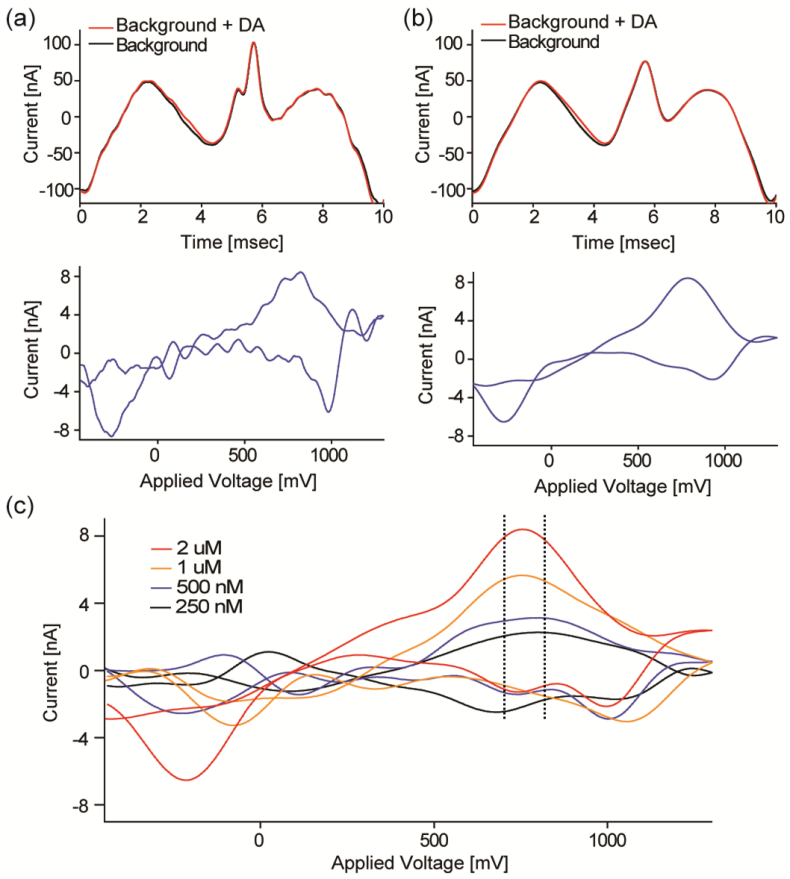

Figure 2.4: Wirelessly transmitted in vitro voltammograms. (a) Background current (black) and current in the presence of 2 µM DA (red) and difference voltammogram (blue) generated from unfiltered data. (b) Currents as in (a) but after 1 kHz Kaiser-Bessel low pass filtering. (c) Voltammogram of 2 µM, 1 µM, 500 nM and 250 nM DA generated from filtered data as in (b).

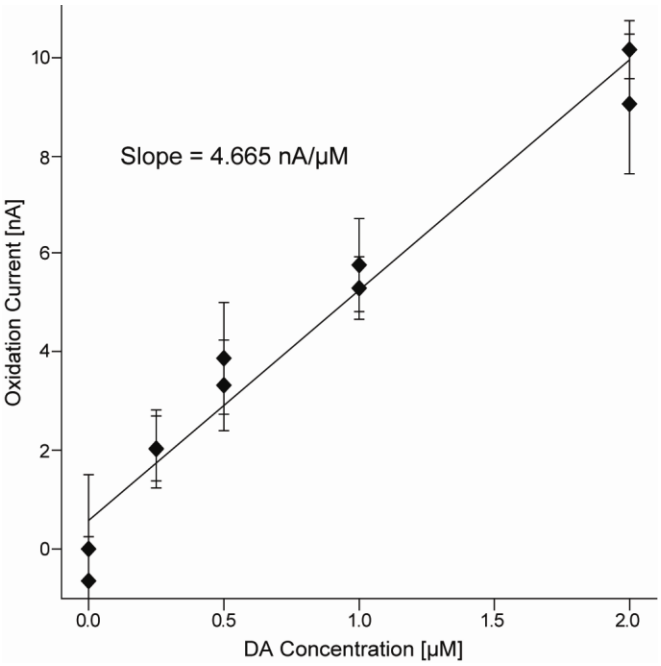

Figure 2.5: A plot of dopamine concentration versus oxidation peak amplitude, with a slope of 4.7 nA/μM. Error bars represent the standard deviation of the peak oxidation current in response to an applied pulse.

Figure 2.6 shows that the wireless device can resolve DA transients with duration <1 s. Figure 2.6a and 2.6b show 3D color plots of DA cyclic voltammograms around the time point where DA was injected. The vertical axis is applied voltage with the upwards voltage ramp starting at the bottom and the downwards voltage ramp finishing at the top of the vertical axis. Background subtracted current is color-coded, with the largest and most positive currents in green and the most negative currents in blue and black. In both, the wired and wireless recordings, the DA oxidation and reduction peaks are clearly visible. Figure 2.6c and 2.6d show the averages of 5 difference cyclic voltammograms recorded at the times indicated by vertical dashed lines in Figure 2.4a and 2.4b, respectively. Figure 2.6e and 2.6f show the time course of the DA oxidation peak current obtained from running averages of the current from 5 signal pulses

providing 500 ms time resolution. The two subsequent DA transients in Figure 2.6f reflect the actual DA concentration changes around the CFE during mixing.

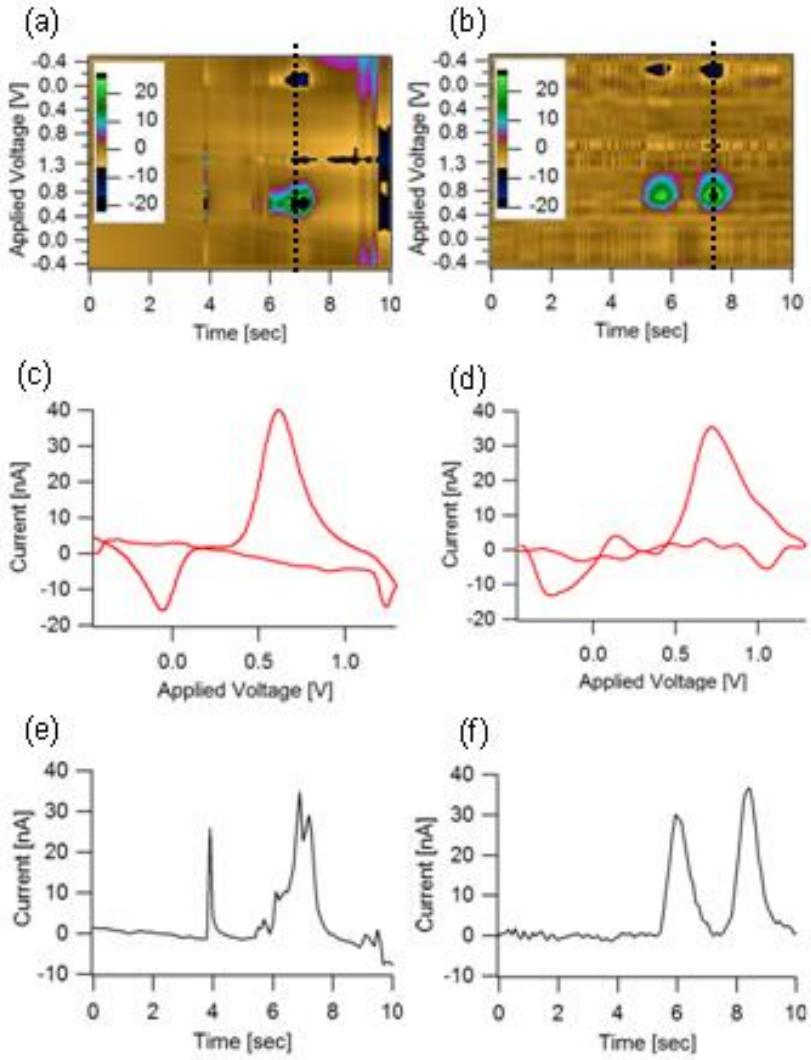

Figure 2.6: DA release from the wired setup (left column) and wireless setup (right column). Color plots for both the wired setup (a) and the wireless setup (b) show a clear DA oxidation peak and reduction peak. The difference voltammograms at the times indicated by vertical dashed lines in panels a,b from the wired (c) and wireless recording (d). The time course of DA concentration indicated by the current amplitude at the DA oxidation peak shows concentration transients with1-2 s duration in both, the wired (e) and wireless (f) recording.

2.4 Discussion

We developed a compact wireless FSCV device that is capable of detecting the release of oxidizable neurotransmitters at concentrations at least down to 250 nM with a sensitivity of 4.7 nA/µM with a standard CFE as used for in vivo recordings. This work extends previous results and shows that bidirectional Bluetooth transmission of audio signals can be used for continuous monitoring of neurotransmitter release in live animals.

Common goals of wireless neurophysiology systems are to achieve a small size, low power consumption and sufficient reliability in recording of oxidizable neurotransmitter release. Integrated circuits are much smaller and lower power than other implementations, but they are more expensive to construct and are typically designed for very specific applications. The device described here, is made entirely of commercially available components. In contrast to previous integrated circuit implementations, which used only unidirectional communication, it allows the user to send arbitrary signals to the remote device from the base station. This feature makes it highly flexible, also for applications beyond FSCV.

In unidirectional communication systems, the triangle pulse waveform is typically programmed onto a chip on the remote device. In bidirectional communication systems, the triangle pulse waveform is digitally defined in software and then wirelessly transmitted to the remote device while current signals are simultaneously recorded from the CFE. In this way, the user may apply voltammetric triangle pulses in one part of the experiment, and then apply amperometric square pulses at another time point without

having to halt the experiment and reprogram a microprocessor. The user may also vary the width, frequency, magnitude and offset of triangle pulses during an experiment to determine optimal settings.

A distinguishing characteristic of our device is that it implements capacitance compensation rather than pulse compensation. Because a CFE behaves very much like a capacitor, capacitance compensation is able to reduce the magnitude of the signal more than pulse compensation, thus increasing dynamic range. An increase in dynamic range means more dopamine sensitivity, allowing the experimenter to more easily record behaviorally evoked dopamine release, which is generally lower in magnitude than artificially evoked dopamine release.

The functionality of the wireless device was demonstrated by in vitro measurements of DA at concentrations down to ~250 nM and measurements of time dependent DA concentration changes. The DA voltammograms are in good agreement with those measured using a conventional wired in vivo recording system. A manuscript describing the application of the wireless device for in vivo recordings form freeley moving unrestrained animals is in preparation.

CHAPTER 3
Wireless *In Vivo* Recording of DA Release in Freely Moving Unrestrained Rats

A Bluetooth-based wireless fast-scan cyclic voltammetry (wFSCV) device that is carried by a laboratory rat in a backpack and connected to an implanted carbon fiber electrode was used to measure dopamine concentration changes in the caudate-putamen. We demonstrate wireless *in vivo* detection of electrically evoked and chemically evoked dopamine release. Changes in dopamine concentration were correlated with anticipation and consumption of food in freely moving unrestrained rats. The results indicate that the wireless device is suitable for *in vivo* recording of DA concentration changes, enabling such measurement in unrestrained rats. DA concentration and its fluctuations are increased in anticipation and early phase of eating but gradually decline during later phase of eating. The bidirectional communication allows adjustment of the voltage waveform according to experimental conditions, making the device highly flexible and also useful for other applications requiring a different stimulation signal.

3.1 Background

Electrochemical measurements of neurotransmitter release are an important tool for better understanding the role of neurotransmitters in brain function and observable animal behavior. Release of oxidizable neurotransmitters such as dopamine (DA) can be recorded with high time resolution by fast scan cyclic voltammetry (FSCV) using an implanted carbon fiber working electrode (CFE) and a reference electrode (Millar et al., 1985). In a conventional set-up, a wired connection is made to the electrodes to apply a

voltage sweep and to measure the resulting current, which displays small changes in response to DA concentration changes around the CFE (Garris et al., 1997). However, the wired connection limits the animal's behavioral freedom and may even alter the observable behavior.

Experiments that benefit the most from wireless neurophysiology technologies are those performed on live awake animals. Neurophysiological recordings on ambulatory animals have always presented challenges that are not encountered with *in vitro* experiments or anesthetized animal experiments. One such challenge is in securing a connection between the computer and the electrodes implanted in the animal. Movement of the animal can cause a break in the computer-electrode connection and/or mechanical disturbances in the wires that lead to signal artifacts. Several FSCV devices have been developed that wirelessly record neurotransmitter release via an infrared transmission system (Crespi et al., 2004), a Bluetooth transceiver (Bledsoe et al., 2009; Garris et al., 2004), or an integrated circuit using RF transmission (Roham et al., 2010; Roham et al., 2008). However, the functionality of most wireless voltammetry technology has only been demonstrated on anesthetized animals (Garris et al., 2007; Bledsoe et al., 2009; Shon et al., 2010). Only a few publications presented results from awake and ambulatory animals (Kagohashi et al., 2008; Roham et al., 2010), but these operated in unidirectional transmission and did not employ bidirectional data transmission that gives the user the flexibility to change the characteristics of the applied waveform during the course of an experiment.

DA plays an important role in governing eating behaviors (Evans and Eikelboom, 1987; Hernandez and Hoebel, 1988; Volkow et al., 2003), obesity (Wang et al., 2001; Geigara et al., 2009) and gnawing and licking behaviors (Antelman et al., 1975). DA also plays a role in binge eating disorders (Wang et al., 2011). The major site of DA release in reward-seeking behaviors is in the dorsal and ventral striatum. Here we present *in vivo* DA recordings from the caudate-putamen, in freely moving rats utilizing a simple bidirectional Bluetooth-based FSCV device, both in the presence and absence of electrical and chemical stimulation.

3.2 Experimental Methods for *In Vivo* Voltammetric Recording

3.2.1 Drugs and Chemicals

Raclopride HCl and GBR-12909 were used to induce chemically-evoked DA release. The drugs were purchased from Sigma-Aldrich (St. Louis, MO, USA) and were used without further purification. Raclopride HCl (2 mg/kg) was dissolved in 0.6 mL of saline. GBR-12909 (15 mg/kg) was dissolved in 0.3 mL of water and diluted with saline to a total volume of 0.6 mL. Both drugs were administered intraperitoneally.

3.2.2 Animals

Male Sprague Dawley rats (250 – 350 g) were purchased from Charles River (Wilmington, MA). Each animal was housed in a temperature-controlled environment on a 12:12 light:dark cycle. Food and water were available ad libitum. All procedures were approved by the Institutional Animal Care and Use Committees of the University of North Carolina and Cornell University.

3.2.3 Surgical Procedure

For surgeries after which the rats are expected to recover, anesthesia was induced with 4% isofluorane and maintained with 1.5–2.0%. Anesthetized animals were immobilized in a stereotaxic frame (David Kopf Instruments, Tujunga, CA) and their dorsal skull exposed. Coordinates were obtained from the Paxinos and Watson Rat Brain Atlas (2007). Using bregma as a reference point, four holes were drilled for the recording, reference and stimulating electrodes. A guide cannula (Bioanalytical Systems, West Lafayette, IL) was positioned 2.5 mm into the skull over the dorsal striatum (+ 1.2 mm anterior-posterior, AP, + 2.0 mm medial-lateral, ML). An insulated bipolar stimulating electrode (Model MS303/1, Plastics One, West Lafayette, IN) was used to electrically evoke DA release. It consists of two pins across which a bipolar square pulse was applied. With pins positioned 1 mm apart, the stimulating electrode was lowered into the ventral tegmental area (- 5.2 AP, + 1.0 ML, - 8.0 dorsal-ventral, DV). Lastly, a Ag/AgCl reference electrode was positioned in the hemisphere contralateral to the guide cannula and stimulating electrode. All items on the skull were secured with stainless steel screws and dental cement. Following surgery, animals were given ibuprofen (15mg/kg). Animals were given at least 2 days of recovery before using a detachable micromanipulator to implant the recording electrode into the dorsal striatum (- 4.0 to 6.0 mm DV).

Experiments with anesthetized animals followed a similar procedure. Animals were anesthetized with urethane (1.5 mg/kg) and placed in the stereotaxic frame. After the

dorsal surface of the skull was exposed, holes were drilled targeting the dorsal striatum and the ventral tegmental area with the same coordinates as described above. Manipulator arms attached to the stereotaxic frame were used to lower the recording and bipolar stimulating electrodes respectively into the dorsal striatum and the ventral tegmental area. A Ag/AgCl reference electrode was again implanted in the contralateral hemisphere and secured with a screw.

3.2.4 Carbon Fiber Electrode Fabrication

Voltammetric recordings were performed using glass-encased, T-650 type carbon fiber (6 μm diameter, Amoco, Greenville, SC) cylindrical electrodes, fabricated as previously described (Cahill et al. 1996). Briefly, carbon fibers were aspirated into glass capillaries (0.6 mm i.d., A-M Systems, Inc., Carlsborg, WA). A micropipette puller (Narashige, Tokyo, Japan) was used to separate a single capillary into two electrodes with tapered seals. Each electrode was then cut under a light microscope so that the exposed length of the carbon fiber was between 75 and100 μm. An electrical connection to the carbon fiber was made by inserting a wire covered with wet silver paint into the open end of the capillary. The recordings of Figure 3.10 were made with a novel chronically implantable carbon fiber electrode developed in the Phillips lab (Clark et al., 2010), which does not require a guide cannula.

3.2.5 Fast Scan Cyclic Voltammetry

For FSCV, a 290-350 V/s triangular voltage ramp was applied at 10 Hz to the carbon fiber, scanning from -0.45 V to +1.0 V or +1.3 V. The +1.3 V waveform boosts the

electrodes' sensitivity for (Heien et al. 2005), but also produces a larger background current. When using this extended waveform the gain of the wireless amplifier was reduced by switching from a 3 MΩ to a 2 MΩ feedback resistor, to prevent saturation of the current-to-voltage converter circuit in the wireless device.

3.2.6 Wired FSCV Setup

The wired FSCV system consists of locally constructed hardware (UNC-Chapel Hill Electronics facility) controlled by HDCV (High Definition Cyclic Voltammetry, UNC-Chapel Hill), a FSCV data acquisition program designed on the LabVIEW programming platform (National Instruments, Austin, TX). The HDCV program sends out a triangle waveform and simultaneously records the response current. The user defines the amplitude of the triangle pulse, the voltage offset, the time between waveforms and the slope of the voltage ramp in V/s. The built-in oscilloscope window shows the measured current superimposed on the applied triangle wave. While recording, the software stores the recorded current on the computer hard drive. During experiments, the user can select the time in the recording at which stimulation pulses are applied. The stimulation train consists of biphasic rectangular pulses of a user-defined amplitude, pulse frequency and number of pulses. To evoke DA release a 24 pulse (±300 μA, 2 ms per phase) stimulation train was applied at 60 Hz.

A block diagram of the wired recording setup is shown in Figure 3.1. The triangle waveform produced by the HDCV software is generated via the PCIe-6363 X-series data acquisition board (National Instruments, Austin, TX) at a 100 kHz sampling rate. To

reduce noise, the output waveform is sent through a voltage divider where it is reduced to 1/3 of its original magnitude and low pass filtered at 2 kHz. The waveform is then sent to the voltammetry circuit on the head stage that contains the current transducer, which is connected to the carbon-fiber and reference electrodes. The output of the head stage voltammetry circuit is fed into an amplifier box with a gain of 200 nA/V before being sent to the computer via the ADC in the PCIe-6363. The pulses for stimulation of DA release are also constructed in software and delivered through the PCIe-6363 data acquisition board to a stimulus isolator (NL 800A, Neurolog, Digitimer Ltd, Hertfordshire, UK). The stimulus isolator outputs a specific amount of current depending on the amplitude of the stimulus waveform. For these experiments the stimulus output was set to 1 mA/V. The output of the stimulus isolator connects directly to the implanted bipolar stimulating electrode. Both the anesthetized and freely moving animal recordings are made within a Faraday cage to reduce noise.

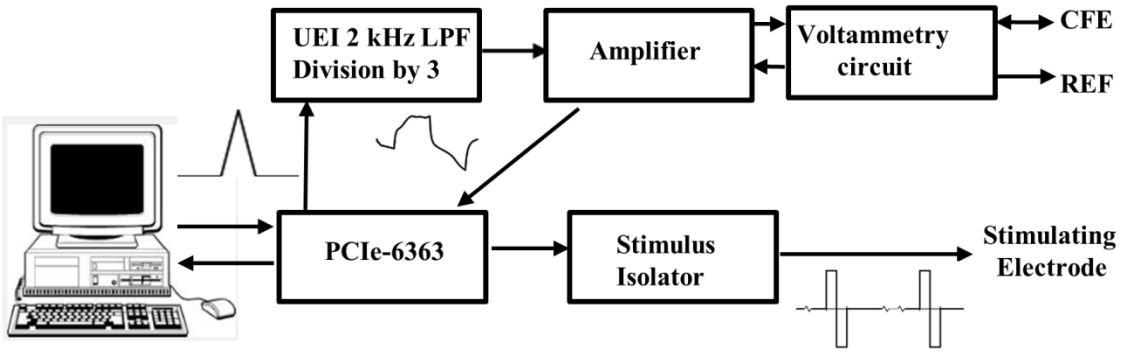

Figure 3.1: Conventional wired recording setup. The setup consists of the voltammetry circuit, amplifier box, the UEI 2 kHz filter, the PCIe-6363 data acquisition board, the stimulus isolator and the desktop computer.

3.2.7 Wireless FSCV Setup

Hardware for the wireless device has been previously described in Chapter 2. The amplifier gain was set to 3 V/μA or 2 V/μA using a 3 MΩ or 2 MΩ feedback resistor, respectively. Figure 3.2A shows the wireless FSCV (wFSCV) printed circuit board. Figure 3.2B shows the wireless voltammetry board placed inside of a pouch with a slit down the side for wires to connect the circuit to the reference electrode (REF) and CFE. A jacket fits around the rat's forelegs from the front and connects to the Velcro on top of the pouch on the rat's back. The battery is placed inside the pouch with the circuit board. To reduce the amount of noise from electrical interference, all recordings are made in a Faraday cage. The Bluetooth USB dongle communicating wirelessly with the remote device is placed inside the Faraday cage with the rat, and is connected to the computer with a USB extension cable.

A pushbutton near the top right hand corner of the wFSCV board is used to activate the Bluetooth transceiver, and the Bluetooth Settings window on the computer screen is used to establish a wireless connection with the remote device.

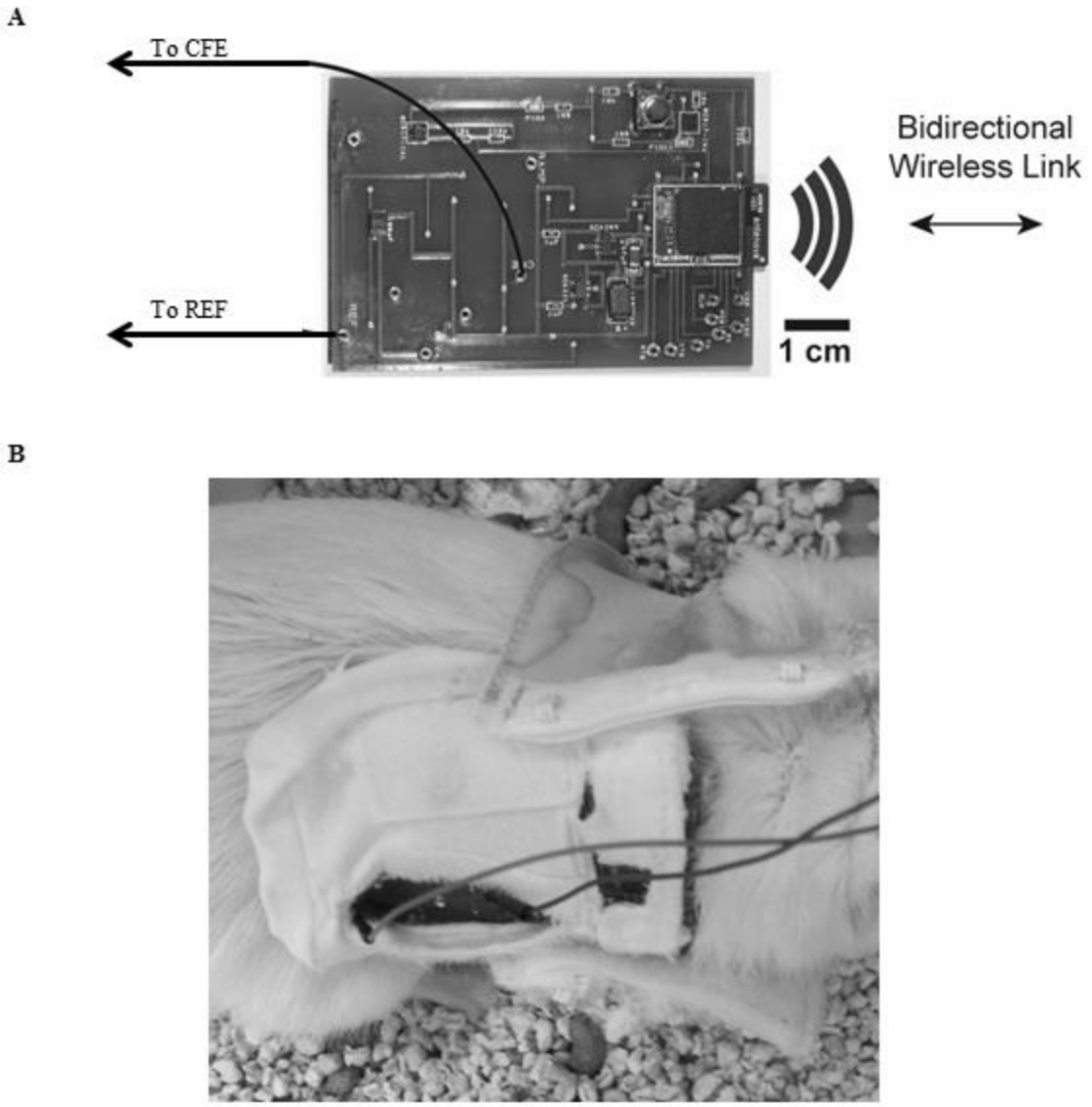

Figure 3.2: (A) The wFSCV circuit board. To the right is the Bluetooth chip that communicates wirelessly with the computer. Also shown are the gold pins that connect to the reference electrode (REF) and the working electrode. (B) Photograph of the wFSCV board inside a pouch on the rat's back like a backpack. The backpack contains the wireless voltammetry printed circuit board and the Tenergy 3.7 V battery. The wires connect the wFSCV circuit to the CFE and reference electrode, respectively.

3.2.8 Anesthetized Animal Recordings

In recordings from anesthetized animals, DA release was evoked by a timed electrical stimulation. At the start of an experiment, the wired system was used to position the recording and stimulating electrodes at depths for maximal DA release within the dorsal

striatum. Once control recordings with the conventional wired setup were completed, the electrodes were connected to the wireless device. The wired system was used to apply the stimulation pulse trains while the wireless device applied the triangle pulse waveform and recorded the resulting current pulses.

3.2.9 Freely-Moving Animal Recordings

Animals were handled each day after their arrival. On the day of recording the rat was dressed in the back pack containing the wFSCV device, but the electrodes were initially connected to the wired head stage amplifier and stimulation output. The wired system was used to position the carbon fiber microelectrode into a region of the dorsal striatum with the highest electrically stimulated DA release. Once this location was found, the electrodes were switched to the wireless system. During experiments where food was presented, a video recording system was used to record the animal's behavior and to mark the time points at which the animal was eating. The animal's overall activity level was also noted.

3.2.10 Data Analysis Methods For Wireless Recordings

Data of electrically and chemically evoked DA release was analyzed as described in Chapter 2 using a program written in IGOR Pro Software. The raw current data was digitally filtered with a 1 or 2 kHz Kaiser-Bessel filter in Igor software. Background pulses were selected from the time point shortly before artificial stimulation began. An average of 10-20 background pulses was subtracted from an average of 5-10 signal pulses in the generation of conventional cyclic voltammogram plots. Color plots were

generated by subtracting the average of 10 background pulses from each individual pulse of the recording, and then plotting the background subtracted signal with respect to time using a color scale as indicated in the figures. Finally, 3-point box smoothing was performed in Igor software. To generate time course plots, the background-subtracted current collected with an applied voltage range associated with peak DA oxidation current was plotted with respect to time. Subsequently, a 5-point moving average was performed for smoothing.

3.2.11 Analysis of Behaviorally-Evoked DA Release

The major data analysis challenge for this study was in the analysis of correlations between DA release and behavior. Behavioral DA signals are often smaller in magnitude and fluctuate slowly over long time scales. While electrically and chemically evoked DA release can take place within a few seconds, behaviorally evoked DA release in reward seeking behaviors extend over much longer time scales. We acquired 4 minute long recordings in the measurement of behaviorally evoked DA release. During a 4-minute time period, electrode drift and subtle changes in the CFE background signal shape can take place. Voltammetry is very sensitive to small changes in the shape of the current signal because the signal of interest is very small compared to the total size of the current pulse. Therefore, special methods were developed to identify long-term behavioral DA signals.

Whenever behavioral recordings were collected, a video was taken of the animal. A sign presented in front of the video camera marked the time at which the wireless FSCV

recording started. In this way, correlations between a behavior of interest observed in the video recording and neurotransmitter signals in the wireless voltammetric recording can be studied.

The difference voltammograms produced by behaviorally evoked DA release are expected to have the same shape and position of the DA oxidation peak as those produced by electrically and/or chemically evoked DA release in the same animal using the same electrode. Therefore, a color plot of the recording during which the animal exhibits reward-seeking behaviors or any behavior potentially associated with DA release is generated. Initially, a reference signal (background voltammogram) is chosen at a time point where no reward seeking behaviors were observed in the video, or at a time point shortly before reward seeking behaviors began. If the reference signal happens to be selected from a time point where the DA concentration is not at its minimum, then time points of lower DA concentration will appear as inverted voltammograms (lower, more negative background subtracted current at the oxidation peak voltage and possibly higher, more positive background subtracted current at the reduction peak voltage). In this case, background voltammograms around the time point of the lowest oxidation current measurement are chosen as the new reference signals.

The color scale is chosen such that DA oxidation peaks become visible. Subsequently, conventional cyclic voltammogram plots are generated for the time points at which DA-like signals appear. The shapes of these cyclic voltammogram plots are compared to

the cyclic voltammogram plots generated from artificially evoked DA release. The position of oxidation peaks are expected to occur at about the same voltage, and to have a similar shape, though likely a different magnitude.

To generate time course plots of DA release, the same averaged background voltammogram is subtracted from each individual signal pulse. The magnitude of the signal averaged over an applied voltage range associated with peak DA oxidation current is plotted after smoothing the time course with a 5 point running average. In wireless data, there may be outlier points from transmission errors that stand out among the other data points. A simple programming script scans the data to detect data points that deviate more than a few standard deviations from other neighboring points, and replaces those points by an interpolated value.

FSCV recordings collected when the animal exhibited no behavior of interest were analyzed in the same way generating color plots with the same color scale as that used for recordings showing DA release.

3.3 *In Vivo* Experimental Results

The results shown below demonstrate the functionality of the wFSCV device for measuring *in vivo* electrically evoked DA release, drug-evoked DA release and behaviorally evoked DA release. To test the wFSCV device, recordings taken with the wFSCV device were compared to recordings taken with a conventional wired FSCV setup, both during experiments with anesthetized animals and during experiments with

a drug that induces DA transients in awake animals. In each case (except Figure 3.10), the wired and wireless setups were used to collect recordings from the same rat with the same electrode in the same experimental session.

3.3.1 DA Release in an Anesthetized Rat in Response to Electrical Stimulation

Figure 3.3 compares the measurement of electrically evoked DA release using the wireless device to that with a conventional wired recording setup. The color plots generated from the data recorded with the wired setup (A) and from the data recorded with the wireless setup (B) indicate DA oxidation peaks at similar voltages. Both the wired and wireless setups show a very similar time course of DA release where the DA signal quickly reaches a peak and decays back to baseline over a time scale of a few seconds (Figure 3.3C,D). The difference voltammograms obtained at the times where the DA currents reach their respective peak values both show a DA oxidation peak at an applied voltage of ~700 mV with a magnitude of ~8 nA (Figure 3.3E,F). The increased noise in the wireless recording was attributed mostly to noise generated by wireless transmission and partly to Johnson noise from the lower feedback resistor of the current-to-voltage converter in the wFSCV device compared to the wired FSCV setup.

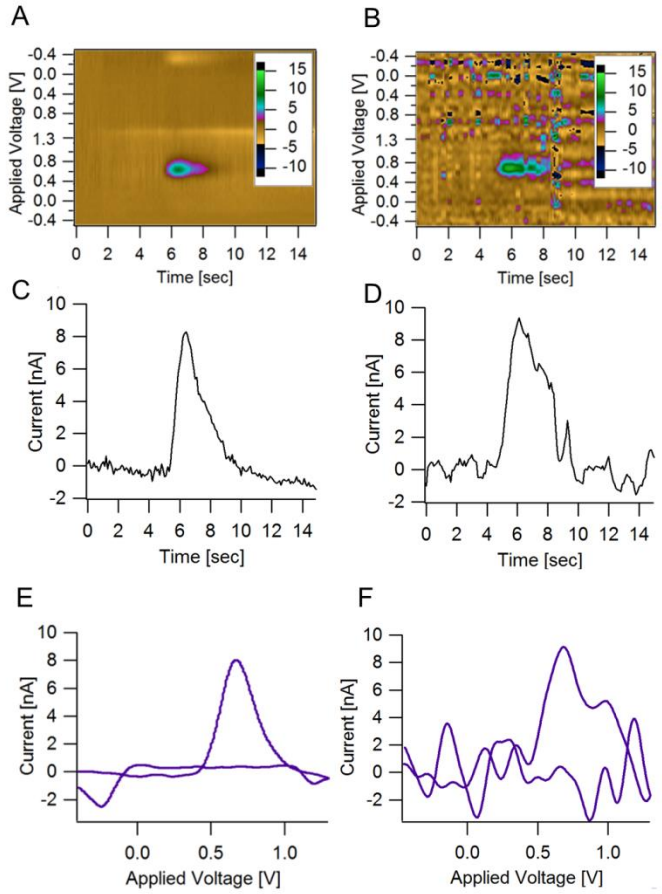

Figure 3.3: Wired (left) versus wireless (right) voltammetric data of electrically evoked DA release in an anesthetized rat. Color plot generated from the wired recording (A) and wireless recording (B) with stimulation aimed at 5 s. Rather than averaging multiple cyclic voltammograms, the color plot was generated from individual signal pulses, followed by 3-point box smoothing in Igor software. Time course of DA release and reuptake from wired recording (C) and wireless recording (D). A moving average of 5 signal pulses was used. Cyclic voltammogram generated with wired setup (E) and wFSCV device (F).

3.3.2 DA Release in a Freely Moving Rat After Drug Administration

Figure 3.4 shows wired and wireless recordings form an awake and freely moving rat under the influence of a drug that increases the occurrence of DA transients in the absence of electrical stimulation. The drug cocktail consisted of a mixture of raclopride (2 mg/kg body mass) and GBR 12909 (15 mg/kg body mass) injected into the

peritoneum. Raclopride blocks D2 receptors, which are autoreceptors that inhibit DA release upon binding. Therefore, blockage of this receptor leads to disinhibition of DA release. GBR 12909 blocks the DA transporter, which is important for DA reuptake (Venton and Wightman, 2007). Recordings began at least 20 minutes after administration of the drug cocktail. First, recordings were performed with the wired setup. Once DA transients were detected with the conventional wired setup, the rat was switched to the wireless recording setup. Wired and wireless recordings were approximately ten minutes apart.

Drug-induced DA transients are smaller in magnitude than electrically evoked DA transients. Nonetheless, the drug-induced DA transients (Figure 3.4C,D) seem to follow a similar time course as the electrically evoked DA transients in both the wired and wireless recordings. In addition, the wired and wireless recordings yield voltammograms of very similar shape (Figure 3.4E,F), indicating that they are reporting the same electrode signal. However, the magnitude of the difference voltammogram is much larger in the wireless recording, perhaps due to the fact that DA transients can vary in magnitude throughout the one hour time period that the rat is under the influence of the drug cocktail. It is, however, also possible that the amplitude of the DA transients in the wired recordings are suppressed due to reduced pleasure in the wired situation.

Both the wired and wireless recordings show a DA oxidation peak at an applied voltage of slightly above +1V (Figure 3.4E,F), which is higher than what would be expected for a DA signal. Such shifts in the DA oxidation signal to higher, more positive voltages

sometimes occur during recordings in live animals, and are thought to be caused by alterations in the electrochemical properties of the reference electrode after implantation into the brain (Bott, 1995). The similar shift evident in the wired and wireless recordings is consistent with it being due to drift in electrode properties.

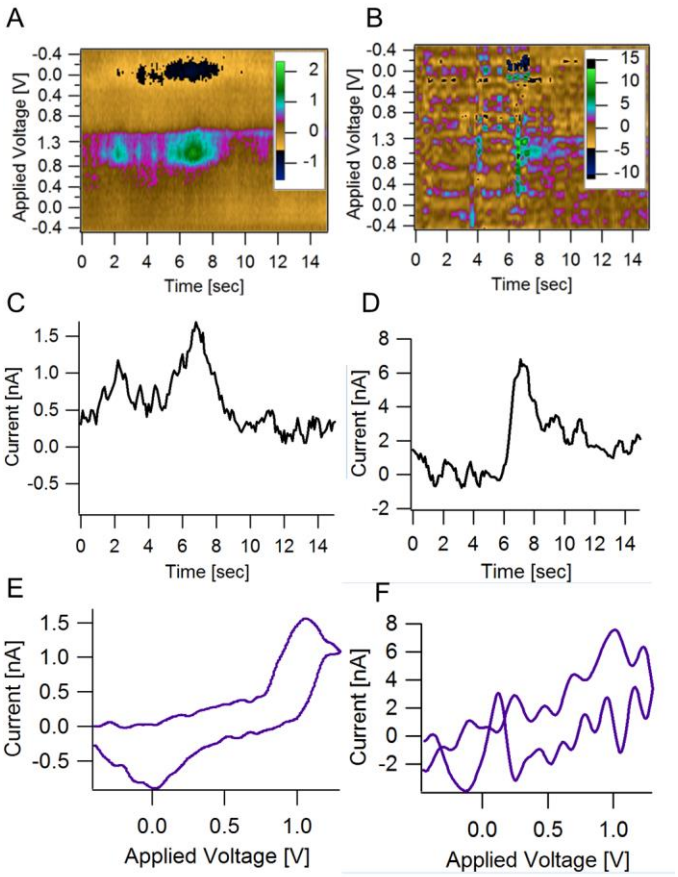

Figure 3.4: Wired (left) versus wireless (right) voltammetric data of drug-evoked DA release in an awake behaving rat (A) Color plot of DA transients from wired setup (B) Color plot of DA transients from wireless device (C) Time course of the DA transient generated from wired setup (D) Time course of the DA transient generated from wireless device (E) Cyclic voltammogram of a DA transient generated with wired setup (F) Cyclic voltammogram of a DA transient generated from wireless device.

Figure 3.5A shows DA transients that were observed prior to the rat's exposure to the drug cocktail. Since the recording is from the same rat with the same electrode as in the recording of Figure 3.4, the difference voltammogram has roughly the same shape as in

Figure 3.4. The similarities between the cyclic voltammogram plots of Figure 3.5B (wireless device) and Figure 3.4E (conventional wired setup) confirms that the wireless device collected a true DA signal in the absence of stimulation.

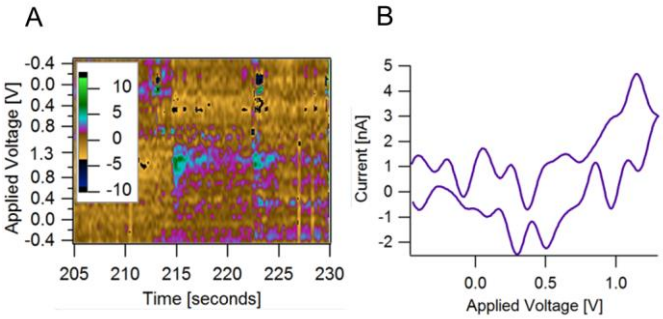

Figure 3.5: Wirelessly recorded DA transients in the absence of electrical stimulation, drugs and reward, illustrated in a color plot (A) and voltammogram at time 215 seconds (B). Compare to a conventionally recorded DA voltammogram generated in the same rat with the same electrode when the rat is under the influence of the raclopride-GBR 12909 cocktail (3.4E).

3.3.3 Behaviorally Evoked DA Release

Unlike in previous applications of wireless FSCV devices, we proceeded to demonstrate our device functionality on the measurement of behaviorally evoked DA release in the absence of electrical and chemical stimulation. The ability to measure behaviorally evoked DA release is important for obtaining an insight into the patterns of DA release in different forms of behavior and at different parts of the brain under natural conditions.

As discussed in the methods section, the first step in the identification of behaviorally evoked DA release is to examine the electrically evoked signal from the same rat with the same electrode. Figure 3.6 shows electrically evoked DA release from an awake rat that exhibited reward seeking behavior later on the same day while moving freely in the cage. It appears that the DA molecules released at ~165 seconds were adsorbed at the

electrode surface, causing the DA signal to be sustained (Figure 3.6A,B). Nonetheless, the difference voltammogram (Figure 3.6C) indicates a DA oxidation peak at +520 mV for this electrode in this particular rat, which is in the expected voltage range.

Figure 3.7 shows data recorded the same freely moving rat with the same electrode as in Figure 3.6. The rat began eating at ~85 s and continued eating until ~170 s. The rat began eating again at around the 210 second time point and continued eating for the remainder of the recording. Figure 3.7A shows DA-like oxidation peaks around +520 mV during the time that the rat was found to be eating in the video. Figure 3.7B shows the time course of DA current during the recording. A large increase in current at +520 mV appears more than 30 s before the rat began eating. To investigate whether this change reflects a change in DA concentration, time course plots were generated for background subtracted currents collected at a range of applied voltages *not* characteristic of DA oxidation or reduction. Figure 3.7C1-2 show such time course plots for applied voltages ranging from -0.25 to +0.25 V during the oxidation ramp (Figure 3.7C1) and +0.75 to +0.25 V during the reduction ramp (Figure 3.7C2). If the observed signals were due to DA release, then such increases in background subtracted current are expected to be evident mainly at applied voltages associated with DA oxidation. Both Figure 3.7C1 and 3.7C2 show little change between 20 s and 60 s, the time period during which the main change in current at +520 mV occurred (Figure 3.7B). Due to an increase in the currents shown in Figure 3.7C1 and 3.7C2 later in the recording the significance of current changes at +520 mV beyond 60 s is uncertain.

Figure 3.8 shows difference voltammogram plots from various time points in the recording during which the rat was eating. At around 20 s into the recording, a DA voltammogram is already visible, with an oxidation peak at about the same applied voltage as that observed in the electrically evoked DA recordings of Figure 3.7. The magnitude of the DA oxidation peak increases after the rat begins eating, indicating that DA release may begin in anticipation of the reward, and continue while the reward is present. The voltammogram collected at the 220 s time point does not resemble a DA voltammogram, suggesting a possible decline in DA release.

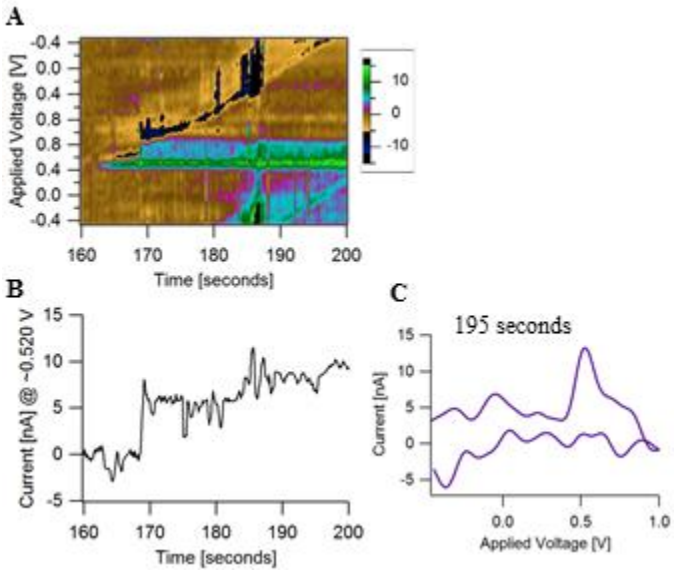

Figure 3.6: (A) Color plot of electrically evoked DA release in a live awake rat. DA molecule adherence to the electrode caused the DA signal to persist through the remainder of the recording. (B) Time course of DA release, 5-point running averaged (C) A sample DA voltammogram, showing a peak at roughly +520 mV (range 471-569 mV). The difference voltammogram was obtained after averaging 5 signal pulses and subtracting 10 background pulses.

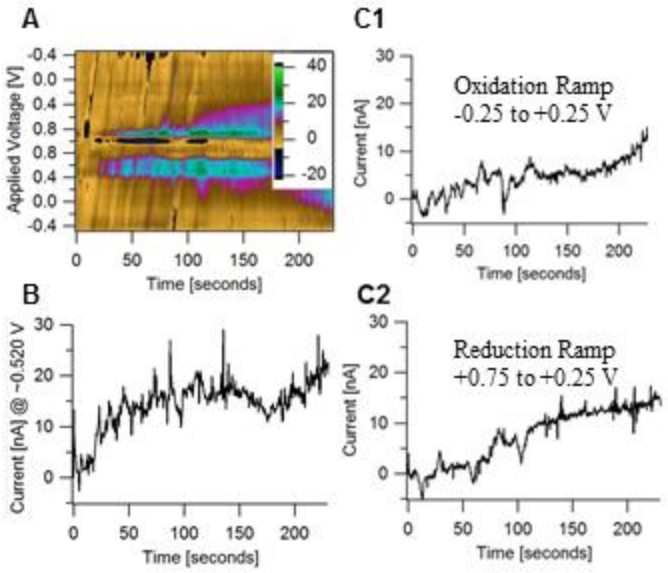

Figure 3.7: (A) Color plot generated from a recording during which the rat was eating, color scale in nA. The rat began eating at around 85 seconds after the start of the recording, and continued eating until around 170 seconds. (B) Time course of DA oxidation current at an applied voltage around +520 mV (range 471-569 mV). (C1-2) Time course of background subtracted current averaged over applied voltage ranges at which neither DA oxidation nor DA reduction occurs.

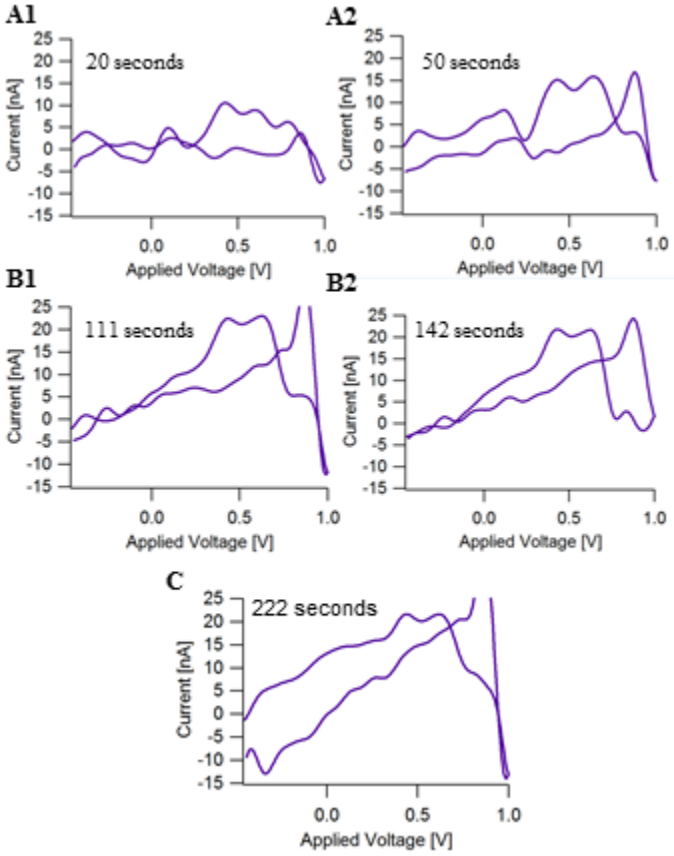

Figure 3.8: Cyclic voltammogram plots from the recording of Fig. 7. DA signals become visible at around 18 seconds into the recording. (A1-2) Cyclic voltammograms from the beginning of the recording before the rat began eating. (B1-2) Cyclic voltammograms from the middle of the recording during which the rat was eating. (C) Cyclic voltammogram from the end of the recording during which the rat began eating again. All cyclic voltammograms were generated by averaging 5 signal pulses from the time point of interest and 10 background pulses from the beginning of the recording at the 4 seconds time point.

3.3.4 Cumulative Histogram Plot of Behaviorally Evoked DA Release

Behaviorally evoked DA release may not necessarily lead to sustained changes or single transient changes, but it could generate rapid fluctuations. In an attempt to obtain evidence for such fluctuations, we generated cumulative histogram plots from time course data shown in Figure 3.8B. In general, a time period during which DA release fluctuates is expected to yield a cumulative distribution plot with a gentler slope, indicating a wider spread over a larger range of oxidation peak current values as compared to a period where DA concentration is approximately constant, yielding a cumulative distribution plot with a steeper slope and a narrower range of oxidation peak current values. The slopes of these cumulative distributions are independent of the choice of the reference background voltammogram.

Figure 3.9 shows cumulative histogram plots of the DA oxidation current shown in Figure 3.7B for different time periods. A sigmoidal fit was performed in Igor software using the equation.

$$Y = Y_0 + \frac{M}{1+e^{(I-I_{1/2})/R}} \quad (1)$$

where Y_0 represents the baseline while M represents the magnitude of the sigmoidal function. $I_{1/2}$ represents the median DA current and R the steepness of the sigmoidal fit,

which decreases with a steeper slope and increases with a gentler slope. The parameter R therefore increases and decreases with increasing and decreasing DA concentration fluctuations, respectively. Figure 3.9A shows cumulative distribution functions generated from time intervals shortly before the rat began eating (50-85 seconds), during the time that the rat was eating (85-170 seconds) and shortly after the rat finished eating (170-210 seconds). The value of R is similar for all 3 curves, suggesting that fluctuations in DA concentration do not change significantly, or may be masked by slow changes over the time intervals analyzed.

To investigate whether anticipation of food increases DA fluctuations shortly before eating, cumulative distribution functions were generated for 20 s time intervals (Figure 3.9B). Figure 3.9C shows R from 20-second time intervals throughout the recording. The overall trend shows an increase in R shortly before a reward-seeking behavior such as eating begins, indicating an overall increase in DA concentration fluctuations. Conversely, R seems to decrease during eating. The results suggest that DA fluctuations are increased in anticipation of food consumption and decrease during food consumption.

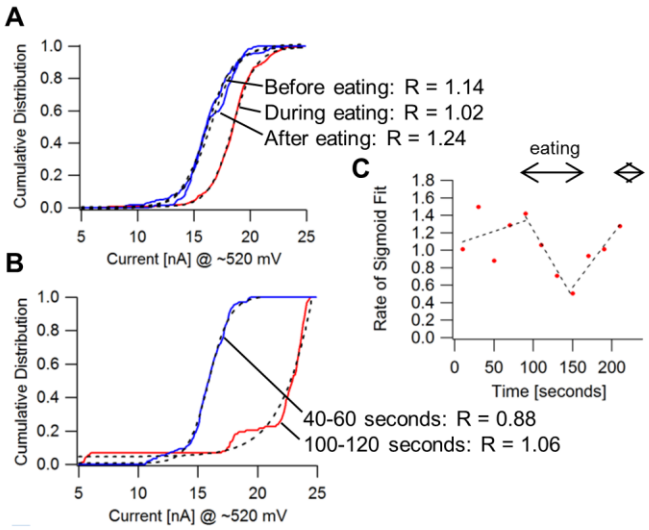

Figure 3.9: Normalized cumulative distribution functions of background-subtracted oxidation current at an applied voltage associated with DA oxidation. (A) Cumulative histograms from a recording during which the rat began eating at 85 seconds, stopped eating at 170 seconds, and started eating again at 210 seconds. Cumulative distribution functions are shown in red when the rat was eating and blue when the rat was not eating. The sigmoid fits to the cumulative histograms are shown as black dashed lines. Sigmoidal fit results yielded before eating (50-85 seconds) $I_{1/2}$=16.16, R=1.14; during eating (85-170 seconds) $I_{1/2}$=18.42, R=1.02; after eating (170-210 seconds) $I_{1/2}$=16.47, R= 1.23 (B) cumulative distribution function from data collected over 20 s time intervals. (C) Time course of rate parameter R from 20-second time intervals throughout the recording. Before the rat began eating, the rate of the cumulative histogram for each 20 second time interval increased at a rate of 0.182 per minute. During eating, the rate decreased at a rate of -0.927 per minute. After eating, and before eating again, the rate increased at a rate of 0.717 per minute.

Figure 3.10 shows three subsequent 240 s long recordings from another rat. The rat began eating fruit-flavored food pellets about 20 s after the start of the first recording, and continued eating the food pellets for the remainder of that recording interval (Figure 3.10 A,B). Figure 3.10A shows a distinct green cluster at ~600 mV from 20 s to 130 s, indicating an increased DA concentration during this time interval. Since the rat began eating at 20 s, this increase in DA concentration in the caudate-putamen may be related to the reward phase. Figure 3.10B shows the time course of the current amplitude at +575 mV, which indicates an increase in DA concentration in the caudate-putamen in

the beginning as well as considerable fluctuations in DA concentration. From about 140 to 195 seconds, the signal shape was temporarily altered, perhaps due to some other temporary change in electrode properties. This alteration in the shape of the current pulse is also evident in the color plot (Figure 3.10A) at all applied voltages. The transient drop in current during this time (Figure 3.10B) is therefore not attributable to a drop in DA concentration.

During the second recording (Figure 3.10 C,D), taken ~10 minutes later, the rat had lost interest in the remaining food. The rat was no longer eating, but was actively moving around the cage. During this phase DA concentration was low and fluctuations were absent (Figure 3.10D). During the third recording (Figure 3.10 E,F), the rat sat still in the cage for most of the recording interval, with some increase in motor activity at the very end. Figure 3.10F suggests that the resting phase may be associated with a small increase in DA concentration, with rapid fluctuations.

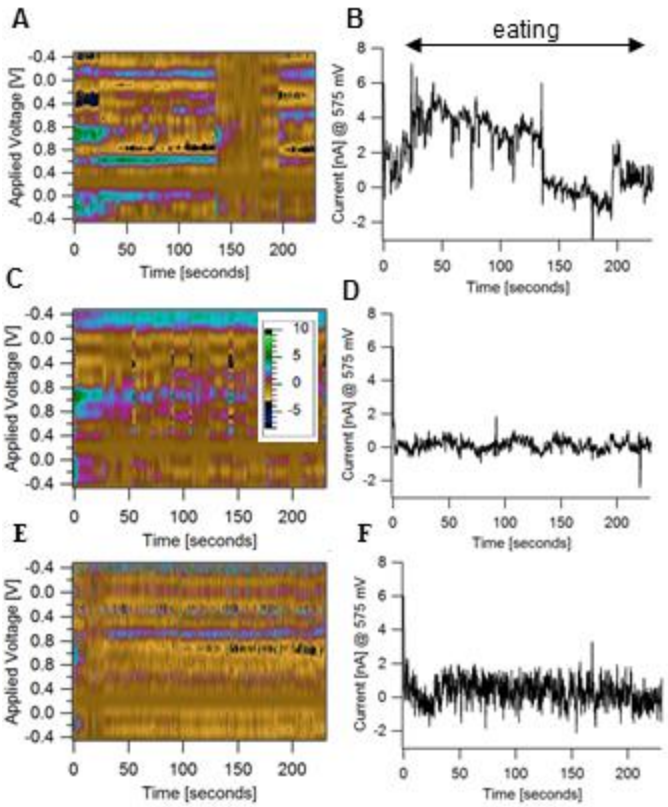

Figure 3.10: Color plots of the background-subtracted currents from 3 subsequent 4 minute recordings (A,C,E) and time course of currents at +575 mV (B,D,F). The rat began eating ~20 s after the start of the first recording (A,B), and continued eating almost until the end of this recording.

3.4 Discussion of *In Vivo* Experimental Findings

In this work we have demonstrated the utility of a simple Bluetooth-based wireless device for the recording of neurotransmitter release in live animals using FSCV. In anesthetized rats, we showed that the wFSCV device reports changes in cyclic voltammograms in response to electrically evoked DA release that are very similar to those recorded with a conventional wired setup in the same animal on the same day with the same electrode. Color plots from wireless and wired recordings show oxidation current peaks located at about the same applied voltage, and time course plots of DA oxidation current show a similar magnitude and time course. Cyclic difference

voltammograms are similar in shape and magnitude. In live ambulatory rats, we showed that the wFSCV device can record chemically evoked and behaviorally evoked DA release. Although behavioral DA release data is more difficult to characterize, we have demonstrated techniques that can be used to distinguish DA current signals from signal artifacts. In future work, the use of electrodes that are less susceptible to electrode drift on the minute time scale may give more stable recordings, aiding in the analysis of time course and magnitude of neurotransmitter release under natural behavioral conditions.

3.4.1 Limitations

The wFSCV color plots and voltammograms show more noise than the corresponding plots generated by the wired recording. The wFSCV device is lower power and a lower feedback resistance must be used to prevent saturation of the CFE signal. In future work, design of a FSCV device that subtracts capacitive current before conversion to a voltage could resolve this tradeoff between low power and SNR.

3.4.2 Relevance to Future Work

Observations of natural animal behavior during a neurophysiological recording experiment can help to elucidate the neurobiological underpinnings of animal behavior. When studying the inner chemical and electrical signaling during natural forms of behavior, wireless technology provides a valuable tool for making recordings less invasive because it abolishes the need for cables and wires. As long as the wireless recording device is sufficiently light-weight and compact, the animal can move more

freely and thus behave naturally. An additional advantage of wireless devices is that they require less power and are not subject to signal artifacts caused by mechanical perturbation of wires.

Many wFSCV systems only offer unidirectional wireless transmission. In these systems, the applied waveform is generated in the remote device, often in a microprocessor. Such a setup does not allow the user the flexibility to change the applied waveform during the course of an experiment. Altering the applied waveform would often mean reprogramming a microprocessor chip, whereas here, the waveform is transmitted from the base station computer and can thus be modified easily. A bidirectional wireless setup bypasses the need for the use of microcontrollers, and allows the user to construct the applied waveform in software. The experimenter may choose to apply voltammetric triangle-shaped pulses at one part of the experiment, and then switch to amperometric square pulses at another phase of the experiment. In addition, if the experimenter finds oxidation peaks at very high voltages, the experimenter may increase the magnitude of the applied waveform during the experiment. It is also easily possible to reduce current amplitudes by reducing the scan rate.

3.4.3 Applications in the Study of Reward-Seeking Behaviors

Wireless technology is useful in the study of reward-seeking behaviors and various behavioral aspects that involve pleasure. When animals eat or copulate, the sense of pleasure may be compromised when wires are protruding from the top of their heads, or when heavy devices are being placed on them. Compact and light weight wireless

technology allows studies of DA release while the animal is engaging in rewarding behaviors in an uninhibited fashion. Although further experiments will be needed to determine whether DA signals differ significantly between wired and wireless recordings, the preliminary results indicating a difference between DA current amplitude in the wired and wireless recordings of Figure 3.4 suggest that this may well be the case.
In experiments with freely behaving animals using the wFSCV device we found preliminary evidence that DA concentration and its fluctuations may increase in anticipation and during the early phase of food consumption. This pattern is consistent with the previous finding that on the short time scale, when a light signal indicates availability of sucrose, a DA transient occurs within 0.2 s, before sucrose has actually been received and declines over the next few seconds (Roitman et al 2004).

A variety of pathological conditions can be studied using the wFSCV technology. One example is the correlation between DA release in the striatum during eating behaviors and obesity. Midbrain DA neurons have been found to play a role in the overconsumption of palatable food (Meye and Adan, 2013). (Baik, 2013) presents a review paper discussing the role of DA signaling pathways in food addiction. Specifically, it was found that food addiction and drug addiction both involve the nucleus accumbens (Hernandez and Hoebel, 1988) and reduced expression of D2 receptors. The technology we demonstrate here could help in exploring the connection between abnormal eating behaviors and abnormalities in DA release versus DA receptor expression.

3.4.4 Applications in the Study of Motor Diseases

When studying diseases of neuromotor control, researchers need to be able to observe unrestrained motor behavior in awake freely moving animals during recording experiments. Noninvasive recording methods are important when researchers want to observe the time course of chemical release in the brain during motor behaviors.

The basal ganglia are a set of structures that are important for learning behaviors leading to a positive outcome and unlearning behaviors that lead to a negative outcome (Frank et al., 2004). With the help of compact wireless recording devices, researchers can record basal ganglia chemical signaling when the animal exhibits motivated behaviors in pursuit of a reward and when the animal avoids a negative stimulus like an electrical shock.

Parkinson's disease (PD) and Huntington's disease are two disease states that cause observable motor deficits. Parkinson's disease is associated with abnormally low DA levels in the basal ganglia while Huntington's disease is associated with DA-induced toxicity. In PD animal studies, it is found that up to an 80% reduction in DA availability may be necessary for PD motor deficits to manifest (Hornykewicz, 1968). Could the primary reason be an increase in DA sensitivity as DA becomes less available? Or perhaps animals do not regularly utilize all of the DA that is available during everyday behaviors. To investigate such possibilities, researchers can conduct recording experiments on animals during every-day behavioral tasks. Noninvasive recording

methods enable the recording of DA release in freely behaving animal models of neurological diseases.

3.4.5 Summary of *In Vivo* Work

In summary we have demonstrated the functionality of a wFSCV device for *in vivo* recordings from live freely moving and freely behaving animals. The wFSCV device was validated by comparison with wired recordings from the same animals on the same day with the same electrode. Preliminary results indicate that DA concentration and its fluctuations increase in anticipation of food and during early phase of food consumption. Further studies using the wFSCV device should shed further light on the associations between DA release and eating behaviors.

Chapter 4

Discussion

4.1 DA and Drug Addiction

As has been discussed in Chapter 3, DA signaling plays a role in motor control and motivated behaviors such as eating. However, there are other behaviors that are influenced by abnormalities in DA release and DA availability. Drug addiction is one example of a behavioral abnormality associated with DA signaling dysfunction. Drug addiction is an abnormal motivated behavior in which the addict uses the drug to artificially stimulate areas of the brain that give a feeling of pleasure. While the drug supplies a feeling of euphoria, withdrawal from the drug often causes dysphoria. Researchers are attempting to better understand the mechanisms underlying euphoria during drug use and dysphoria associated with withdrawal. Among the most addictive drugs is cocaine, which blocks DA reuptake (Ritz et al., 1987). (Dackis and Gold, 1985) present a review of DA depletion in cocaine addiction, discussing how blockage of DA reuptake allows more DA molecules to diffuse away before they are endocytosed into synaptic vesicles and recycled. If DA molecules are not recycled, DA can become less available, possibly explaining the dysphoria associated with withdrawal. More recent experimental studies showed a decrease in occupancy of D2/D3 receptors in the ventral striatum, caudate and putamen that was attributed to a higher binding potential and lower endogenous DA levels (Martinez et al., 2009).

DA depletion was found not only in cocaine addiction, but also in addiction to morphine, alcohol and amphetamine (Rosetti et al., 1992). During cocaine and amphetamine

addiction, DA depletion could last for several days after drug exposure. Wireless voltammetry technology can provide a minimally invasive recording environment in which to record from animal models of drug addiction. Researchers can use wFSCV to study not only DA transients during cocaine administration, but also the impact of physiological drug addiction on the time course of DA release in normal behaviors such as eating. One would expect that if drug addiction causes DA depletion, DA release would be lower magnitude than normal in response to natural reward-seeking behaviors. If so, then the DA depletion can explain why cocaine can cause a loss of appetite for food. A study on rhesus monkeys found that when given the choice between cocaine and food, the monkeys always chose cocaine (Aigner and Balster, 1978).

4.2 DA and Sexual Function

DA also plays a role in sexual function (Guiliano and Allard, 2001). In particular, D1 receptor agonists (D'Aquila et al., 2003) and D2 receptor agonists (Depoortère et al., 2009) were found to induce penile erections in animals. Furthermore, DA signaling is involved in motivated behaviors as was described previously, and sexual activity is a motivated behavior. The role of DA release in sexual behaviors can be explored with the help of compact wireless recording technology. Investigations of the chemical signaling underpinnings of unrestrained sexual activity can help to elucidate the time course of DA transients before, during and after copulation.

4.3 Stray DA Transients

Even in the absence of a reward-seeking behavior and artificial stimulation, we found stray DA transients, which have been reported in previous literature (Robinson et al., 2002). The significance of such stray DA transients is still unknown.

4.4 Serotonin and Depression

The wFSCV system can be used to study release of any kind of oxidizable signaling molecule in the brain, including other neurotransmitters. Serotonin, also an oxidizable neurotransmitter, plays a role in depression, which is associated with abnormally low serotonin levels (Coppen and Doogan, 1988). However, wFSCV cannot measure baseline serotonin levels, but rather the kinetics of serotonin release during the recording time frame. Furthermore, changes in serotonin levels often occur over very long time scales on the order of two hours, which are not time scales that are ideal for voltammetry. Nevertheless, (Wood and Hashemi, 2013) used FSCV to find an increase in electrically evoked serotonin release after administration of serotonin reuptake inhibitors, which are used to treat depression. By studying the dynamic changes in serotonin levels after acute administration of the serotonin reuptake inhibitors, the researchers developed a better understanding of increased depression and suicide after beginning antidepressant treatment. In future work, behavioral experiments on depression can offer insight into the link between serotonin depletion and observable depressive behaviors.

4.5 Other Applications of wFSCV

In addition to studying the brain's reward system and motor control system, noninvasive recording methods are important for studying an array of other behaviors involving chemical signaling such as sleep (Siegel, 2004), cognition and neuropsychiatric disorders (Sarter et al., 2006). In all cases, recordings should be collected in a natural behavioral setting for best results.

Cognition and sleep are two areas of study that can benefit from the use of wireless recording methods. Recording of neurotransmitter release throughout the sleep-wake cycle must be noninvasive so that animals can comfortably sleep and move about when awake. Recordings taken during cognitive tasks such as navigation through a maze can become difficult when the animal is connected to cables and wires. Wireless recording technology is useful for allowing animals to crawl wherever they please without something dragging behind them.

4.6 Summary

Wireless voltammetry will continue to be used to study neurotransmitter abnormalities in normal behavior and in diseased states. With ongoing improvements in technology, wireless recording devices are expected to become more compact, more reliable, lower power, and easier to use. More generally, bidirectional wireless transmission will continue to be useful for any remote application where currents are measured in response to an applied voltage waveform.

CHAPTER 5

K-12 Outreach

Cornell's Learning Initiative in Medicine and Bioengineering (CLIMB) is an NSF-funded program that pairs biomedical engineering graduate students with a high school or middle school teacher. During the summer, the graduate student and his/her lab assign a project for the teacher to complete during a six-week period. The summer experience is meant to give the teacher a glimpse of real cutting-edge science research. Some concepts learned from the summer research experience are brought into the classroom in hopes of improving the science curriculum at the teacher's school. The teacher and graduate student work together to form a curriculum for the students in the teacher's classroom throughout the academic year. Students do projects and/or activities that teach them about real-world science and engineering. Learning is inquiry-based where students learn how to design an experiment in order to answer a question. Students learn how to interpret the results of their experiments, and draw conclusions from their findings.

One major objective of the program is to get students excited about pursuing science and engineering careers. Students learn about the fun of following one's curiosity and/or designing a device that performs a useful function. There has been recent talk that not enough American high school graduates are pursuing science and engineering careers. Math and science standardized test scores are lower for American K-12 students than in many other countries. Students may lack confidence to pursue STEM (Science Technology Engineering Mathematics) careers, or they may have false notions

that math-based careers are hard and boring. An aim of the CLIMB outreach program is to improve the math and science curriculum in school districts so that students get a glimpse of the more interesting aspects of STEM careers.

Another major objective of the program is to make teachers more well-informed of science beyond the textbook. Teachers are often unaware of the interdisciplinary nature of science fields, thinking of physics, mathematics, chemistry and biology as separate entities. The summer experience in the graduate student's laboratory allows the teacher to observe researchers from a diversity of backgrounds working together. Biomedical engineering is a great environment for middle school and high school teachers to learn about interdisciplinary research because biomedical engineering is a combination of biology, engineering, physics, chemistry and mathematics. Many labs in biomedical engineering have researchers from different fields of study.

5.1 Summer Project

For the K-12 CLIMB program, I was paired with a high school physics teacher named Deb. Unlike most other science teachers, Deb had some laboratory experience, making it easier for her to learn how to do her summer research project.

The objective of the summer research project was to perform *in vitro* voltammetry experiments on DA release and determine the relationship between the length of exposed carbon fiber and DA oxidation current magnitude. Prior to performing the

experiments, Deb needed to learn about voltammetry theory. (Phillips and Wightman, 2003) provided good introductory information on the basic theory and rationale behind fast-scan cyclic voltammetry. After developing an understanding of the basic theory, Deb learned how to use the Tar Heel voltammetry software. She learned how to change the program settings in order to apply a triangle pulse that sweeps from -450 mV to +1000 mV, and has a time width of 10 ms. She also learned how to use the head stage to connect the recording setup to a carbon fiber electrode and reference electrode. The carbon fiber electrode and reference electrode were both placed in a dish a buffer solution, but at different parts of the dish. To measure DA release, a solution of known DA concentration was squirted in the vicinity of the carbon fiber electrode at a specific time point in the recording interval. After using Tar Heel software to collect data, Deb learned how to use the Tar Heel software analyze the data by subtracting the pulses from two different time points in the recording.

Deb also learned how to fabricate her own carbon fiber electrodes. Deb learned how to use the suction device to suck the carbon fiber into the glass capillary tube. Next, she learned how to use the pipette puller to form a pointed tip. Deb used the microscope to view the carbon fiber protrusion from the glass tip. She learned what a good glass seal looks like versus a bad glass seal in which the glass is broken. Deb used a scalpel to trim the carbon fiber under a microscope until the carbon fiber protrusion length was the desired length. Deb labeled each carbon fiber electrode .based on the length of protrusion of the carbon fiber.

Next, Deb learned how to use buffer solution to make her own DA dilutions. Soon, Deb was able to perform all experiments on her own, provided that she had enough buffer solution. She spent hours at the wired recording setup measuring *in vitro* changes in DA concentrations. One challenge we faced was in detecting smaller changes in DA concentrations. Deb tried to squirt in the DA solution in the exact same way every time, but eventually we determined that we would need to change the entire solution in the dish during the course of the recording so that by the end of the recording, the dish would be all DA solution. In this way, the change in DA concentration during the recording interval would be more precisely known and easier to measure.

Deb ran into some challenges in determining what a DA oxidation peak looks like, and what a mere signal artifact looks like. She learned to make observations of the voltage at which peak oxidation current is observed. If data was too ambiguous, then she would simply not use it and collect more data.

After much work, Deb was able to plot curves of DA oxidation current magnitude and length of carbon fiber protrusion. Deb also plotted curves of DA concentration versus DA oxidation current magnitude for the same electrode. The curves were linear, and contained error bars representing standard deviation.

Deb's work was useful to us in allowing us to predict how much oxidation current to expect from an electrode of a known carbon fiber protrusion length and for a given DA concentration. Because carbon fiber exposure area is linearly proportional to the

electrode sensitivity, the curve of DA oxidation current versus DA concentration will vary from one electrode to the next. Deb's experimental results allowed us to predict how sensitive our carbon fiber electrode is to DA concentration changes based on the length of exposed carbon fiber.

To summarize, Deb learned how to use experimental neuroscience methods to detect the release of DA in an *in vitro* solution. In particular, Deb learned about how to use voltammetry, an electrochemistry technique, to measure the amount of DA release during the recording time interval. Critical assessment of data was important for being able to distinguish a DA oxidation peak from a signal artifact. Furthermore, the magnitude of the oxidation peak often varies from one experiment to the next even when measuring the same DA concentration with the same electrode. A large number of experiments needed to be run to find statistically significant differences in the magnitude of the DA oxidation peak from one DA concentration to the next and from one electrode to the next. Interpretation of the data also was important for determining the dual effect of DA concentration and carbon fiber exposure length on the magnitude of the DA oxidation peak. Deb made calibration plots of DA concentration versus DA oxidation current magnitude for a single electrode, and Deb made plots of carbon fiber exposure length versus DA oxidation current magnitude when DA concentration remained constant. At the end of the summer, Deb learned how to illustrate and present her findings in a poster.

5.2 Curriculum for the Classroom

For the classroom, I put together a series of projects that were easier and more fun than the project for Deb. The projects involved the building and design of simple electronic circuits. Before the students started my curriculum, I gave a lecture to the class that was about half an hour long. The lecture included information on how electronics is used in the real world both among scientists and engineers. Surprisingly, the students in the lower level physics class seemed more interested in the presentation than the advanced placement class. When I discussed this observation with one of my K-12 outreach colleagues, she said that sometimes students in accelerated academic programs are primarily concerned with getting the highest grades rather than in the material itself. Students in lower level classes are not as interested in the highest grades, so that when they take an interest in something that you are teaching, their interest is more genuine.

After listening to the introductory lecture, students would learn how to use a breadboard to build a circuit. The first circuit they build would be a light bulb connected to a battery. Students would experiment with parallel and series resistance by placing the light bulb in series and in parallel with a resistor. Students were asked to observe whether a parallel or series connection makes the light bulb brighter, and why. What if the resistor value were varied? Could the students correctly predict what would happen?

I wanted the students to build amplifier and filter circuits, and probe various parts of the circuit on an oscilloscope. However, oscilloscopes were too expensive for our limited

budget, so one of the biggest challenges was in figuring out what to use as an oscilloscope. One idea was to use the computer's sound port to input and output signals. I downloaded a free software called SoundScope that allows the user to input and output audio waveforms through the computer's sound port. The user can define the shape, frequency and magnitude of the generated waveform. The problem with using the sound port is that the microphone port has AC coupling, which causes overshoots and undershoots in square pulses. This posed a major problem for the RC circuit lab where students apply a square pulse to an RC circuit. Therefore, I had to come up with another solution. The answer was a USB oscilloscope device from Measurement Computing. The USB device is a small box with a series of pins. It is attached to a USB cable that connects to the computer. It comes with software. Unfortunately, the software is limited in what types of waveforms it can generate. Therefore, Audacity software was used as the waveform generator while the USB device was used as an oscilloscope.

To generate input waveforms and probe the outputs of a circuit, students needed to learn how to use three types of software: SoundScope, Audacity and the USB oscilloscope software. In some lab sessions, both SoundScope and Audacity were used so that SoundScope generates the waveform while Audacity generates noise. With this setup, students would learn how to design an RC low pass filter that can filter out noise.

Still another major challenge was that each class was at a different level. Deb taught two advanced placement physics classes and one conceptual physics class for students who wanted to fulfill the bare minimum physics requirement to graduate. My curriculum was less extensive for the conceptual physics class. The conceptual physics class did not build any RC circuits or operational amplifier circuits. These students learned how to use a breadboard to build a simple light bulb circuit discussed in the next section, and they experimented with the Audacity software presented in section 5.2.2.

The sections to follow each present a self-guided tutorial for the high school physics students to follow. The tutorial assigns tasks and asks questions about what observations were made following each set of tasks. At times, students are expected to come up with an optimum low pass filter design that filters out as much unwanted signal noise as possible while still preserving the signal of interest.

5.2.1 Building Resistive Networks with Breadboards

OBJECTIVE

Electronic circuits consist of multiple interconnected components where each component has some degree of resistance to current flow. Circuit analysis methods attempt to determine the voltages and currents across the individual components. The series of simple experiments presented here involves the construction of resistive circuits on a breadboard and observations of how voltage is distributed across a resistive element when the resistive element is in series versus in parallel with other resistors.

Unlike other lab activities that may already exist in the high school classroom, this lab teaches students how to build electronic circuits on a breadboard, which is a valuable skill for both engineers and physicists. In this experimental inquiry-based laboratory activity, students gain an intuitive feel for how resistors in series versus in parallel change the distribution of voltages and currents. Students make observations not only by reading numbers for current or voltage, but also by viewing the change in the visual brightness of a light bulb.

Students will first connect a power supply to a light bulb and watch the light bulb light up brightly. Next, students will place the light bulb in series and in parallel with resistors of known resistance and observe what happens. In the end, students should write up a lab report or have an in-class discussion regarding what they observed and why. Students are expected to know about the meaning of current flow, voltage, electric charge and Ohm's Law. Students also should know how to use a digital multimeter.

Supplies

Each lab station will need one power supply, one or more light bulbs, connection wires, a resistor set, a digital multimeter, light bulb holders and a bread board.

Potential Hazards

Resistors can get very hot when connected to power supplies.

Using a Breadboard

Figure 5.1 shows what a breadboard looks like. They are used for assembling electronic circuits by simply sticking circuit parts into the holes. Figure 5.1 also shows how the holes are connected. Notice that the holes that are along the red and blue lines are vertically connected to each other while the other holes in the middle are horizontally connected to each other.

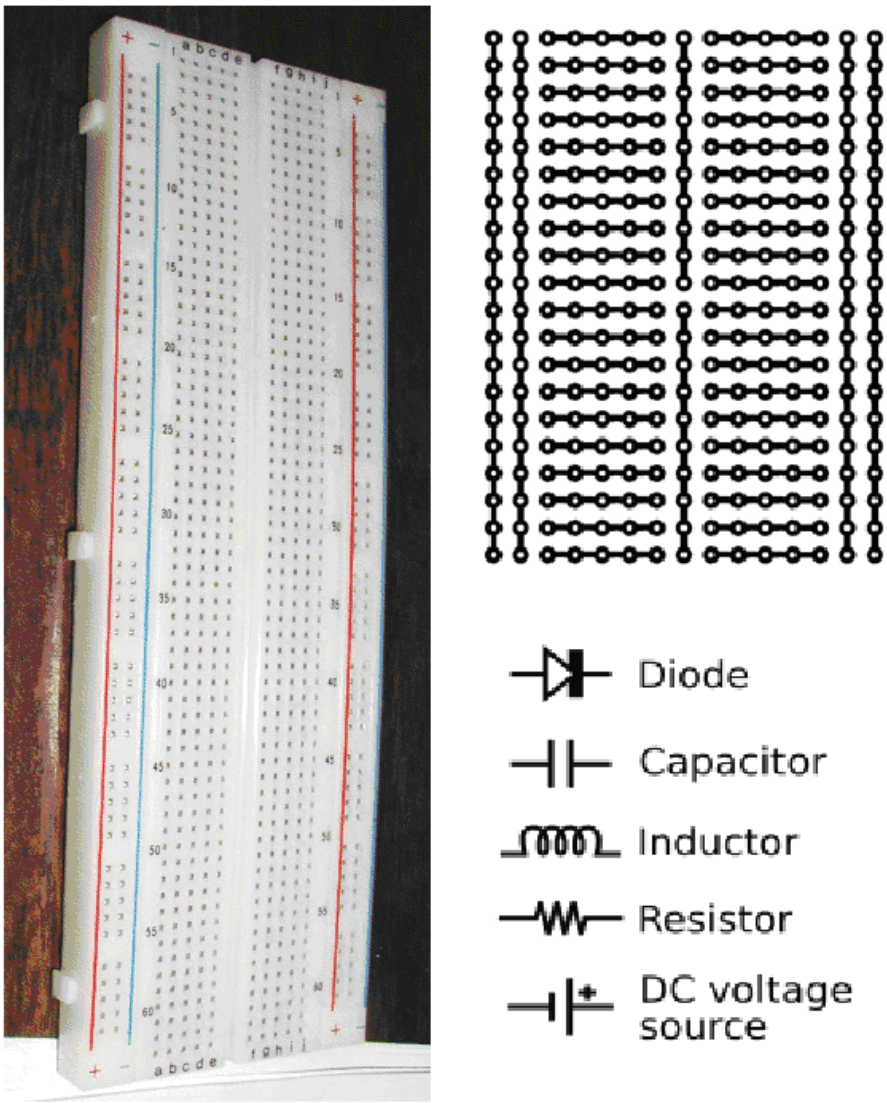

Figure 5.1: (Left) a photo of the breadboard that you will use to assemble your circuits. (Right) an illustration of the connections that exist within the breadboard along with the symbols that correspond to each type of circuit element.

Figure 5.2 shows different ways that we can connect a capacitor, resistor and battery. The blue component you see is a capacitor. The component next to it is a resistor.

Using the symbols in Figure 5.1, see if the students can draw a circuit schematic that corresponds to each set of connections. Two of these sets of connections have something wrong with them. Ask the students if they can tell which ones?

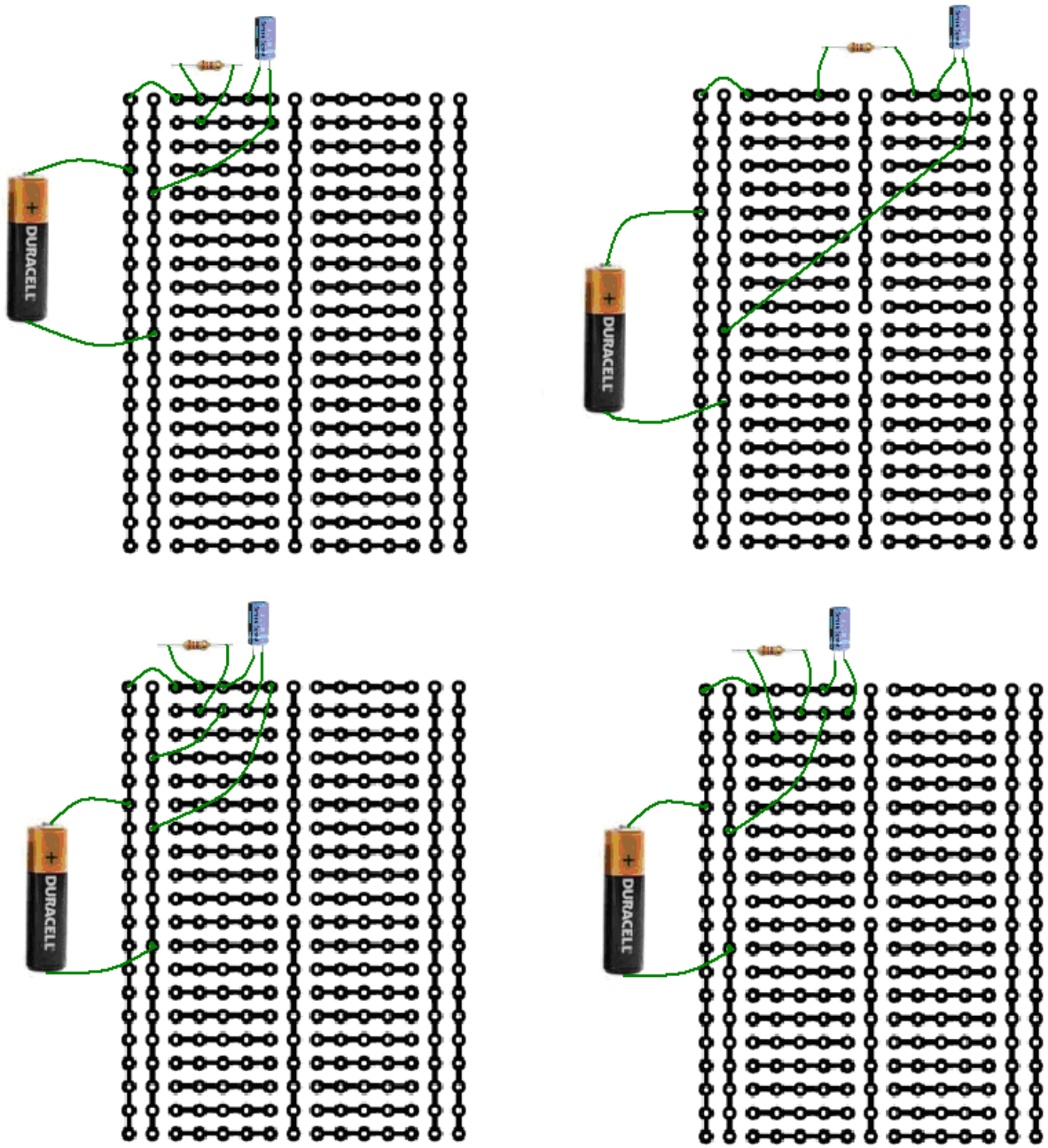

Figure 5.2: These are 4 different sets up connections that one can make between a capacitor, resistor and battery. Have the students write the circuit schematic for each set of connections. The blue component is a capacitor and the other component is a resistor.

Experiment 1: Lighting up a light bulb

You will notice that batteries and power supplies have a '+' end and a '–' end. Figure

5.3 illustrates how to use a voltage source to light up a light bulb. Different light bulbs

have different voltage ratings, so have the students choose a power supply that matches the voltage rating of the light bulb. Warn the students not set your voltage too high in order to prevent the light bulb from burning out.

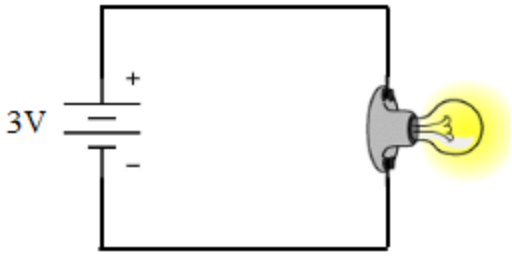

Figure 5.3: First have the students connect the light bulb between the + and – end of your power supply. The side of the light bulb is connected to the + end of the power supply while the bottom tip of the light bulb is connected to the – end of the power supply.

Students can use the digital multimeter to measure the voltage across the light bulb.

Experiment 2: Connecting a light bulb in series with a resistor

Have the students use a digital multimeter to measure the resistance across the light bulb. Next, place the light bulb in series with a resistor that is about the same resistance as the light bulb. Assemble the circuit shown in Figure 5.4 on the breadboard.

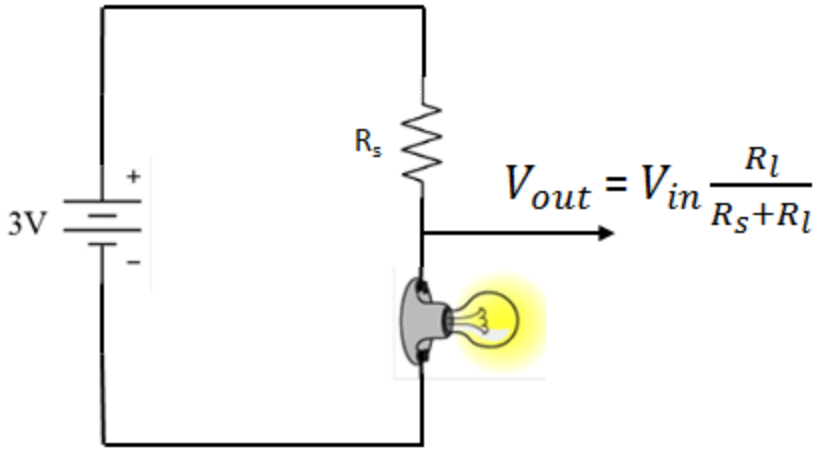

Figure 5.4: This is a light bulb connected in series with a resistor, R_s. R_l denotes the resistance of the light bulb. V_{in} denotes the total voltage applied across the resistive network, and V_{out} denotes the voltage across the light bulb.

Students should observe how brightly the light bulb lights up compared to before, and then record their observations.

Next, students will vary the resistor value to both higher and lower values. Have them observe the brightness of the light bulb each time. Also have them measure the voltage across the light bulb each time, and record the voltage measurement across the light bulb with respect to the series resistance.

Experiment 3: Connecting a light bulb in parallel with a resistor

Now students will place the light bulb in parallel with the same resistor as shown in Figure 5.5. How brightly does the light bulb light up now? Have students record their observations

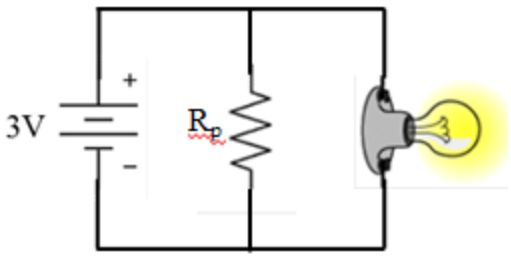

Figure 5.5: Connect the light bulb in parallel with the resistor, R_p

Next, tell students to vary the resistor value, R_p, and record any changes in the brightness of the light bulb.

Experiment 4: Resistors in parallel and in series

Finally, students will experiment with a combination of series and parallel connections. First, students will connect the light bulb in series with one resistor and in parallel with another resistor as illustrated in Figure 5.6. To start, let both resistor values have resistance approximately equal to the resistance of the light bulb.

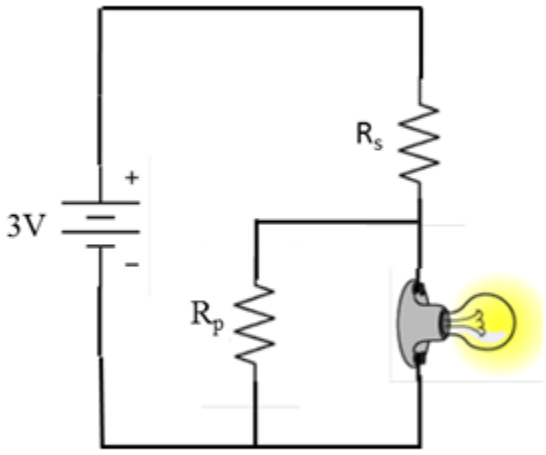

Figure 5.6: Connect the light bulb in parallel with one resistor and in series with another resistor

Students should measure the voltage across the light bulb, and observe the level of brightness of the light bulb. Is the level of brightness closer to what was observed in Experiment 2 or Experiment 3? As students why they think this is?

Next, students can vary the parallel resistance, R_p, to both higher and lower values. Students should record the voltage across the light bulb each time and note the level of brightness.

Finally, students vary the series resistance, R_s, to both higher and lower values, record the voltage across the light bulb each time, and note the level of brightness.

Other Experiments

For more experiments, ask students to try hooking up multiple light bulbs in series and in parallel. Have them measure the voltage across each light bulb each time and note the level of brightness.

Discussion

To ensure that the students have an improved understanding of how voltages and currents are distributed across resistive networks, it is important to have either an in-class discussion or have students turn in lab reports that present their observations as well as the meaning of those observations.

An important take-home message: the series resistance has much more influence over the brightness of the light bulb than does the parallel resistance.

5.2.2 Signal Frequency Spectra with Audacity®

The primary objective of the activity presented here is to allow students to explore the frequency components of various signals. Analysis of the frequency components of a signal allows students to design filters that filter out unwanted components of a signal while conserving the shape and magnitude of the relevant portion of a signal. For example, signal noise is often contained in higher frequency (fast-changing) components whereas signal drift is contained in lower frequency (slow-changing) components of the signal. A low pass filter allows lower frequency components *below* a cutoff frequency to pass through, whereas a high pass filter allows higher frequency components *above* a cutoff frequency to pass through.

Students will use Audacity® software to generate and observe the frequency spectra of various audio waveforms from simple waveforms such as sine waves to more complex waveforms such as voice recordings. In this inquiry-based activity, students will learn what a frequency spectrum says about a signal, and students will learn how to use their understanding of frequency components to design a low pass filter that filters out unwanted signal noise while preserving the signal components of interest.

Audacity® is a sound recording software that allows users to experiment with sound waveforms and their frequency spectra. It is available for free download from the following link:

http://audacity.sourceforge.net/download/

Other supplies necessary for this exercise are a microphone and sound speakers.

Audacity® User Interface

Figure 5.7 illustrates the user interface of Audacity®.

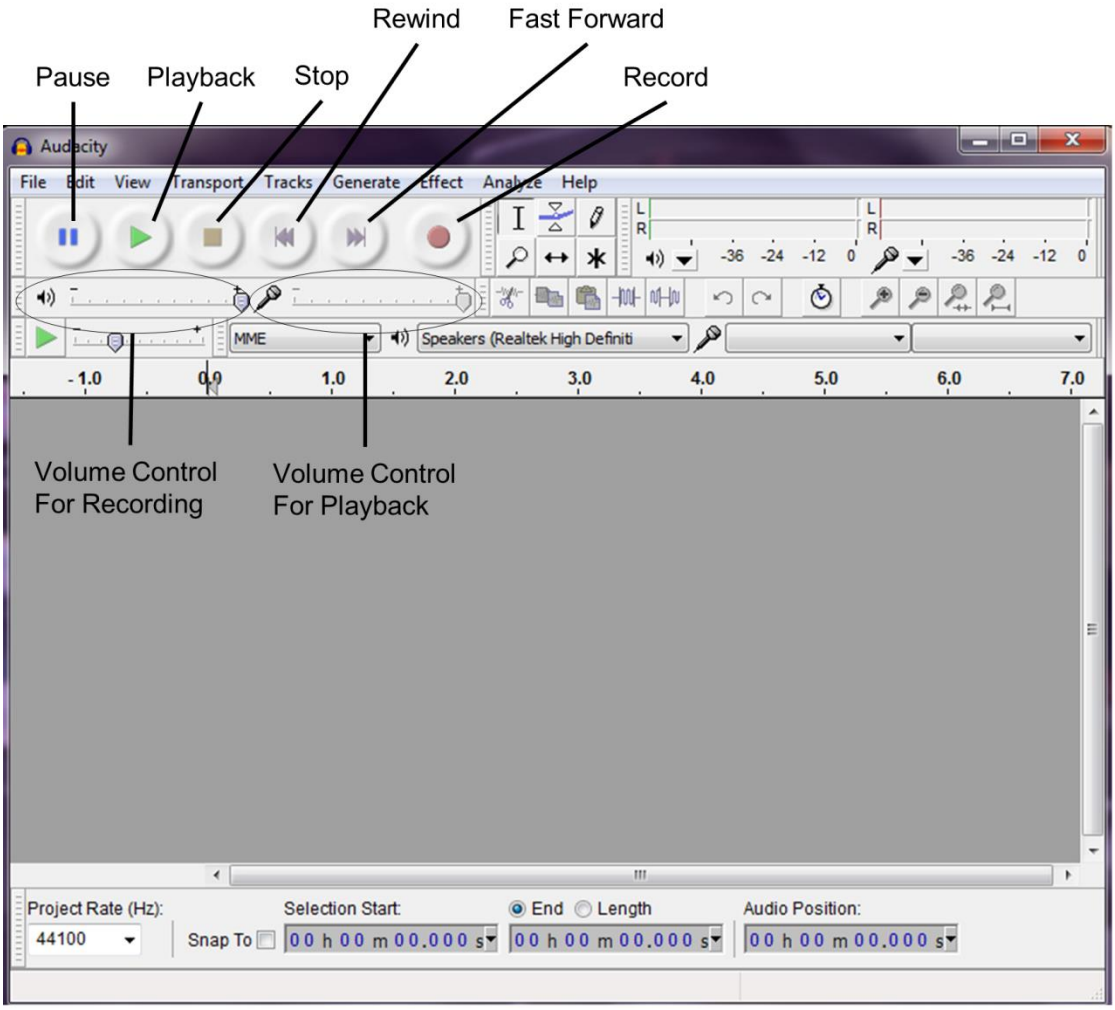

Figure 5.7: Audacity® user interface. The record button starts recording a signal and the stop button stops the recording. The green arrow allows you to play back the signal you just recorded. While playing a sound, you may pause it or click stop to stop playing the signal and start over.

While students are playing a song or speaking into the microphone, they may click the RECORD button to start recording the sound. When students are finished recording, they will click on the STOP button that looks like a square. To play back the sound that was just recorded, students will click on the PLAY button, which has a green arrow. To

stop playing back the song, students will click the STOP button or click PAUSE if they want to stop the playback and then continue playing the recording where they left off.

The volume control for recording determines how much the sound gets amplified when it is being recorded. The volume control for playback determines how loudly a sound is being played.

Generating Different Waveforms

Have students generate a sine waveform and record it. Waveforms can be generated by clicking on the Generate button at the top of the Audacity® window. Select *Tone* from the dropdown menu. A tone generator window will show up. Click on waveform and select *sine*. Click on the text box next to Frequency and type in 5000. Set the amplitude to 1.0. Next to Duration, click on the downward arrow and select *seconds*. Type in 20 seconds. These selections will generate a sine waveform that is 5000 cycles per second at an amplitude of 1 unit for 20 seconds.

Click OK and immediately press the PLAY button. Students should hear a simple tone. If the tone is too loud, reduce the playback volume by clicking and dragging.

Generating a Frequency Spectrum

To generate a frequency spectrum of the sine wave, click on Analyze at the top of the Audacity® window and select *Spectrum*. A window will appear as shown in Figure 5.8

that shows the frequencies contained within your signal. At the bottom of this window, make sure that Algorithm is set to *Spectrum*, and Function is set to *Hanning Window*.

The vertical axis represents amplitude. Note that amplitude is highest at 5000 Hz and is not visible for most of the other frequencies. This is because a sine wave has only one frequency harmonic.

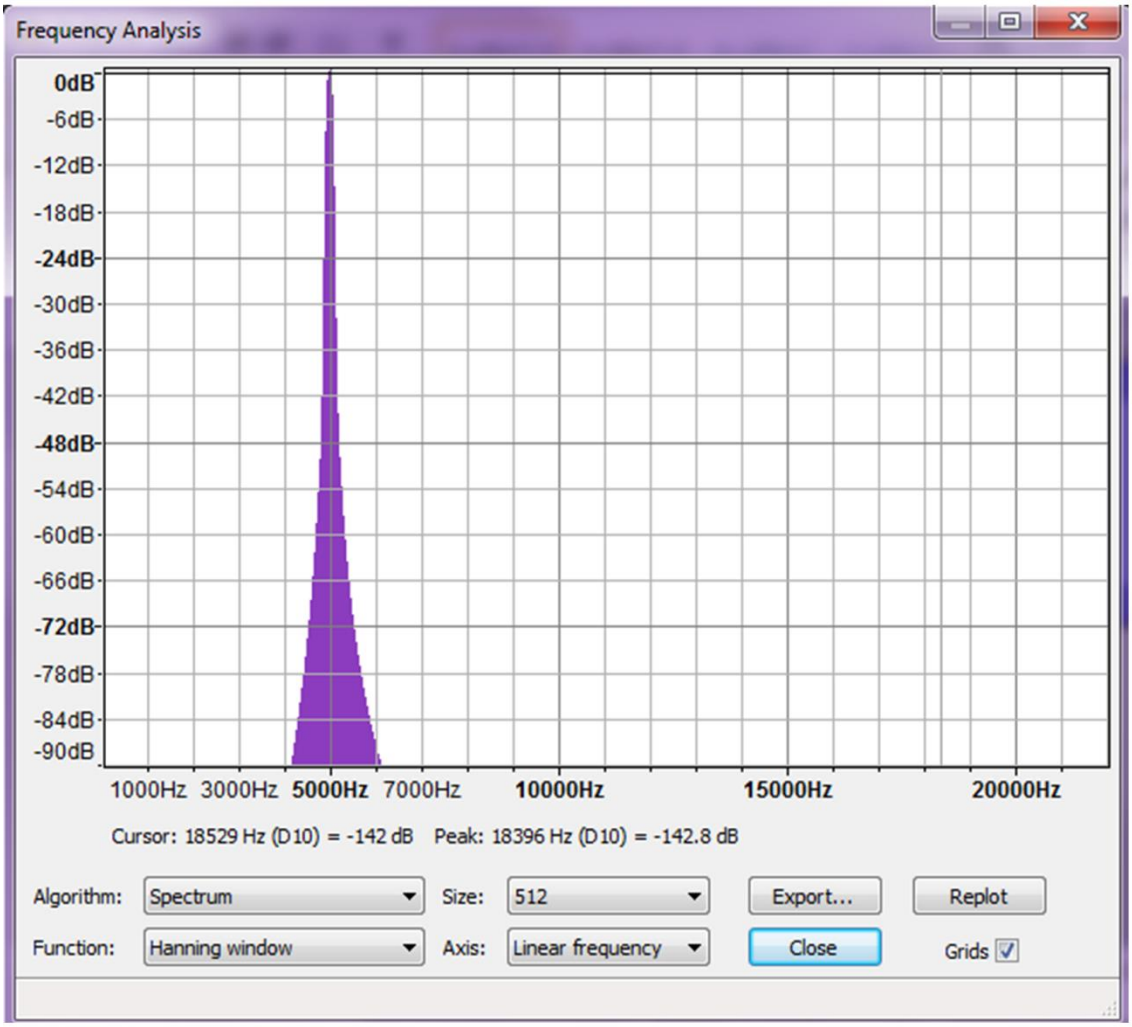

Figure 5.8: The frequency analysis window, which shows the frequency spectrum for a 5000 Hz sine wave. The sine wave has only one frequency harmonic, which is centered at 5000 Hz.

Experimenting with a Different Frequency Sine Wave

Generate another tone as before, only this time change to a different frequency. Click PLAY and listen. Here, students can observe how this sound is different from the previous sound.

Once again, students can generate the frequency spectrum of this new sine wave and observe how the frequency spectrum is different from the frequency spectrum of the first sine waveform.

Experimenting with a Different Signal Shape

Here, students will generate a square waveform. To do so, select square wave as shown in Figure 5.9. Select *Square* next to Waveform. Enter 5000 next to Frequency and make sure the duration is still set to 20 seconds.

Click OK and immediately click PLAY.

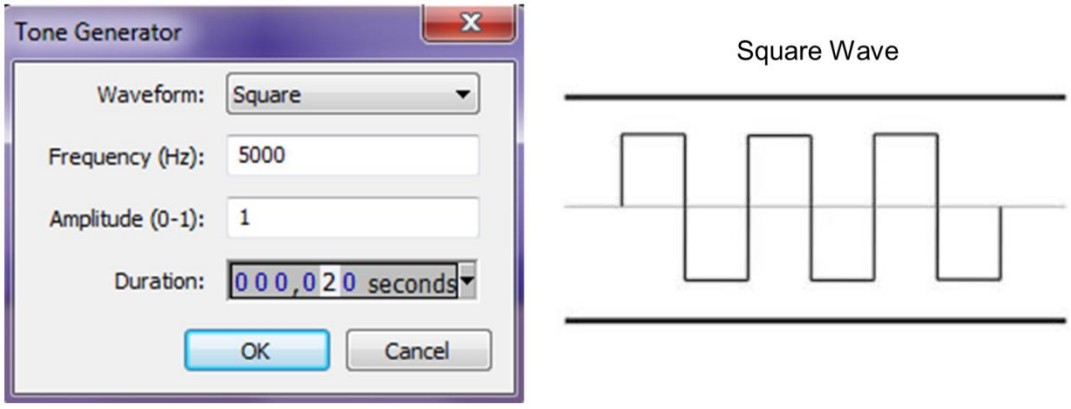

Figure 5.9: Generate a square wave that runs 5000 cycles per second for 20 seconds

Click on the Analyze tab and once again click on *Spectrum*. This time, students should see many different frequencies because the square wave has rising and falling edges. During a rising or falling edge, the signal changes very quickly from low to high or high to low. Fast changing parts of a signal give the signal higher frequencies than the 5000 Hz base frequency.

When students listen to the square waveform, they may notice that even though the square wave is set to the same frequency as the sine wave, it sounds like a combination of tones of variable pitch. This is because a square wave is an infinite summation of sine waves of different frequencies.

Students should keep a record of the frequency spectra that they generate for different waveforms. To keep a record of the frequency spectrum, students can make a screen shot of the frequency spectrum for the square wave. Press the print screen button on your keyboard, and open up Microsoft Paint in the Programs list. After Microsoft Paint is opened, click on Edit and select *Paste*. You should see a picture of the computer screen with the frequency spectrum in it. Save this image for later use.

Changing the Frequency of the Square Wave

Have students generate another square wave of a different frequency. Have students record the sound and then look at the frequency spectrum again. Students can compare the frequency spectrum to the frequency spectrum of the previously generated

square wave. In particular, students can be prompted to record the frequency in the spectrum plot that appears to have the highest magnitude for each of the square waves.

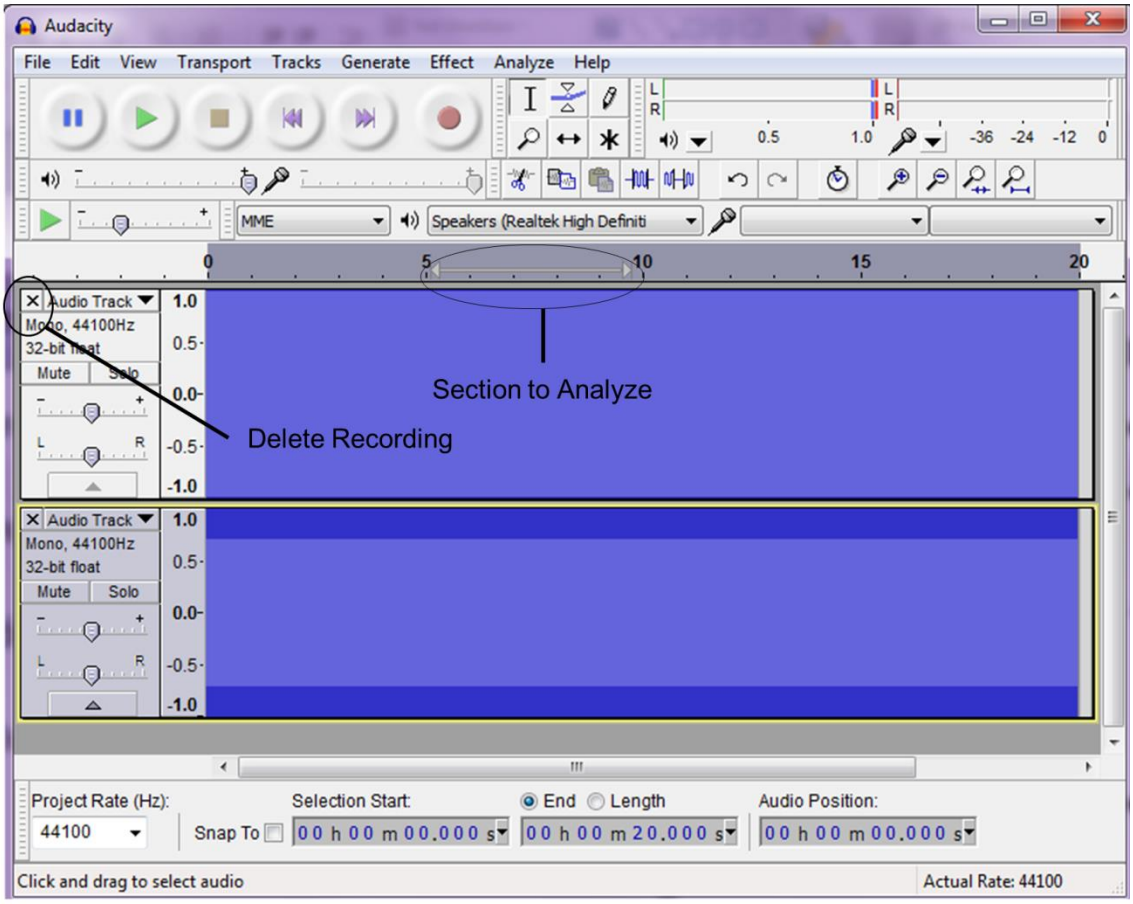

Figure 5.10: Recorded waveforms shown in the Audacity user interface. Because the frequency is 5000 Hz, zooming in is necessary to make out the waveform shape. To analyze a previously recorded waveform, just click on the waveform and drag the mouse. As illustrated above, the section that you are analyzing will be highlighted. You may then click on the Analyze tab at the top. If you want to delete the recording, click on the X at the upper left as shown above.

Experimenting with a Sawtooth Wave

Have students generate a sawtooth wave. A sawtooth wave can be generated by selecting Sawtooth Wave in the Tone Generator window. Set the frequency to 5000 Hz

and make sure the duration is still 20 seconds. Click OK, then immediately click PLAY. Compare how the sawtooth wave sounds compared to the square wave and sine wave. Does it sound higher pitched? Lower pitched?

Students should compare the frequency spectrum of the sawtooth wave to the frequency spectrum of the sine wave and square wave of the same frequency. How does the distribution of frequency harmonics compare to that of a sine wave or square wave? Could differences in frequency distribution explain the differences in the overall sound of the signal?

Voice Recording

The objective of this section is to allow students to record a real-life noisy signal, and learn how to filter out the signal noise. Sometimes in the real world, recordings are difficult because there is noise that can make the signal harder to read. For example, there may be static noise on certain radio stations. Scientists and engineers also have problems with noise when they try to record and analyze signals.

First, students will hook up a microphone to the computer and record their speech. After hooking up the microphone, click RECORD and speak into the microphone. To finish the recording, click STOP. To play back the recording, click PLAY.

After hearing their voices on the recording, students can view the frequency spectrum of the signal that they have recorded. When viewing the frequency spectrum of their

voices, students can observe how this frequency spectrum compares to the frequency spectrum of the simpler waveforms from before, namely sine waves, square waves and sawtooth waves. Figure 5.11 shows an example of a recording of a voice signal.

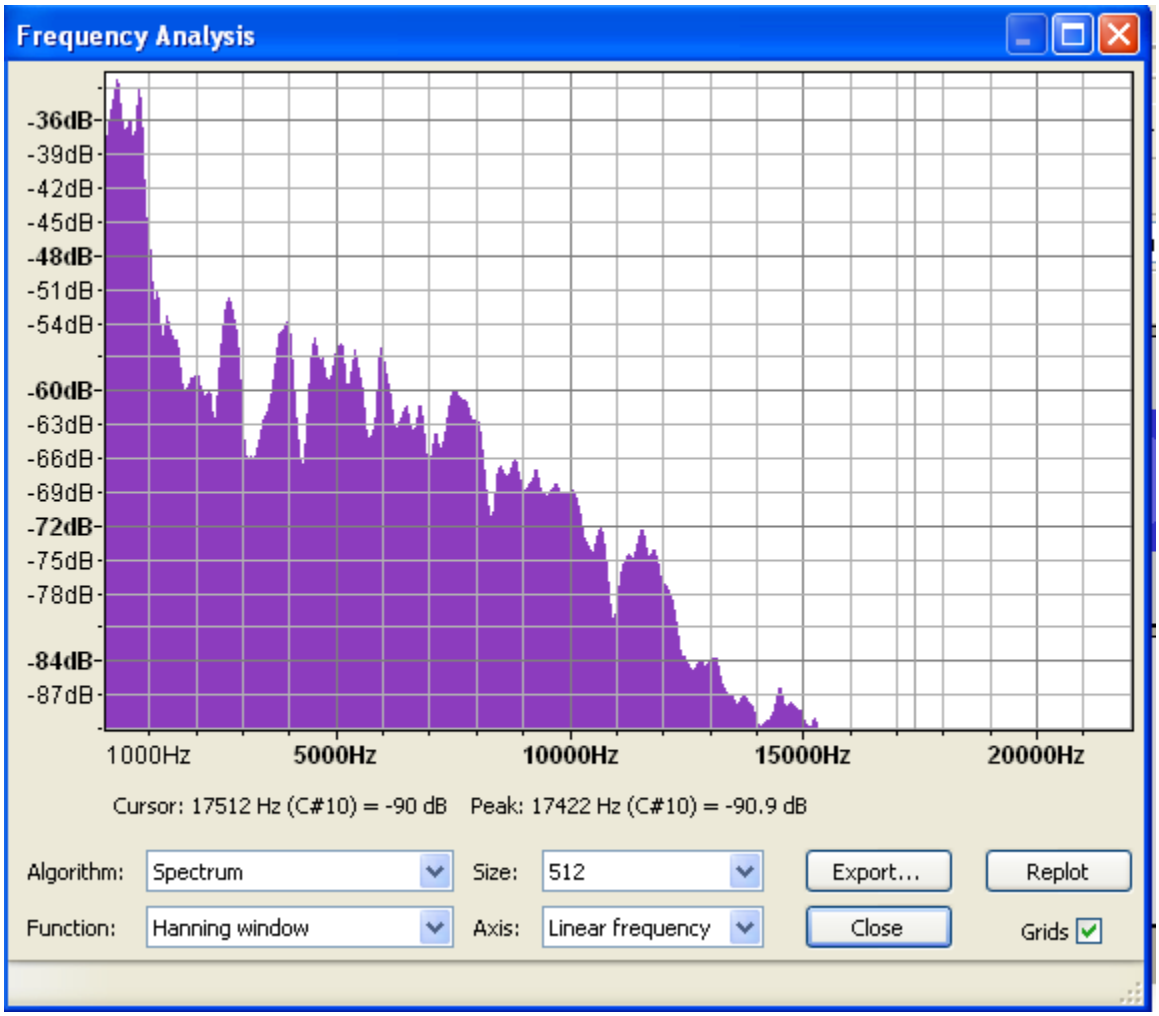

Figure 5.11: Frequency spectrum of a voice recording

Next students can record their voices again, only make their voices higher pitched, and then lower pitched. Each time, students should generate a frequency spectrum of the recorded signal and view how the frequency spectrum changes as they change the pitch of their voices.

To keep a record of the frequency spectrum of each voice recording, students can press the *print screen* button and paste the image for each frequency plot into imaging software such as Microsoft Paint.

Generating a Noisy Signal

In this part of the activity, students will add noise to their voice recordings. To generate noise, click on the Generate tab and select *noise*. The noise generator window should open up as shown in Figure 5.12. For noise type, select *white*. Let the amplitude by equal to 0.5, and make sure that the time duration is about 20 seconds.

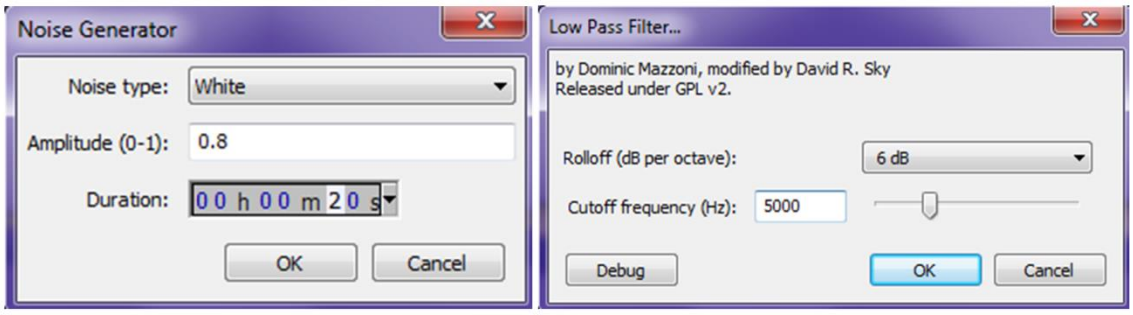

Figure 5.12: Window for generating noise on the left and for generating a low pass filter on the right.

Click OK. Figure 5.13 shows the Audacity user interface after generation of a white noise signal and recording of the voice signal. Note that the voice signal and the white noise signal are in separate tracks, which both play at once when the PLAY button is pressed. After clicking PLAY, students should hear a very noisy version of the same voice signal.

Students should generate a white noise frequency spectrum and compare it to the frequency spectrum of their voice recording. Figure 5.14 shows the frequency spectrum of the white noise signal. Have students record how the distribution of frequencies changes between the voice recording and the white noise signal. In particular, what is the ratio of magnitude at lower frequencies versus higher frequencies? How does the overall magnitude of the voice signal compare to that of the white noise signal? In other words, what is the approximate signal-to-noise ratio?

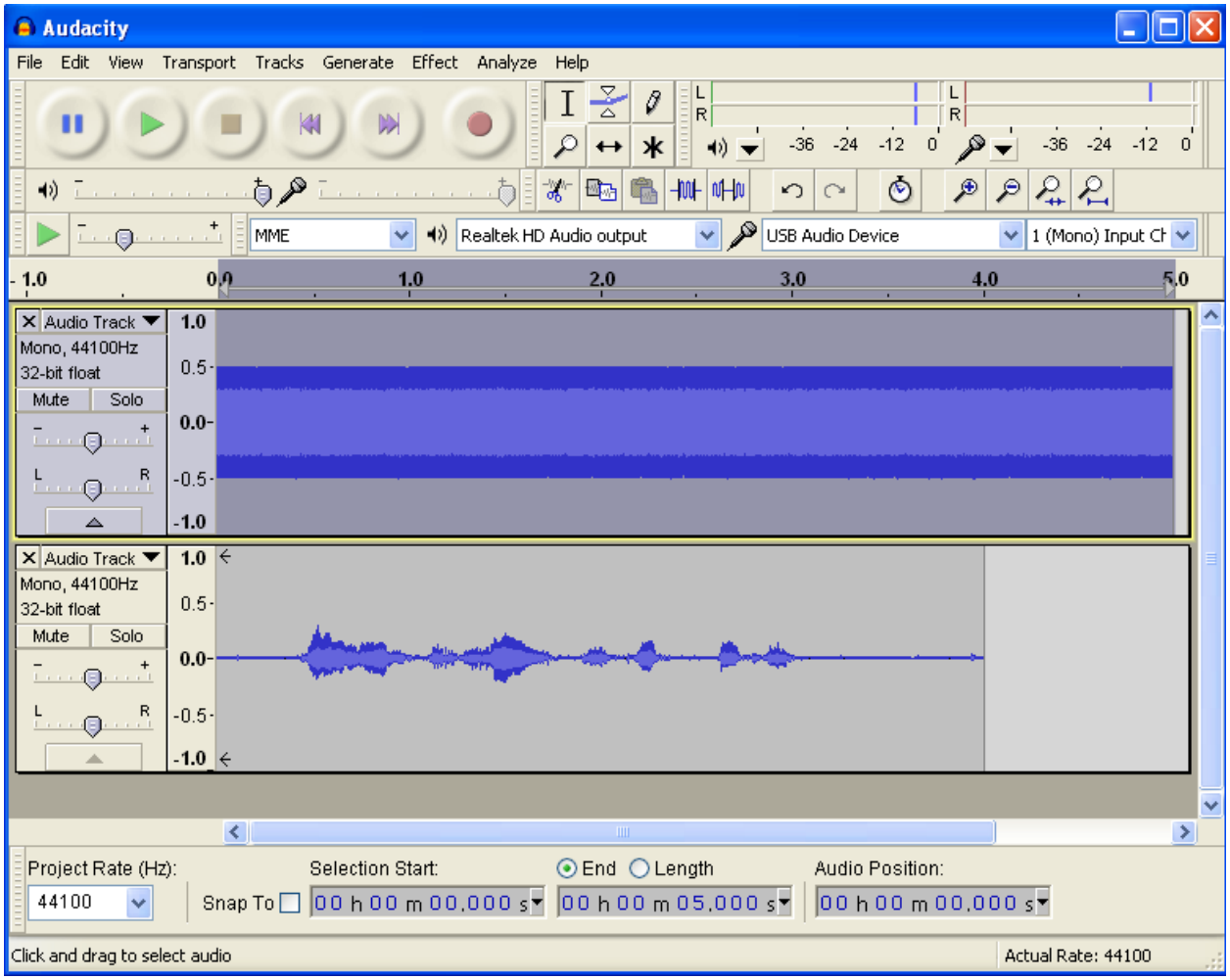

Figure 5.13: Voice recording with white noise

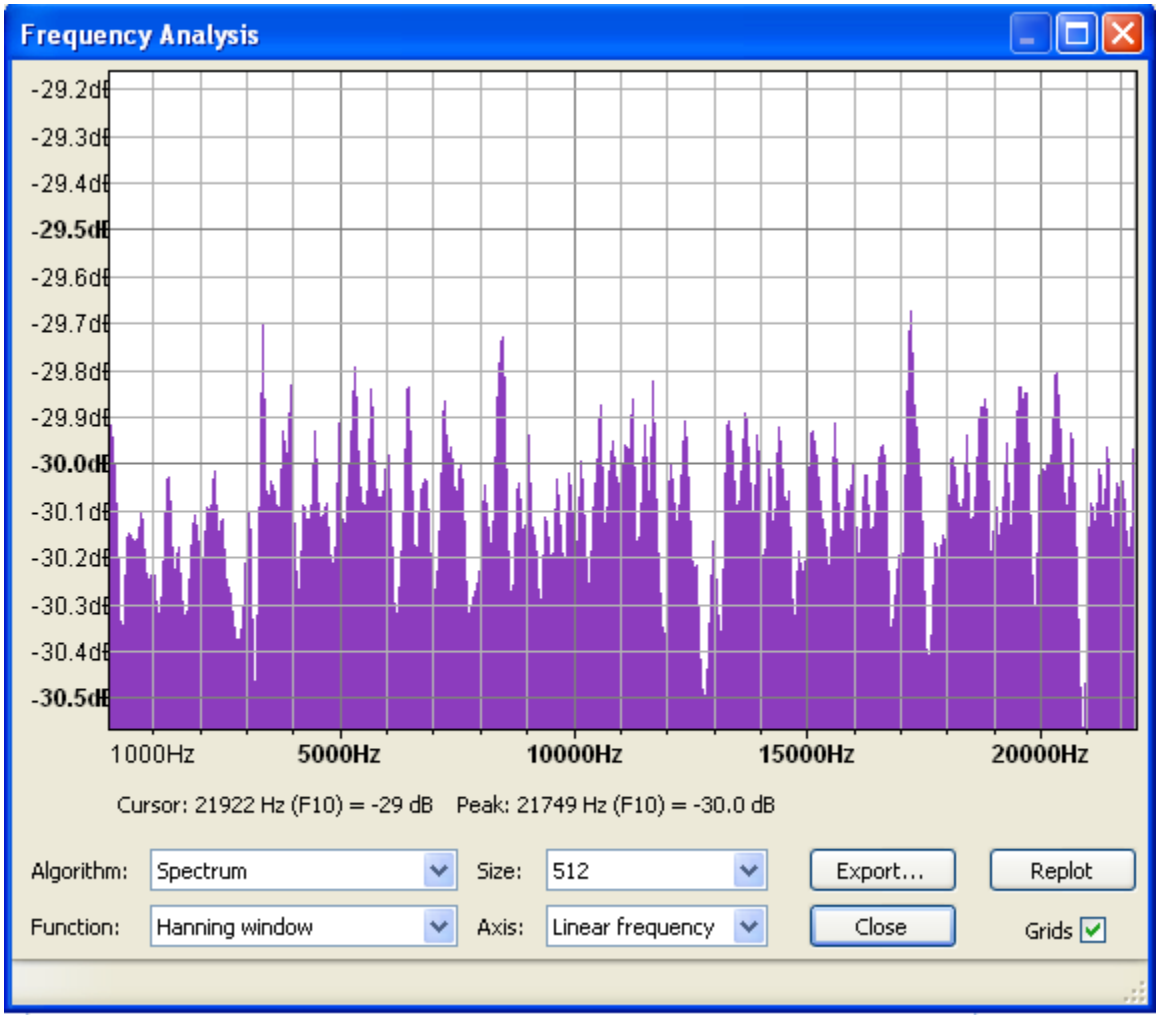

Figure 5.14: Frequency spectrum of the white noise signal

To examine the frequency spectrum of the noisy voice signal, the frequency spectrum of the white noise signal and the voice signal need to be summated. After generating the frequency spectrum, click the Export button on the lower right. This button generates a text file with frequency in the left column and magnitude in dB in the right column, which could be imported into software such as Excel. Before summation, convert from dB to non-dB units. After summation, convert back to dB units. Plot the result with respect to

frequency. The combined frequency spectrum represents the frequency spectrum of a noisy voice signal.

Filtering a Signal

Students may notice that the frequency spectrum of the noisy signal has a larger magnitude at higher frequencies than the signal without noise. One way of getting rid of noise is to filter out higher frequencies so that the noise becomes quieter and the voice signal becomes audible again.

Each track needs to be low pass filtered individually. To low pass filter a track in Audacity® software, highlight the part of the signal to be filtered, click on the Effect tab and select *Low Pass Filter*. A low pass filter window should show up as shown in Figure 5.12. If prompted to enter filter quality, set the filter quality to a high value such as 17.4 dB (otherwise it will not be very effective at filtering out unwanted frequencies). Select a cutoff frequency of 7000 and set the rolloff to 48 dB. Click OK.

Students may notice that the waveform in the recording changes as shown in Figure 5.15. For each track, click on the Analyze tab and select *spectrum*. Students should notice that for both the white noise signal (Figure 5.15) and the voice signal (Figure 5.16), the higher frequencies have decreased in amplitude while the lower frequencies retain higher amplitudes.

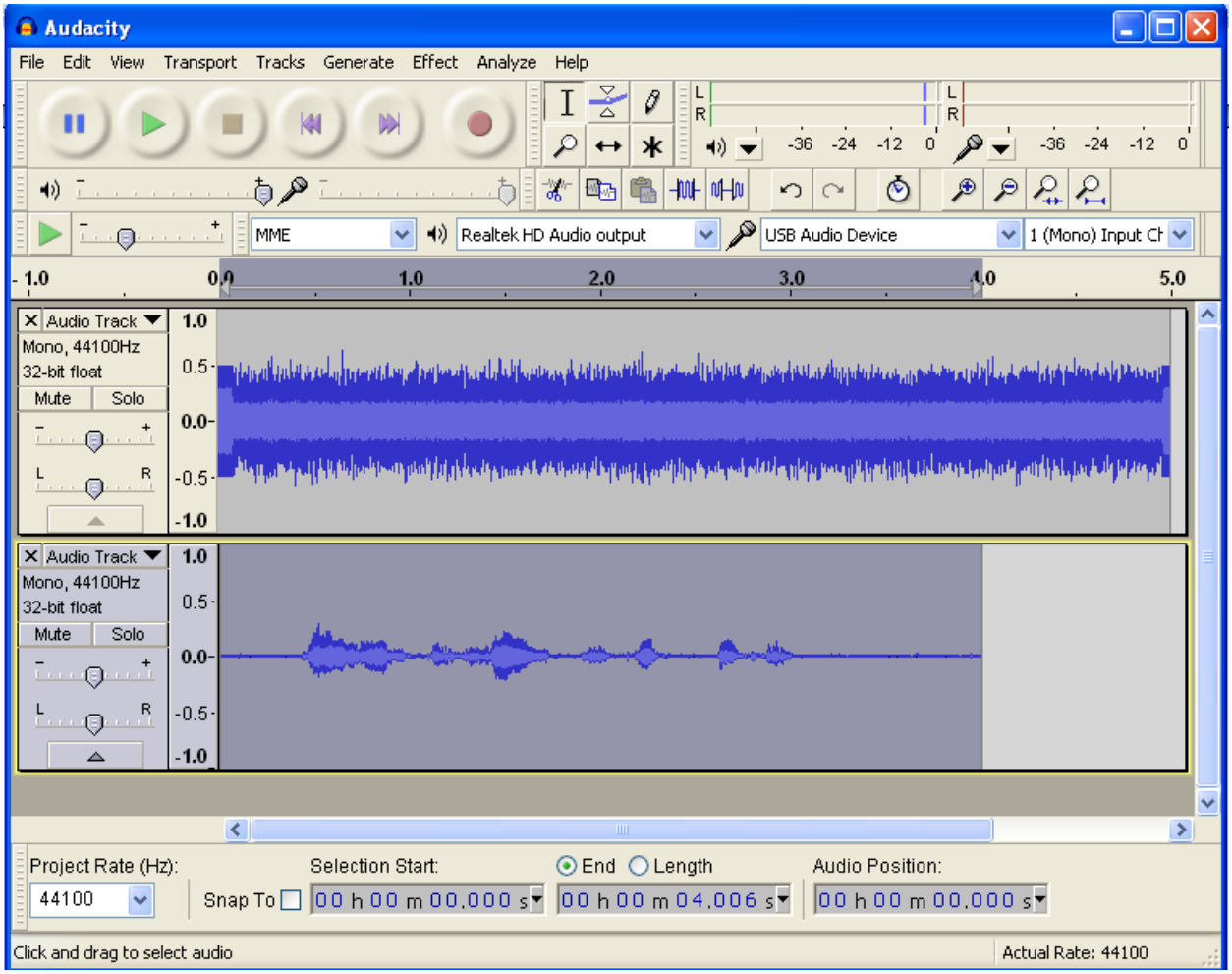

Figure 5.15: Voice recording with white noise after low pass filtering with a cutoff frequency of 7000 Hz and a 48 dB/octave rolloff

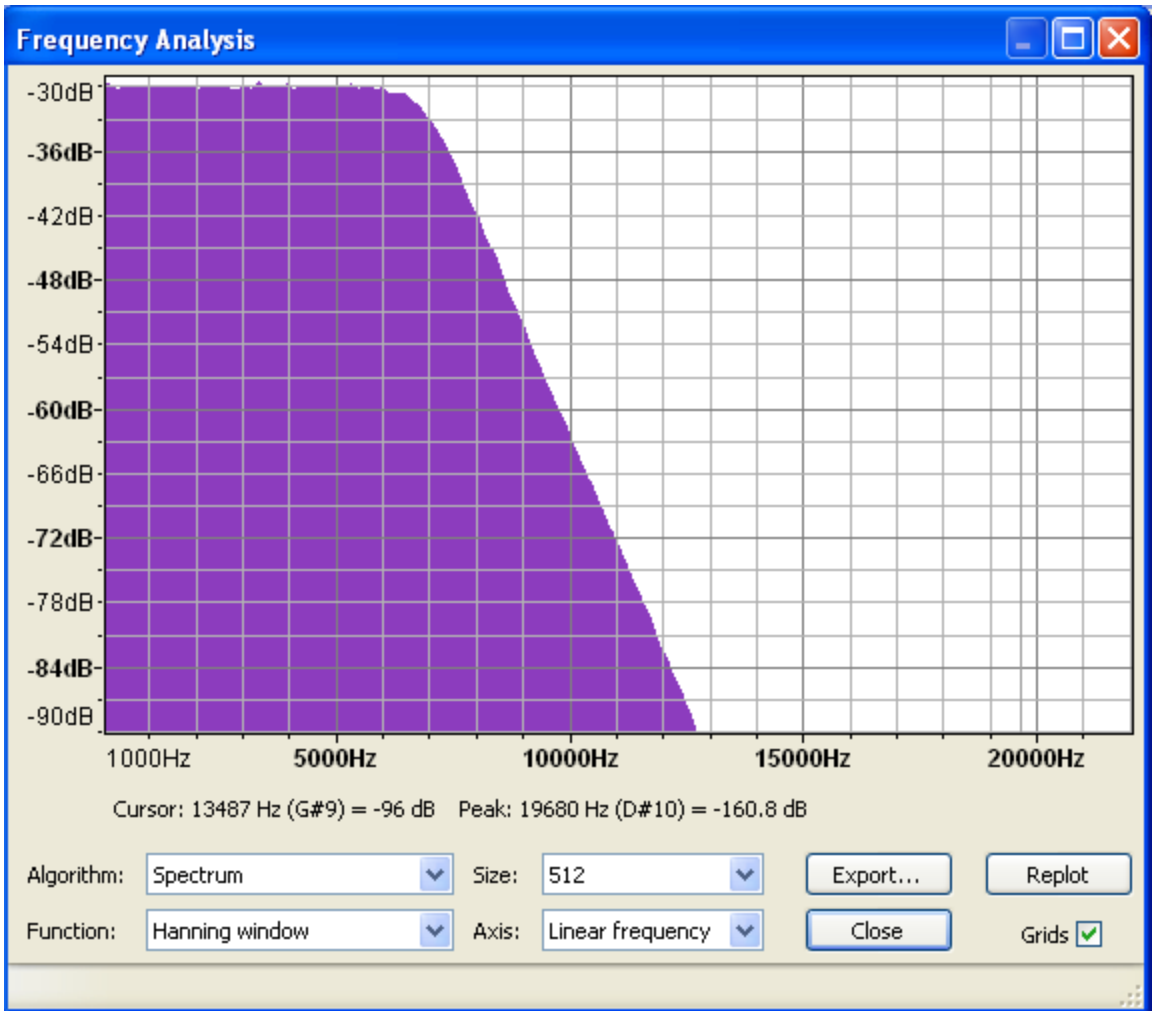

Figure 5.16: Frequency spectrum of noise after low pass filtering with a cutoff frequency of 1000 Hz and a 48 dB/octave rolloff.

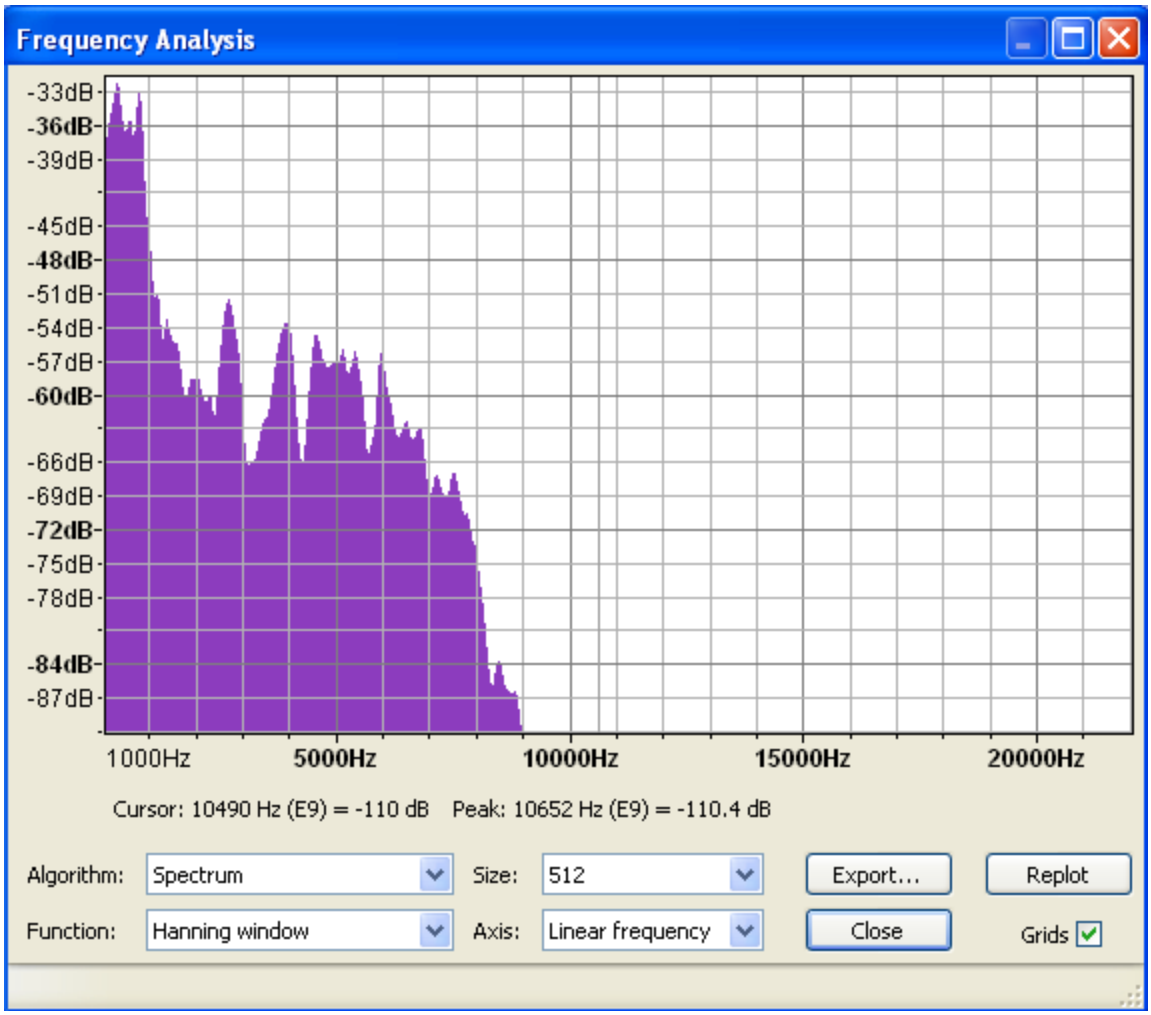

Figure 5.17: Frequency spectrum of voice signal after low pass filtering with a cutoff frequency of 7000 Hz and a 48 dB/octave rolloff

Have the students play back the newly filtered noisy signal, and let them decide if the signal quality has improved. If students think that the signal quality could be better, then students should undo the low pass filtering for each waveform by selecting the waveform, then clicking Edit>>Undo Filter. The Undo feature allows students to restart with the same signal. Students shall continue to experiment with different cutoff frequencies and different rolloff values until they find a cutoff frequency and rolloff that

are optimal. The best cutoff frequency and rolloff eliminate the most noise while preserving the voice signal.

When the optimal cutoff frequency is found, students should generate the frequency spectrum of the resulting noise signal and voice signal. The noise signal can be compared to the frequency spectrum of the unfiltered noisy signal and the voice signal can be compared to the frequency spectrum of the voice recording without the added noise.

Students should generally notice that their voices sound clearer as the low pass filtering parameters becomes more optimal. If the cutoff frequency is too low, their voice recordings may start to sound muffled, and the frequency plot may start to look less like the frequency spectrum of the original voice recording.

In the end, students should have a record of voice signal in the time domain and frequency domain 1) without noise; 2) with noise and 3) filtered with noise.

Reflection

After the laboratory activity is completed, students should have an in-class discussion or submit a lab report of their observations and the underlying meaning. Recordings of observations during the laboratory activity are important for helping students draw conclusions at the end of the activity. One way of recording observations is to take screen shots of frequency spectra each time a new waveform is generated.

Discussion

Signal analysis and signal processing are important skills to acquire in many career paths including physics. Experimental physicists typically measure a variety of signals such as electromagnetic signals and/or acoustic signals. A common method for characterizing a signal is by analyzing its frequency spectrum. The frequency components of a signal can give important information about the entity being measured. Furthermore, when designing a filter, it is important to know the frequency range of the signal of interest and the frequency response of the filter in order to optimally attenuate unwanted components of the signal such as noise, and ensure that the signal of interest is preserved.

Still another use for frequency component analysis is in the analysis of signal distortion. Attenuation, for instance, causes distortion in the signal because higher frequency components attenuate faster than lower frequency components. When different frequency components experience different levels of attenuation, the signal becomes distorted. White noise is useful in the analysis of signal distortion because the frequency spectrum of white noise is flat. When white noise is passed through a system, the shape of the frequency spectrum at the output can show whether distortion is to be expected.

5.2.3 Building Operational Amplifier Circuits with Breadboards

OBJECTIVE

The objective of this lab is to learn how to design and build an inverted operational amplifier circuit. Operational amplifier circuit have multiple uses including amplification of signals and current-to-voltage conversion. By learning how to build an inverted op amp circuit on a breadboard, students will learn how to interpret the pin diagram of a circuit chip and connect other circuit components to the correct pins. This inquiry-based learning activity allows students to vary the resistor values on the inverted op amp circuit, and observe how variations in resistor values influence the output signal. What happens if one or more of the resistor values is extremely large? What happens if one or more resistor values is extremely small? Students will be able to explore such questions by building the circuit and drawing conclusions from their own observations.

Supplies

Each lab station will need an LM741 op amp chip, resistors, wires, a breadboard, a BNC cable, twin alligator clips, a function generator and an oscilloscope.

Not all learning facilities have access to a function generator. In such cases, signals can be output through the computer's speaker port. SoundScope software is a free software that can be downloaded from the internet. It can generate various waveforms of user-defined amplitude and frequency. A TRS to BNC adapter can be used to collect the signal from the speaker port and deliver it to the circuit via the twin alligator clips.

Many learning facilities also are without an oscilloscope. While the microphone port may be used as the poor man's oscilloscope, the microphone port performs AC coupling, which can cause large amounts of distortion in certain waveforms such as square waveforms. Another option is to purchase TracerDAQ software from Measurement Computing Inc. The software comes with a USB device with multiple pins that serve as input and output channels. This software can more reliably probe different parts of the circuit, which is important for observing what the circuit is doing to a signal.

Operational Amplifiers

Operational amplifiers are often used to amplify signals. The circuit shown in Figure 5.18 is an operational amplifier circuit that amplifies the input voltage signal, V_{in}, to obtain a larger output voltage signal, V_{out}. So how much is the input signal amplified? How many times larger will the output voltage be? This can be computed by the following equation:

$$\frac{V_{out}}{V_{in}} = -\frac{R_f}{R_{in}}$$

An operational amplifier chip has 8 pins as shown in Figure 5.18. One pin is for the inverting input, one pin is for the noninverting input, one pin is for the output, one pin is for the + end of the power supply and another pin is for the – end of the power supply. The offset null pins and the NC pin will not be used in this lab, and therefore are not connected to anything.

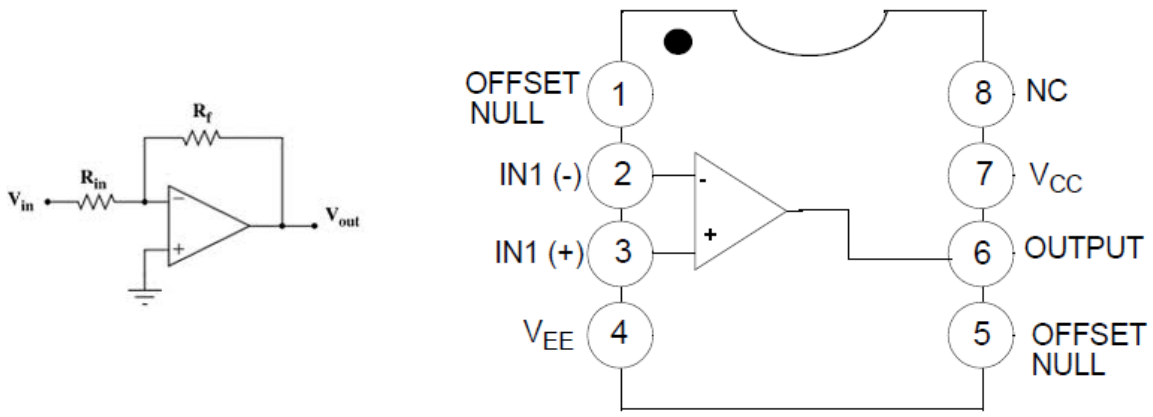

Figure 5.18: An operational amplifier circuit that amplifies a signal by a factor of R_f/R_{in}. To the left is the circuit diagram of an operational amplifier and to the right is the pin diagram for the LM741 operational amplifier chip.

Manufacturing the Waveform

First, students will make sure that they can generate the waveform and probe it on the oscilloscope or TracerDAQ software. If using the sound port to generate the waveform, open the SoundScope software. If using the USB device in place of the oscilloscope, open the TracerDAQ software. Connect the BNC cables to the speaker port via the TRS to BNC adapter. At the other end of the BNC cable, connect to pins 1 & 2 of the USB device via the twin alligator clips as shown in Figure 5.19.

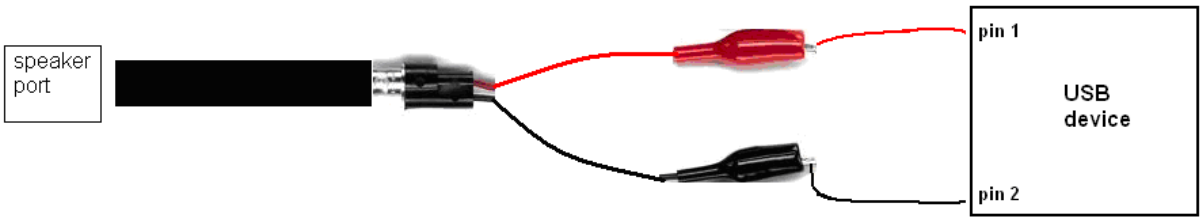

Figure 5.19: To make sure everything is working properly, you should connect the speaker port to pins 1 & 2 of your USB device as shown above. Make sure the waveforms produced by Sound Scope show up on your TracerDAQ oscilloscope.

First, students will use Sound Scope software or the function generator to produce sine waves, and then square waves. Make sure that each time a different waveform is generated, it shows up on your TracerDAQ oscilloscope.

Next students can vary the amplitude and frequency of the waveform. Have students make a sine wave with amplitude = 0.1 and frequency = 500 Hz, and then view the signal on the Tracer DAQ oscilloscope. The observed signal amplitude should be recorded along with the time between peaks (also known as the period).

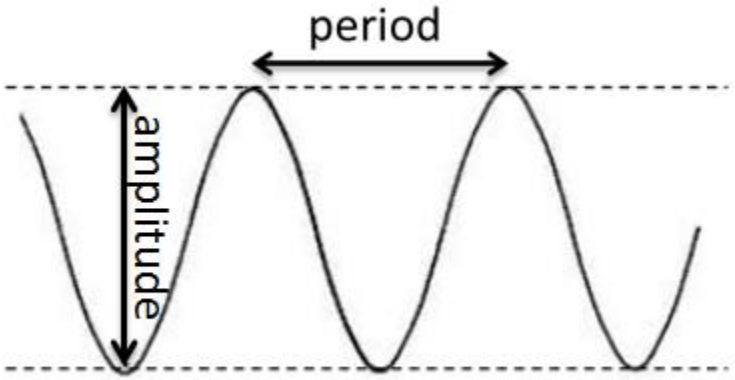

Figure 5.20: A diagram illustrating the peak-to-peak amplitude and period of the waveform.

Constructing the Circuit on the Breadboard

Using your breadboard, assemble the circuit illustrated in Figure 5.15, which uses an LM741 op amp. On the left, you can see what an LM741 operational amplifier chip looks like. Note that there is a little circle in one corner of the chip. *Place the chip on the breadboard so that the little circle is on the upper left.*

WARNING: Placing in the chip backwards causes power supply to go to the wrong pin, which can burn/destroy your chip.

NOTE: The vertical columns in the top half of the board are *not* connected to the vertical columns on the bottom half of the board, so either build your circuit on the top half or bottom half of your board.

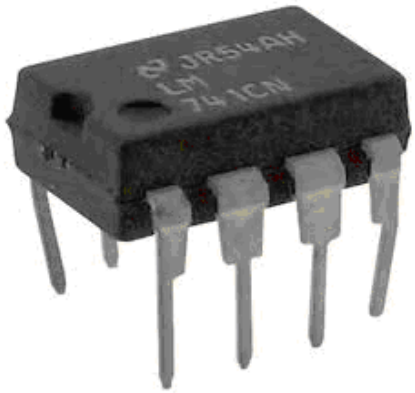

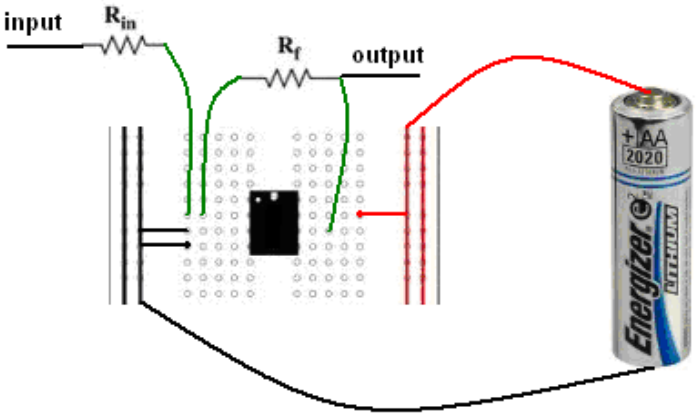

Figure 5.21: On the left is a picture of an LM741 operational amplifier chip. Notice that the chip has a circle in one of the corners. Place the chip on the breadboard so that the little circle is on the upper left. Assemble the circuit as shown on the right

The right hand side of Figure 5.15 shows how to connect the resistors, wires and power supply.

Let R_f = 2 kΩ and R_{in} = 1 kΩ

The LM741 chip requires a power supply of at least 15 V. In this activity, 25 V is recommended.

Probing the Circuit on the Oscilloscope

At this stage of the activity, students will connect the output of the circuit to the oscilloscope or USB device. An input waveform will simultaneously be connected to the circuit input as shown in Figure 5.16 below.

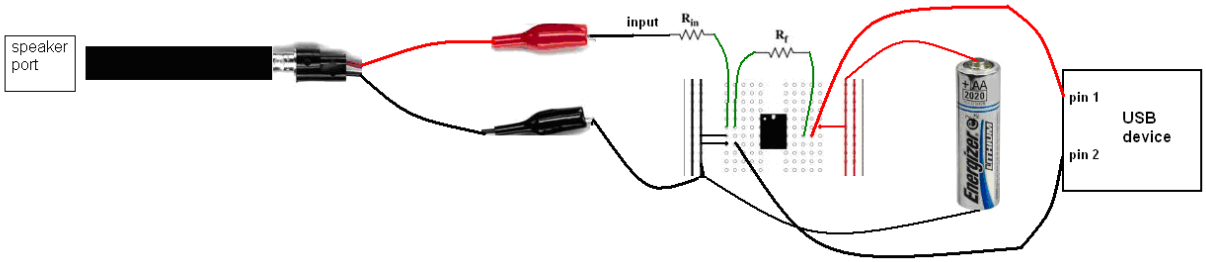

Figure 5.22: Setup for connecting the speaker port to the input of your amplifier circuit and connecting the USB device to the amplifier output. Use 25 V power supply

Students should select an input signal amplitude that is not too large in order to avoid saturation at the signal output. Next, any changes in the amplitude and signal frequency should be recorded.

Varying the Resistor Values

Have students select new resistor values to increase the amplification of the input signal. Students should use the equation presented on the first page to help them select a set of resistor values that increases or decreases amplification. Students can choose to change R_f, R_{in} or both.

For each combination of resistor values, students should record the set of resistor values they used and the resulting amplitude and period of the output signal, as illustrated in the blank table below.

R_f	R_{in}	Amplitude	Period

At one point, students should experiment with very large and very small resistor values. For example, students should experiment with what happens to the output signal when R_f = 1 MΩ.

Filtering a Noisy Input Signal

An op amp circuit can easily be converted to a low pass filter by placement of a capacitor in parallel with the feedback resistor, R_f.

For this activity, let R_f = 3 kΩ and R_{in} = 1 kΩ. To generate a noisy signal, use the Sound Scope software to generate a sine wave signal as before, and then use another software that is capable of sending noise out of the speaker port. Audacity software is one example of software that can produce a noisy signal.

Observe the output signal with the resistor values given above. Next, have students place a 47 nF capacitor in parallel with R_f. Students should record the changes that occur in the output signal.

Reflection: How may such an amplifier circuit be useful for scientists? What about engineers?

5.2.4 Summary of the Projects

The projects for this curriculum consisted of a set of self-guided tutorials where students split into groups of 2-4. Each group had its own computer work station and set of circuit components. Prior to each laboratory session, I would give a brief lecture on the nature of the project the students were about to do and the theory behind it.

The first tutorial taught students how to build a circuit on a bread board, how to use a digital multimeter, and how to avoid bad connections that can cause unwanted short circuits. Students experimented with the fundamental principles of Ohm's Law governing parallel and series resistance circuits.

The Audacity tutorial presented in 5.2.2 allowed students to experiment with waveforms of variable shape and frequency. Prior to this project, I discussed with students the meaning of signal frequency. What does a signal look like before and after certain frequencies are filtered out? What does cutoff frequency mean? Throughout the tutorial, students learned about how the signal frequency is related to the pitch. A major aim was to give students an intuitive feel for what the frequency spectrum of a signal can indicate. Eventually, students were asked to record their voice, and look at the frequency spectrum of their voice. Next, students recorded their voice while simultaneously playing a bunch of noise with Sound Scope. Students were asked to filter the noisy recording by using an inbuilt low pass filter in Audacity. The goal was to find the correct cutoff frequency that filtered out as much noise as possible while still

preserving the voice recording. Many groups found that they were hardly able to hear the voice over all the noise, but were able to hear the voice again after low pass filtering.

Advanced placement students were able to build amplifier circuits and RC circuits. First students built an RC circuit on the breadboard. They used Audacity and Sound Scope to make a noisy sine wave. The goal was to find the best resistor and capacitor value for filtering out the noise and preserving the sine wave signal. To measure the time constant of the RC circuit, students applied a square wave to the circuit and studied the output signal in the oscilloscope window. The students were given the equation relating time constant to resistance and capacitance. Did the equation correctly predict their measurements of the time constant?

The amplifier circuit lab presented some difficulties. Sometimes, amplification of a signal can cause a large shift in the signal offset, moving the signal out of the limited field of view in the oscilloscope. For this reason, I had put together an alternative amplifier tutorial that uses dual power supplies. The reference point of the amplifier circuit would be directly in between two power supplies, allowing the signal to keep the same offset after amplification.

5.3 Results

One way of assessing how much the students learned is to give the students a pre-test and post-test. Both tests ask basic questions about electronic circuits.

5.3.1 The Pre-Test

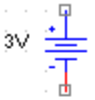

3 Volt battery

resistor

capacitor

ground or reference voltage

This test is meant to assess how much you already know about the basics of electronic circuits. The questions contain circuit diagrams where circuit elements such as batteries and resistors are represented by symbols. To the left is an illustration of what symbol is used to represent each type of circuit element.

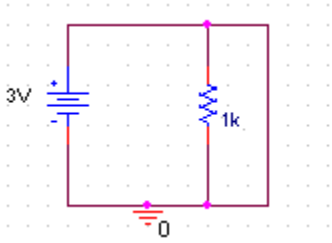

1) What is wrong with this circuit?

2)

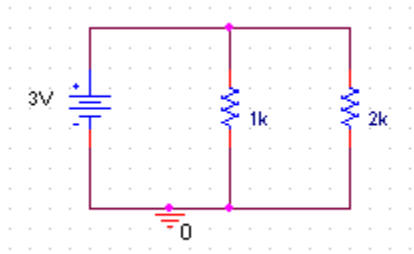

One resistor shown here is 1kΩ or 1000 ohms. The other resistor is 2kΩ or 2000 ohms. Which resistor draws more current? Try using Ohm's Law to explain your answer.

3)

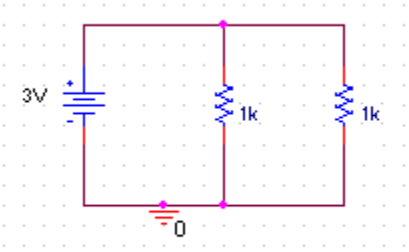

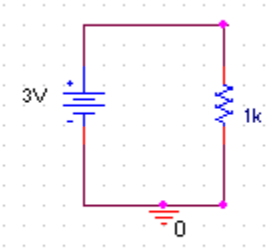

Shown above are two different circuits. One circuit has two 1000-ohm resistors in parallel while the other circuit has only one resistor that is 1000 ohms. Which circuit draws more current? Use Ohm's Law to explain your answer.

4) In addition to batteries, electronic power may come from an outlet you see on the wall. Sometimes an electronic power supply is used to power a large system with many circuit components such as a television set, or it may power a smaller system such as a light bulb.

Why may larger electronics systems with more circuit components draw more current than smaller systems?

5) Low pass filters only let lower frequencies through. High pass filters only let higher frequencies through. Which circuit below is a low pass filter? And which is a high pass filter? Can you explain your answer based on how capacitors work?

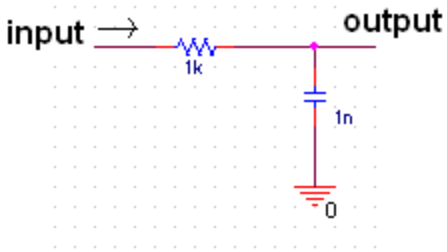

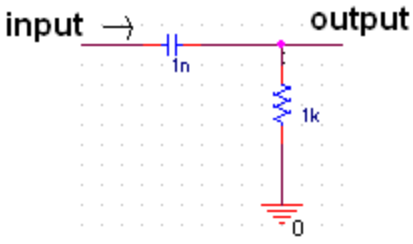

6) If a low pass filter has a cutoff frequency of 2 kHz and the input signal is a 1 kHz sine wave, will the filter:

a) increase signal amplitude

b) decrease signal amplitude

c) alter the signal's shape

d) no change in the signal

7) If a low pass filter has a cutoff frequency of 2 kHz and the input signal is a 1 kHz *square* wave, will the filter:

a) increase signal amplitude

b) decrease signal amplitude

c) alter the signal's shape

(d) no change in the signal

8) You start with a signal with a wide range of frequency components. If you place the signal through a low pass filter with cutoff frequency 5 kHz and then pass the signal through a high pass filter with cutoff frequency 1 kHz, what range of frequencies most easily show up in the output signal?

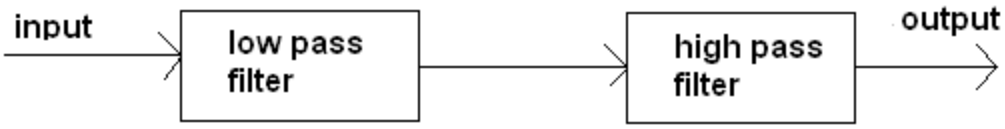

9) What can voltage dividers be used for? What are their disadvantages?

10) You connect a miniature light bulb across a 3 Volt battery and it shines brightly. Given that the resistance across the light bulb is about 40 ohms, predict what you think will happen if you construct each of the circuit below. Will the light bulb a) light up brightly, b) light up less brightly, or c) not light up visibly at all.

Note: In the lower left circuit, 20 means 20 ohm resistance. 5k means 5000 ohms and 1k means 1000 ohms.

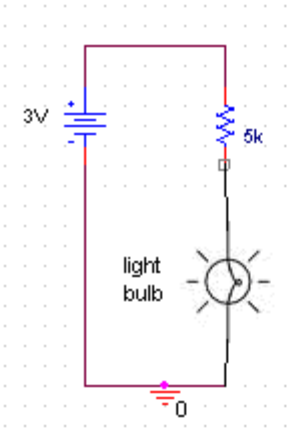

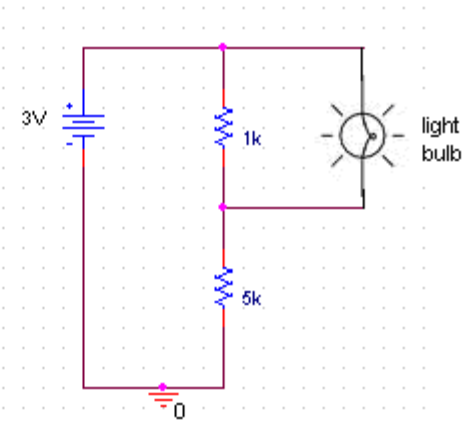

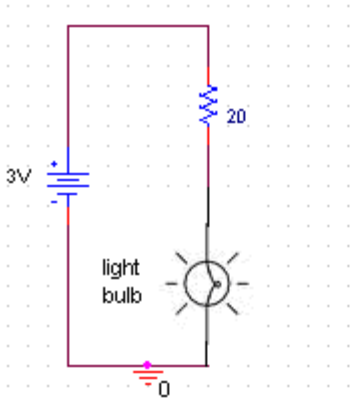

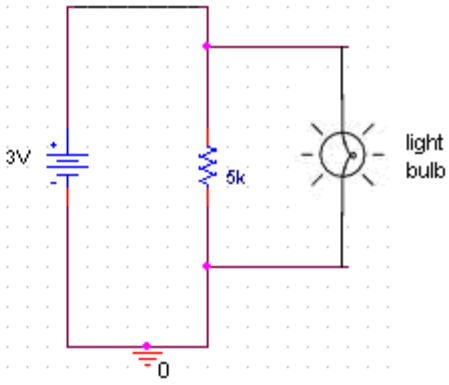

5.3.2 Student Performance Before and After

A few of the advanced placement physics students did well on the first eight questions on the pre-test because they had already learned about Ohm's Law and about what resistances draw the most current. However, most students did not know the answers from the 4th question onward. They knew the basics of Ohm's Law, but did not have an understanding of filter circuits. In particular, most students did not understand what a high pass filter versus a low pass filter circuit does to a signal. A large portion of the students also did not know how the brightness of a light bulb changes when a resistor is placed in series with the light bulb versus in parallel.

The post test questions were exactly the same as the pre-test questions. The only difference between the pre-test and post-test was that the pre-test was administered before the curriculum, the post-test after the curriculum. Results showed improved, but still incomplete, understanding of low pass versus high pass filtering. In particular, while more students were able to determine which frequencies can successfully pass through a filter of a certain cutoff frequency, some were still not able to determine when a filter changes a signal and when a filter does not. The reason for this outcome may be that students were not asked to filter signal of different shapes or frequencies. Rather, they were only prompted to filter a sine waveform with an RC circuit and their voice recording with an inbuilt Audacity filter. If students were prompted to filter signals of variable shapes and frequencies, then perhaps they would have developed more of an intuitive understanding of what a filter does to a signal given the signal's shape and frequency components.

The 10th question had a wide cross section of answers during both the pre-test and post-test, but the general trend showed that more students answered correctly on the post-test than on the pre-test. The portion of question 10 that caused the most confusion was the circuit with the light bulb in parallel with the 1k resistor and in series with the 5k resistor. Many students thought that this set of connections would allow the light bulb to light up brightly, but in reality the light bulb would not light up visibly at all. Perhaps this confusion could have been prevented if the light bulb tutorial had prompted the students to build a circuit with the light bulb in series with one resistor and in parallel

with another resistor. Students seemed to develop a better understanding of what happens when a light bulb is placed in series versus in parallel with a resistor, but they got confused when they saw a diagram of the light bulb in series with one resistor and in parallel with another resistor.

The overall post test results did not meet the standards of the curriculum, but nonetheless provide valuable feedback in terms of how the curriculum can be improved. A few simple additions and modifications can make a big difference in the outcome the next time around.

5.4 Materials and Cost

Table 5.1 shows the items used for this curriculum along with their cost. Each lab station would require 1 USB device, two BNC cables, two sets of twin alligator clips, 1 bread board, capacitors, resistors, one LMV751 chip, a few light bulbs and one digital multimeter. Lab stations can share the same capacitor set and resistor set. The number of lab stations that can share a resistor set and capacitor set is dependent on the number of each type of resistor and capacitor. On hobbyengineering.com, the 610 piece resistor set has 10 of each resistor value.

Table 5.1

Item Description	**Unit Cost**
USB-1208FS from Measurement Computing	$189 each
BNC cables	~$15 each
Twin alligator clips	~$10 each
Bread boards	~$10 each

Capacitor set	~$15
Resistor set	~$10
LMV751 op amp chips	$1.92 each
Miniature light bulbs	~$5 per pack of 10
Digital multimeters	~$20 each
Microphone	~$30 each

Adding up the cost of each item in Table 4.1 yields a total cost of roughly $305 per lab station plus the resistor and capacitor set that is shared among lab stations. Our classroom had 6 lab stations, yielding a total cost of $1860. The CLIMB fellowship provided a budget of $2500 for the academic year.

5.5 Discussion of K-12 Outreach Program

Bringing real-world science and engineering into the classroom has been both rewarding and challenging. Some major challenges included the limits in resources available and the variety of students with different academic backgrounds. Limits in resources are often an issue because real-world science often involves the use of expensive equipment. A tax-funded public school will not have as much funding as a science lab with a research grant. Fortunately, electronics equipment is not as expensive as some of the equipment that other scientists use. The most expensive component in my setup was the USB oscilloscope device. While the sound port could be utilized as a poor man's oscilloscope in some applications, its use is limited because of the AC coupling in the microphone port. However, with some creativity and resourcefulness, one can find an oscilloscope for a cheap price.

Students of variable academic and technical backgrounds also can present a challenge. Some students may already have extensive experience in the design and building of electronic devices while other students may not have any technical experience. In these cases, a pre-test is useful for assessing what students already know. Students with the most technical experience should not all be in the same group.

Yet another challenge is in keeping students motivated and reminded of how their lab projects are useful for real-world applications. Working closely with the school teacher is very helpful in fine tuning the curriculum so that it is more appealing to students. Many students had fun with the Audacity tutorial because they could record their voices and see what happens when they process their voice recording with different cutoff frequencies. The students also enjoyed viewing the real-time generated waveform of their voice on the Sound Scope program oscilloscope.

The RC circuit lab was useful for the advanced placement students because they had already learned about RC circuits as a part of their advanced placement physics curriculum. Some were even excited about building a real RC circuit.

Deb said that after the curriculum was complete, she got mixed reviews from the students. Some students liked the projects more than others. The mixed feedback did not surprise me because the projects were challenging to some extent, and troubleshooting was sometimes necessary in cases where the circuit did not output the expected signals. Although the need for troubleshooting is typical in engineering,

getting students interested in engineering may need to involve less gruesome troubleshooting. Students seemed to get frustrated sometimes when the circuit did not work as expected right away.

Fine tuning a curriculum for students of a specific grade level and academic background can be challenging. The projects need to be easy enough for the students to successfully complete them, but still have some challenge so that students do not get bored. Because of the lack of oscilloscopes available, a special USB device had to be used. The introduction of a USB device can present an additional source of complication when completing a project.

APPENDIX

A.1 Bluetooth

The Bluetooth sampling frequency is 44,100 samples/s. An advantage to using Bluetooth is that it employs adaptive frequency hopping spread spectrum (AFH). Frequency hopping spread spectrum (FHSS) means that Bluetooth hops from one carrier frequency to the next at 1600 times per second during active transmission. There are 79 different carrier frequencies in the hopping sequence, and all carrier frequencies are at least 1 MHz different from each other. FHSS is more robust and has little interference from noise, reflections, environmental factors and other radio stations. Adaptive frequency hopping has an additional feature: it allows Bluetooth to adapt to its environment by identifying fixed sources of interference and eliminating those frequencies from the hopping sequence. The quality of wireless transmission for each carrier frequency is evaluated with RSSI (Received Signal Strength Indication) or PER (Packet Error Rate). PER involves repeatedly testing and reassessing bad channels. It is less accurate than RSSI, but consumes less power.

AFH works better for slow-changing environments (Golmie et al., 2003) where the same hopping sequence can be used for a longer time. A disadvantage to AFH is that it can lead to additional packet loss.

We are using an F2M03MLA chip that is programmed in headset mode, which has bidirectional transmission in one channel for each direction. The triangle pulse waveform comes out of Out-P-Left and Out-N-Left. Because Bluetooth cannot output a

signal much larger than 500 mV peak-to-peak, the triangle pulse waveform is sent directly to the ramp amplifier circuit of the remote device as shown in Figure 2. For a pin diagram, see the datasheet of the F2M03MLA chip on the Free2move website.

To transmit a signal to the computer, the voltammetry circuit output is connected to the Audio In-P-Left pin. Audio In-N-Left is kept open. Audio In-P-Right and Audio In-N-Right are connected to Vref. To receive signals from the computer, the input of the voltammetry circuit is connected between Out-P-Left and Out-N-Left. Out-N-Right and Out-P-Right are kept open. The GND pins are connected to V-. Power supply is delivered across +VCC and GND. RESET is connected to +VCC so that when power supply gets too low, the circuit automatically resets. RX, TX, CTS and RTS are connected to the RS-232 circuit for temporarily connecting the remote device to the hyperterminal of the computer via the RS-232 port.

Audio In-N-Left is kept open to allow the voltammetry output to be transmitted to the computer without saturation or distortion. Out-P-Right and Out-N-Right are kept open because connection to the reference voltage causes an increase in the amount of current drawn by the Bluetooth chip.

A.2 Voltage Regulator

Voltage is regulated with the XC6209 chip, which outputs a fixed voltage of 3.3 V for the Bluetooth circuit. A 100 µF capacitor is placed across the +3.7-V battery to allow the

capacitor to charge up during periods of low power consumption and discharge during brief periods of high power consumption. During brief periods of high power consumption, such as when a wireless connection is first established, the battery may not be able to keep up with the large amount of current demanded by the circuit, so rather than rely on the battery for supplying current, a sufficiently large capacitor can discharge.

The reference voltage is stabilized with an XC6221 voltage regulator circuit, which outputs a stable voltage of +1.5 V relative to V-.

A.3 Switching Between Active Mode and Inactive Mode

The Bluetooth chip is preprogrammed so that when the PIO11 pin goes high, the Bluetooth transceiver starts to actively send out signals that can be picked up by the computer. When Bluetooth is actively sending out signals, the PIO3 pin goes high and remains high until the wireless connection is lost and Bluetooth enters an inactive state. The user is able to push a button down for a few seconds in order to activate Bluetooth, and view an LED that lights up when Bluetooth is maintaining an active connection. The circuit board has two LEDs. One LED lights up when the pushbutton is pressed, and the other LED lights up when Bluetooth is actively transmitting signals.

A.4 Bluetooth Setup on a New Computer

To establish an interface between the remote device and a computer Bluetooth must be installed on the computer. A Free2move installation CD can be purchased from the Free2move website along with a Bluetooth USB dongle. Insert the installation CD and install the FTDI USB to serial converter. The FTDI USB to serial converter software will allow the Bluetooth chip to communicate with the computer through a virtual COM port.

The next item to install is a Bluetooth Toshiba stack. The Toshiba stack is for constructing the user interface that allows the user to establish a connection between the computer and a Bluetooth device. The software is free, and can be found by typing "Bluetooth Toshiba stack" into an internet search engine.

The next step is to insert the Bluetooth USB dongle into a USB port. At the bottom right corner of the screen, there should be a couple of Bluetooth symbols, one of which is a white symbol with blue background. Right click on that symbol, and then click on Bluetooth settings. The Bluetooth settings user interface should show up.

Before establishing a new connection, the remote device must be paired with the computer through the hyperterminal. Our wireless voltammetry system comes with a printed circuit board that connects to the computer via an RS-232 cable. It has six gold pins: VCC, GND, CTS, RX, RTS and TX. Use wires to connect VCC of the RS-232 circuit to V+ of the remote device, and connect GND of the RS-232 circuit to V- of the remote device. Connect the CTS gold pin on the RS-232 board to the CTS pin of the remote device. Similarly, connect the RX, TX and RTS pins of the RS-232 board to the

RX, TX and RTS pins of the remote device. Next, make sure that the VCC and GND pins are connected to a power supply between 3.7 V and 6 V. Insert the RS-232 cable into the RS-232 port of the computer.

To pair the remote device with a laptop that has no RS-232 port, connect the RS-232 circuit to a desktop computer with an RS-232 port while simultaneously inserting the Bluetooth USB dongle into the laptop. Open the Bluetooth Settings user interface on the laptop and launch the desktop computer hyperterminal, selecting the correct COM port. On the next screen, select a baud rate of 38400 bits per second, with 8 data bits, no parity, 1 stop bit and hardware flow control. Before typing anything in the hyperterminal, one needs to activate the echoing of typed characters. Go to File>>>Properties. Click on the Settings tab. Click on ASCII setup at the lower right. Check the box next to “Echo typed characters locally” and check the box next to “Append line feeds to incoming line ends.” Click OK, then click OK to get out of the Properties box.

Type in DO POWER ON. If nothing happens, then you have connected into the wrong COM port and must establish a new hyperterminal connection all over again. The response you should get is DO POWER ON OK. Once power is on, type DO PAIR ON. You should see DO PAIR ON OK.

Now go to the Bluetooth settings box. Click on New Connection and go through the New Connection wizard. Select Custom Mode, and then select Free2move on the

menu of remote devices. On the next panel, click Headset. When prompted for a password, type in 0000. Choose a name for your connection, and click Finish. You will be returned to the Bluetooth Settings box, only now your new connection icon shows up. To officially establish a connection, right click on the new icon and click connect. If connection fails, just right click on the icon again. When connection succeeds, you will be prompted to press the headset button. Press the pushbutton on your remote device, and a connection should be established.

The microphone gain and HFP gain need special settings in order to maximize the amplitude of the transmitted signal in both directions. Each gain is set on a scale of 0-15. To expand the dynamic range of the signal that is recorded on the computer from the remote device, the microphone gain needs to be as low as possible without being set to 0 both in the hyperterminal and the computer's audio properties settings. HFP gain and A2DP gain should be maximized to 15. Tone gain is maximized to 22. All four gains can be set by typing in the following command:

SET VOLUME 1 15 15 22

In the computer's sound properties box, minimize the microphone volume to as low as possible without making it 0. Maximize the speaker volume.

After establishing a Bluetooth connection in the Bluetooth Settings box, and after modifying the volume settings for microphone and speaker, the Bluetooth connection

can may be tested. End the hyperterminal connection, and disconnect the RS-232 circuit from the remote device. Make a triangle pulse waveform in software, and convert it to an audio file. Play the audio file. To see if the triangle pulse waveform has been received at the remote device, connect an oscilloscope probe between the RAMP pin (test point #1 in Fig. 3a) and the REF pin, both of which are labeled on the printed circuit board. A triangle pulse waveform should show up on the oscilloscope. To test wireless transmission from remote device to computer, continue to play the triangle pulse waveform and simultaneously record a sound for a few seconds. View the recorded sound on a graph and make sure that a waveform of pulses is shown with the same number of pulses per second as the triangle pulse waveform.

Once the wireless voltammetry device has been paired with a computer, and volume settings have been modified, connection to the hyperterminal via the RS-232 port will no longer be necessary for successive experiments. To start an experiment, simply connect the battery to the V+ and V- pins, press the pushbutton until the PIO3 LED turns on, use the Bluetooth Settings window to establish a connection, and press the pushbutton again when prompted.

A.5 Constructing a Triangle Pulse Waveform

The first step to generate a triangle pulse waveform is to choose the desired waveform parameters. As illustrated in Figure A.1, this includes the period, pulse width, pulse amplitude and offset. In Matlab, an audio file is on a magnitude scale from 0.0 to 1.0 whereas in Igor, an audio file is on a scale from -32768 to +32767. The offset

represents the holding voltage between pulses, the maximum voltage is equal to the offset + amplitude. The slope in V/s is the amplitude divided by half the pulse width.

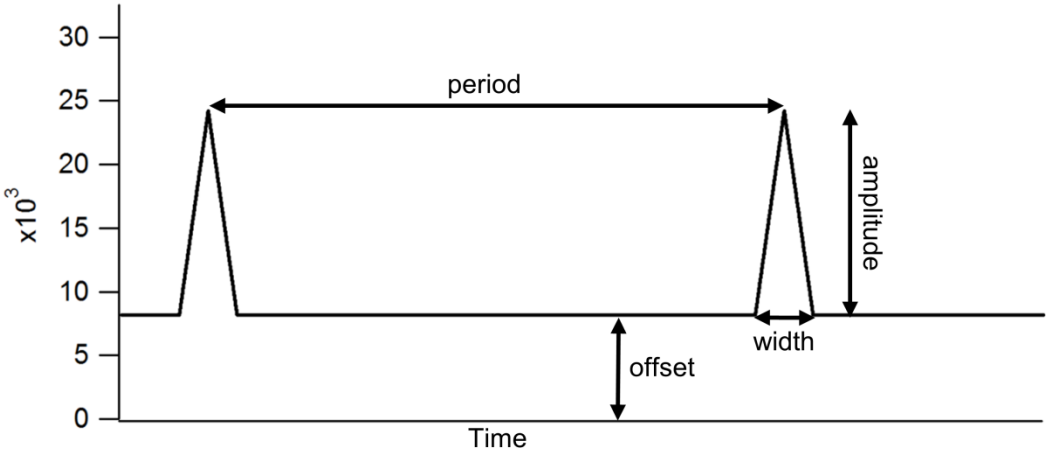

Figure A.1: Digital triangle pulse waveform that is constructed in Igor software. The user can select the period (time between peaks), pulse width, pulse amplitude and offset.

The digital waveform must be converted to an audio file and played with a software that can play audio files such as Windows Media Player or Igor. To calibrate the triangle pulse waveform, an oscilloscope probe is placed between the RAMP pin and the REF pin on the remote device and the offset and amplitude of the digital triangle pulse waveform are adjusted until the oscilloscope shows the correct offset and amplitude of the voltage ramp. Once we have the correct amplitude and offset values are found, the calibration of the triangle pulse amplitude and offset should be constant, provided that the volume settings are set correctly in the hyperterminal, as discussed in section A.4.

If the user wants to vary any features of the triangle waveform in the course of an experiment, then he/she may calibrate multiple triangle pulse waveforms to the desired amplitudes and offsets, and then freely switch from one waveform to the next during the experiment. For example, the user may want to calibrate a triangle pulse waveform that

sweeps from -450 mV to +1300 mV while another triangle pulse waveform sweeps from -500 mV to +1000 mV. Another triangle pulse waveform may have pulses that are 20 ms wide. Another waveform may have square pulses used for amperometry.

The syntax for sending out a sound signal in Matlab named SawWaveform is: sound('SawWaveform', 44100, 16) where 44100 is the sampling frequency in samples per second and 16 is the number of bits resolution. The syntax for sending out a sound signal in Igor name SawWaveform is playsound/A SawWaveform where /A allows for the execution of other commands while the sound file is played.

If Windows Media Player is chosen to send out the triangle waveform, then the waveform needs to be converted to an audio wmp file. The syntax for storing data in a sound file in Matlab is wavwrite('SawWaveform', 44100, 16, 'SawWaveform_sound_file'). This command converts the data file SawWaveform into an audio file named SawWaveform_sound_file. The same process can be performed in Igor by clicking on the SaveWaveSoundFile tab and selecting SawWaveform from the menu of wave files.

A.6 Recording Data

Data transmission to and from the remote device was performed in Igor software. However, other types of software, such as Matlab, can be used as well. To record data in Igor, a waveform needs to be defined with a specific number of samples. For our

application, there are 44100 samples per second, or 1/44100 seconds per sample. The soundinrecord command records a soundwave and stores it into the specified waveform. The time length of the recording depends on the number of samples per second and the number of samples in the waveform. To record in Matlab, the wavread command is used. The user defines the sampling frequency in Hz and the number of samples to record.

A.7 Low Pass Filtering

Low pass filtering is done in hardware and in software. The hardware low pass filter is in the form of an RC feedback circuit between the inverting input and output of the LM751 operational amplifier (see Figure 2). The cutoff frequency = $1/(2\pi RC)$, making a cutoff frequency of 531 Hz for the CFE circuit. However, there is still some noise on the wireless recording. Most of the noise is filtered out with the in-built filters in Igor. We can choose among many different classes of filters, and select the cutoff frequency. As in many other laboratories, we used a cutoff frequency of 2 kHz. However, for the calibration experiments shown in Figures 5 and 6, we used a cutoff frequency of 1 kHz in order to improve the SNR for smaller DA oxidation signals. The specific filter model we use is the Kaiser-Bessel20, which is an in-built low-pass filter in Igor.

Running averaging has been experimented with as well, but the frequency response of a running average oscillates due to the nature of running averaging. Therefore, in-built low pass filters are better.

A.8 Data Analysis

The major goal of data analysis is to perform background subtraction, generate cyclic voltammogram plots, generate color plots and generate dotted plots that show the time course of dopamine release.

Unfortunately, the acquisition of the current pulses is not perfectly synchronized with the applied triangle pulses. However, the collected current is practically constant between triangle pulses, allowing us to determine the start of a current pulse by the rising or falling edge for each pulse. In practice, we determine first the time point in the waveform at which to collect the reference signal. The reference signal is typically collected from the time point in the recording just prior to dopamine release. A cursor is placed at the start of the first reference pulse in the line of consecutive reference pulses to be averaged. Next the software moves forward by exactly 100 ms to the next pulse (given that the triangle pulse waveform has applied 10 pulses per second). The starting point of each successive pulse is determined so that the pulse is optimally aligned with the average of the preceding pulses. The pulses are considered to be optimally aligned when the RMS of their difference is minimized.

Next, we determine the time point in the waveform at which to collect the signal pulses. A second cursor is placed at the start of the first signal pulse in the line of consecutive signal pulses to be averaged. The starting point of the first signal pulse is selected so that the signal pulse is optimally aligned with the average of the reference pulses. After

the first signal pulse, the software moves forward by exactly 100 ms to the next signal pulse. The starting point of each successive signal pulse is determined so that the pulse optimally aligns with the average of the preceding signal pulses.

To generate a voltammogram, a user-defined number of background pulses is averaged, and then subtracted from an average of a user-defined number of signal pulses. The background-subtracted signal is plotted with respect to the applied voltage.

While a cyclic voltammogram plot shows the dopamine signal at one point in time, a color plot shows the dopamine signal over an entire time window from before dopamine release to after dopamine diffusion and reuptake. A color plot is a 3D plot that shows time on the horizontal axis and applied voltage on the vertical axis. A color code is used in which green represents the largest and most positive background subtracted currents while blue represents the most negative background subtracted currents, and yellow represents a background subtracted current equal to 0. Any background subtracted currents that are out of range appear black. In a color plot, a dopamine oxidation signal would appear as a green blotch near an applied voltage of roughly +450 to +650 mV. A dopamine reduction signal would appear as a bluish blotch at a more negative applied voltage. Figure 2.7A shows a color plot generated from injection of dopamine solution into a dish of buffer solution.

To generate a color plot, an additional cursor is placed at the starting point of the first pulse to be included in the color plot. Our color plot function inputs the length of time in

seconds and the number of voltammograms generated per second while the cursor marks the starting time. Each voltammogram in the color plot may be generated from only one signal pulse or multiple signal pulses averaged together. Depending on the scenario, we may choose to generate only one voltammogram per second where each voltammogram represents an average of 10 signal pulses. In another scenario, we may generate 10 voltammograms per second with a moving average of 10 signal pulses.

A time course plot is used to show the time course of neurotransmitter oxidation current over a certain time window. Each point represents the average background-subtracted current for a range of applied voltages. The range of applied voltage represents the voltages at which the peak oxidation current is observed. The trace is expected to shift upwards to more positive values when neurotransmitter release occurs, and shift back down to baseline levels as the neurotransmitter diffuses away from the CFE.

In the recording software, a recorded sound waveform is on a scale of 0 to 1 in Matlab, and a scale of -32768 to +32768 on Igor given 16 bits of resolution. It is important to convert from software units to nA in order to know how many nA of current was collected. To compute the conversion factor, we need to know the gain of the CFE current-to-voltage converter and the wireless transmission gain. The gain of the CFE current-to-voltage converter is determined by the feedback resistance. A 3 MΩ feedback resistance yields a CFE current-to-voltage conversion gain of 3 mV/nA. Subtraction of the capacitance compensation signal at the differential amplifier does not change the mV/nA gain. After the capacitance compensation signal is subtracted, the

magnitude of the differential output is noted in volts. The magnitude of the software recording is noted in software units. With this information, the formula below can be used to convert from software units to nA:

$$data\_amp\_per\_nA = (1 \times 10^{-9} A)(3 \times 10^{6} \Omega) \times \frac{recording\_amp}{diff\_output\_amp}$$

A.9 Cost

In vivo neurophysiology setups are rather expensive. The mechanical set-up for the wired connection, head stage, amplifiers and data acquisition boards add up to several thousand dollars. The wireless FSCV device described here includes all required system components at a cost below $500 including PCB fabrication and assembly.

Table A.1 shows the unit price per device based on purchase of three boards. The PCB manufacturing cost and assembly cost will vary depending on the manufacturer you choose. Because the Bluetooth chip can only be soldered by machine, it is often necessary to pay for assembly. Our printed circuit board design was done in PCB Artist software. Manufacturing and assembly were done by Advanced Circuits in Aurora, Colorado, with a 5-day turn time.

Table A.1

Item Description	Cost Per Board
PCB manufacturing	172.67
PCB assembly	229.80
F2M03MLA chip	55.39
Resistor 3.01K 0.1%	1.08
Resistor 10K 0.1%	1.31
Resistor 10K 1%	0.50
Resistor 3 MΩ 5%	1.20
Resistor 100K 1%	0.08
Resistor 15K 1%	0.08
Resistor 180 Ω 1%	0.20

Resistor 220K 1%	0.16
Capacitor 1 μF 20%	1.20
Capacitor 300 pF	0.10
Capacitor 47 μF	0.69
Capacitor 1 nF	0.24
Capacitor 33 nF	0.03
Capacitor 100 pF	0.90
Capacitor 100 μF	1.30
Yellow Standard LED	0.23
Diode Schottky	1.15
Pushbutton	0.26
NPN Bipolar Transistor	0.52
LMV751 op amp chip	4.67
INA132 diff amp chip	3.53
XC6209 voltage regulator	0.58
XC6221 voltage regulator	1.11
Gold Pins from Newark	12.33
Total	491.31

BIBLIOGRAPHY

Acquas E, Carboni E and Chiara GD (1991) “Profound depression of mesolimbic dopamine release after morphine withdrawal in dependent rats” *Eur. J. Pharm.* 193: 133-134

Agid Y, Ruberg M, Javoy-Agid F, Hirsch E, Raisman-Vozari R, Faucheux B, Michel P, Kastner A, Blanchard V, et al., (1993) “Are dopaminergic neurons selectively vulnerable to Parkinson’s disease?” *Adv. Neurol.* 60: 148-164

Aigner TG and Balster RL (1978) “Choice of Behavior in Rhesus Monkeys: Cocaine Versus Food” *Science* 201(4355): 534-535

Agnesi F, Tye SJ, Bledsoe JM, Griessenauer CJ, Kimble CJ, Sieck GC, Bennet KE, Garris PA, Blaha CD, Lee KH (2009) “Wireless instantaneous neurotransmitter concentration system-based amperometric detection of dopamine, adenosine, and glutamate for intraoperative neurochemical monitoring” *J. Neurosurg*. 111: 701–711

Ahlskog JE and Muenter MD (2001) “Frequency of Levodopa-Related Dyskinesias and Motor Fluctuatios as Estimated From the Cumulative Literature” *Movement Disorders* 16(3): 448-458

Akai T, Yamaguchi M, Mizuta E and Kuno S (1993) “Effects of terguride, a partial D2 agonist, on MPTP-lesioned parkinsonian cynomolgus monkeys” *Ann Neurol.* 33(5): 507-511

Anglade P, Vyas S, Javoy-Agid F, Herrero MT, Michel PP, Marquez J, Mouatt-Prigent A, Ruberg M, Hirsch EC and Agid Y (1997) “Apoptosis and autophagy in nigral neurons of patients with Parkinson’s disease” *Histology and Histopathology* 12(1): 25-31

Annovazzi-Lodi V and Donati S (1988) “An Optoelectronic Interconnection for Bidirectional Transmission of Biological Signals” *IEEE Trans. Biomed. Eng*. 35(8): 595-606

Antelman SM, Szechtman H, Chin P and Fisher AE (1975) “Tail pinch-induced eating, gnawing and licking behavior in rats: Dependence on the nigrostriatal dopamine system” *Brain Research* 99(2): 319-337

Badiani A, Oates MM, Day HEW, Watson SJ, Akil H and Robinson TE (1998) “Amphetamine-Induced Behavior, Dopamine Release, and *c-fos* mRNA Expression: Modulation by Environmental Novelty” *J. Neurosci.* 18(24): 10579-93

Baik JH (2013) “Dopamine signaling in food addiction: role of dopamine D2 receptors” *BMB Reports* 46(11): 519-526

Berardelli A, Rothwell JC, Thompson PD and Hallett M (2001) “Pathophysiology of bradykinesia in Parkinson’s disease” *Brain* 124: 2131-2146

Bergh C, Eklund T, Soderstein P and Nordin C (1997) “Altered dopamine function in pathological gambling“ *Psych. Med.* 27(2): 473-475

Berke JD and Hyman SD (2000) “Addiction, Dopamine and the Molecular Mechanisms of Memory” *Neuron* 25: 515-532

Benabid AL (2003) “Deep brain stimulation for Parkinson’s Disease” *Current Opinion in Neurobiology* 13(6):696-706

Benabid AL, Chabardes S, Mitrofanis J and Pollak P (2009) “Deep brain stimulation of the subthalamic nucleus for the treatment of Parkinson’s Disease” *The Lancet Neurology* 8(1): 67-81

Benabid AL, Pollak P, Louveau A, Henry S and de Rougemont J (1987) “Combined (Thalamotomy and Stimulation) Stereotaxic Surgery of the VIM Thalamic Nucleus for Bilateral Parkinson’s Disease” *Appl. Neurophysiol.* 50:344-346

Bledsoe JM, Kimble CJ, Covey DP, Blaha CD, Agnesi F, Mohseni P, Whitlock S, Johnson DM, Horne A, Bennet KE, Lee KH and Garris PA (2009) “Development of the Wireless Instantaneous Neurotransmitter Concentration System for intraoperative neurochemical monitoring using fast-scan cyclic voltammetry” *J. Neurosurg*. 111(4): 712-723

Breier A, Su TP, Saunders R, Carson RE, Kolachana BS, de Bartolomeis A, Weinberger DR, Weisenfeld N, Malhotra AK, Eckelman WC and Pickar D (1997) “Schizophrenia is associated with elevated amphetamine-induced synaptic dopamine concentrations: Evidence from a novel positron emission tomography method” *Proc. Natl. Acad. Sci. USA* 94(6): 2569-2574

Butcher SP, Fairbrother IS, Kelly JS and Arbuthnott GW (1988) “Amphetamine-Induced Dopamine Release in the Rat Striatum: An In Vivo Microdialysis Study” *J. Neurochem.* 50(2): 346-355

Cenci MA, Lee CS and Björkland A (1998) “L-DOPA-induced dyskinesia in the rat associated with striatal overexpression of prodynorphin- and glutamic acid decarboxylase mRNA” *Eur. J. Neurosci.* 10(8): 2694-2706

Chase TN (1998) “The Significance of Continuous Dopaminergic Stimulation in the Treatment of Parkinson’s Disease” *Drugs* 55(1) Suppl. 1: 1-9

Chen N and Reith MEA (2000) “Structure and function of the dopamine transporter” *Eur. J. Pharmacol.* 405(1-3): 329-339

Chesselet MF, Cheramy A, Reisine TD and Glowinski J (1981) “Morphine and δ-opiate agonists locally stimulate *in vivo* dopamine release in cat caudate nucleus” *Nature* 291: 320-322

Chesselet MF, Cheramy A, Reisine TD, Lubetzki C, Glowinski J, Fournie-Zaluski MC, and Roques B (1982) “Effects of various opiates including specific delta and mu agonists on dopamine release from nigrostriatal dopaminergic neurons *in vitro* in the rat and *in vivo* in the cat” *Life Sciences* 31(20-21): 2291-2294

Chiara GD and Imperato A (1988) “Opposite effects of mu and kappa opiate agonists on dopamine release in the nucleus accumbens and in the dorsal caudate of freely moving rats” *J. Pharmacol.* 244(3): 1067-1080

Chow RH, Rüden L and Neher E (1992) “Delay in vesicle fusion revealed by electrochemical monitoring of single secretory events in adrenal chromaffin cells” *Nature* 356: 60-63

Cooper AJ and Stanford IM (2001) “Dopamine D2 receptor mediated presynaptic inhibition of striatopallidal $GABA_A$ IPSCs in vitro” *Neuropharmacology* 41(1): 62-71

Crespi F, D Dalessandro, Annovazzi-Lodi V, Heidbreder C and Norgia M (2004) “In vivo voltammetry: From wire to wireless measurements” *J. Neurosci. Methods* 140: 153-161

Dackis CA and Gold MS (1985) “New Concepts in Cocaine Addiction: The Dopamine Depletion Hypothesis” *Neurosci Biobehav. Rev*. 9:469-477

D’Aquila PS, Panin F, Cossu M, Peana AT and Serra G (2003) “Dopamine D1 receptor agonists induce penile erections in rats” *Eur. J. Pharmacol*. 460(1): 71-4

Depoortère R, Bardin L, Rodrigues M, Abrial E, Aliaga M and Newman-Tancredi A. (2009) “Penile Erection and Yawning Induced by Dopamine D2-Like Receptor Agonists in Rats: Influence of Strain and Contribution of Dopamine D2 But Not D3 and D4 Receptors” *Behav. Pharmacol*. 20(4): 303-11

De Simoni MG, De Luigi A, Imeri L and Algeri S (1990) “Miniaturized optoelectronic system for telemetry of in vivo voltammetric signals” *J. Neurosci. Methods* 33: 233-240

Deumens R, Blokland A and Prickaerts J (2002) “Modeling Parkinson’s Disease in Rats: An Evaluation of 6-OHDA Lesions of the Nigrostriatal Pathway” *Exp. Neurol.* 175:303-317

Deuschl G, Raethjen J, Baron R, Lindemann M, Wilms H and Krack P (2000) “The pathophysiology of tremor: a review” *J. Neurol*. 247(5): V/33-V/48

Dong Y, Cooper D, Nasif F, Hu XT, and White FJ (2004) “Dopamine Modulates Inwardly Rectifying Potassium Currents in Medial Prefrontal Cortex Pyramidal Neurons” *J. Neurosci.* 24(12): 3077-3085

Dos Santos WTP, Gimenes DT, de Almeida EGN, Eiras SP, AlbuquerqueYDT and Richter EM (2009) “Simple flow injection amperometric system for simultaneous determination of dipyrone and paracetamol in pharmaceutical formulations” *J. Brazil. Chem. Soc*. 20(7): 1249-1255

Drevets WC, Gautier C, Price JC, Kupfer DJ, Kinahan PE, Grace AA, Price JL and Mathis CA (2001) “Amphetamine-induced dopamine release in human ventral striatum correlates with euphoria” *Biol. Psych.* 49(2): 81-96

Driver-Dunckley E, Samanta J and Stacy M (2003) ”Pathological gambling associated with dopamine agonist therapy in Parkinson’s disease” *Neurology* 61(3): 422-423

Ehringer H and Hornykiewicz O (1998) “Distribution of noradrenaline and dopamine (3-hydroxytyramine) in the human brain and their behavior in diseases in the extrapyramidal system” *Parkinsonism & Related Disorders* 4(2): 53-57

Einhorn LC, Gregerson KA and Oxford GS (1991) “D2 dopamine receptor activation of potassium channels in identified rat lactotrophs: whole-cell and single-channel recording” *J. Neurosci.* 11(12): 3727-3737

Engbar TM, Susel Z, Juncos JL and Chase TN (1989) “Continuous and intermittent levodopa differentially affect rotation induced by D-1 and D-2 dopamine agonists” *Eur. J. Pharm*. 168: 291-298

Evans KR and Eikelboom R (1987) “Feeding induced by ventricular bromocriptine and amphetamine: A possible excitatory role for dopamine in eating behavior” *Behavioral Neurosci.* 101(4): 591-593

Fabbrini G, Brotchie JM, Grandas F, Nomoto M and Goetz CG (2007) “Levodopa-Induced Dyskinesias“ *Movement Disorders* 22(10): 1379-1389

Fernandez I, Arac D, Ubach J, Gerber SH, Shin O, Gao Y, Anderson RGW, Südhof TC and Rizo J (2001) “Three-Dimensional Structure of the Synaptotagmin 1 C_2B-Domain: Synaptotagmin I as a Phospholipid Binding Machine” *Neuron* 32: 1057-1069

Garris PA, Christensen JRC, Rebec GV and Wightman RM (1997) “Real-Time Measurement of Electrically Evoked Extracellular Dopamine in the Striatum of Freely Moving Rats” *J. Neurochem.* 68: 152-161

Garris PA, Ensman R, Poehlman J, Alexander A, Langley PE, Sandberg SG, Greco PG, Wightman RM and Rebec GV (2004) “Wireless transmission of fast-scan cyclic

voltammetry at a carbon-fiber microelectrode: proof of principle" *J. Neurosci. Methods* 140: 103-115

Garris PA, Greco PG, Sandberg SG, Howes G, Pongmaytegul S, Heidenreich BA, Casto JM, Ensman R, J Poehlman, Alexander A and Rebec GV (2007) "In vivo voltammetry with telemetry" Electrochemical Methods for Neuroscience (Chapter 12) Boca Raton, FL: CRC Press

Geigera BM, Haburcaka M, Avenab NM, Moyerc MC, Hoebelc BG, Pothos EN (2009) "Deficits of mesolimbic dopamine neurotransmission in rat dietary obesity" *Behavioral Neurosci*. 159(4):1193-99

Giorguieff MF, Kernel ML, Glowinski J and Beson MJ (1978) "Stimulation of dopamine release by GABA in rat striatal slices" *Brain Res.* 139: 115-130

Griessenauer CJ, Chang SY, Tye SJ, Kimble CJ, Bennet KE, Garris PA and Lee KH (2010) "WINCS-based wireless electrochemical monitoring of serotonin (5-HT) using fast-scan cyclic voltammetry: Proof of principle" *J. Neurosurg.* 113(3): 656-665

Guiliano F and Allard J (2009) "Dopamine and sexual function" *Inter. J. Impotence Res*. 13(Suppl 3): S18-28

Hadipour-Niktarash A (2006) "A computational model of how an interaction between the thalamocortical and thalamic reticular neurons transforms the low-frequency oscillations of the globus pallidus" *J. Comput. Neurosci*. 20: 299-320

Hernandez L and Hoebel BG (1988) "Food reward and cocaine increase extracellular dopamine in the nucleus accumbens as measured by microdialysis" *Life Sciences* 42(18): 1705-1712

Hochstetler SE, Puopolo M, Gustincich S, Raviola E, and Wightman RM (2000) "Real-Time Amperometric Measurements of Zeptomole Quantities of Dopamine Release From Neurons" *Anal. Chem.* 72(3): 489-496

Hornykewicz O (1986) "Parkinson's disease and the adaptive capacity of the nigrostriatal dopamine system" *Adv. Neurol.* 60: 140-147

Hyman SE and Malenka SC (2001) "Addiction and the brain: The neurobiology of compulsion and its persistence" *Nature Rev. Neurosci.* 2: 695-703

Ikemoto S and Panksepp J (1999) "The role of nucleus accumbens dopamine in motivated behavior: a unifying interpretation with special reference to reward seeking" *Brain Research Reviews* 31: 6-41

Ito R, Dalley JW, Howes SR, Robbins TW and Everitt BJ (2000) "Dissociation in Conditioned Dopamine Release in the Nucleus Accumbens Core and Shell in Response

to Cocaine Cues and During Cocaine-Seeking Behavior in Rats" *J. Neurosci.* 20(19): 7489-7495

Ito R, Dalley JW, Howes SR, Robbins TW and Everitt BJ (2002) "Dopamine Release in the Dorsal Striatum during Cocaine-Seeking Behavior under the Control of a Drug-Associated Cue" *J. Neurosci.* 22(14): 6247-6253

Jakel RJ and Maragos WF (2000) "Neuronal cell death in Huntington's disease: a potential role for dopamine" *Trends in Neurosci.* 23(6): 239-245

Jenkins IH, Fernandez W, Playford ED, Lees AJ, Frackowiak RSJ, Passingham RE, Phil D and Brooks DJ (1992) "Impaired Activation of the Supplementary Motor Area in Parkinson's Disease Is Reversed When Akinesia Is Treated With Apomorphine" *Annals Neurol.* 32(6): 749-757

Jenner P (2003) "The contribution of the MPTP-treated primate model to the development of new treatment strategies for Parkinson's disease" *Parkinsonism and Related Disorders* 9: 131-137

Jeon BS, Jackson-Lewis V and Burke RE (1995) "6-Hydroxydopamine Lesion of the Rat Substantia Nigra: Time Course and Morphology of Cell Death" *Neurodegeneration* 4: 131-137

John CE and Jones SE (2007) Fast Scan Cyclic Voltammetry of Dopamine and Serotonin in Mouse Brain Slices In Michael AC and Borland LM (Eds) *Electrochemical Methods for Neuroscience* (pp. 49-62) Boca Raton, FL: CRC Press

Johnson DC (1986) "Carbohydrate detection gains potential" *Nature* 321: 451-452

Kagohashi M, Nakazato T, Yoshimi K, Moizumi S, Hattori N and Kitazawa S (2008) "Wireless voltammetry recording in unanesthetized behaving rats" *Neurosci. Res.* 60(1): 120-127

Kandel ER, Schwartz JH and Jessell TM Principles of Neural Science, Fourth Edition. New York: The McGraw-Hill Companies, Inc., 2000

Kanterewicz BI, Urban NN, McMahon DBT, Norman ED, Giffen LJ, Favata MF, Scherle PA, Trzaskos JM, Barrionuevo G and Klann E (2000) "The Extracellular Signal-Regulated Kinase Cascade Is Required for NMDA Receptor-Independent LTP in Area CA1 But Not Area CA3 of the Hippocampus" *J. Neurosci.* 20(9): 3057-3066

Katz B (1969) "The Release of Neural Transmitter Substances" Springfield, IL: Liverpool University Press

Kim JS, Lee KS, Lee KH, Kim Yi, Kim BS, Chung YA and Chung SK (2001) “Evidence of thalamic disinhibition in patients with hemichorea: semiquantitative analysis using SPECT” *J. Neurol. Neurosurg. Psychiat.* 72: 329-333

Kiyatkin EA, Wise RA and Gratton A (1993) “Drug- and behavior-associated changes in dopamine-related electrochemical signals during intravenous heroin administration in rats” *Synapse* 14(1): 60-72

Koepp MJ, Gunn RN, Lawrence AD, Cunningham VJ, Dagher A, Brooks DJ, Bench CJ and Grasby BM (1998) “Evidence for striatal dopamine release during a videogame” *Nature* 393: 266-268

Kruk ZL, Cheeta S, Milla J, Muscat R, Williams JEG and Willner P (1998) “Real time measurement of stimulated dopamine release in the conscious rat using fast cyclic voltammetry: dopamine release is not observed during intracranial self stimulation” *J. Neurosci. Methods* 79: 9-19

Kühn AA, Tsui A, Aziz T, Ray N, Brücke C, Kupsch A, Schneider GH and Brown P (2009) “Pathological synchronization in the subthalamic nucleus of patients with Parkinson’s disease relates to both bradykinesia and rigidity” *Exp Neurol.* 215(2): 380-387

Kuhr WG, Ewing AG, Caudill WL and Wightman RM (1984) “Monitoring the Stimulated Release of Dopamine with *In Vivo* Voltammetry. I. Characterization of the Response Observed in the Caudate Nucleus of the Rat” *J. Neurochem.* 43(2): 560-569

Langston JW, Ballard P, Tetrud JW and Irwin I (1983) “Chronic Parkinsonism in humans due to a product of meperidine-analog synthesis” *Science* 219(4587): 979-980

Laruelle M, Abi-Darghum A, van Dyck CH, Gil R, D’souza CD, Erdos J, McCance E, Rosenblatt W, Fingado C, Zoghbi SS, Baldwin RM, Seibyl JP, Krystal JH, Charney DS and Innis RB (1996) “Single photon emission computerized tomography imaging of amphetamine-induced dopamine release in drug-free schizophrenic subjects” *Proc. Natl. Acad. Sci. USA* 93(17): 9235-9240

Li L and Chin LS (2003) “The molecular machinery of synaptic vesicle exocytosis” *Cell. Mol. Life Sci.* 60: 942-960

Maina FK, Khalid M, Apawu AK and Mathews TA (2012) “Presynaptic dopamine dynamics in striatal brain slices with fast-scan cyclic voltammetry” *J. Vis. Exp*. 59: 3791-3464

Martinez D, Greene K, Broft A, Kumar D, Liu F, Narendran R, Slifstein M, Van Heertum R, and Kleber HD (2009) “Lower Level of Endogenous Dopamine in Patients With Cocaine Dependence: Findings From PET Imaging of D2/D3 Receptors Following Acute Dopamine Depletion” *Am J. Psychiatry* 166(10): 1170-77

Martinez D, Slifstein M, Broft A, Mawlawi O, Hwang DR, Huang Y, Cooper T, Kegeles L, Zarahn E, Abi-Dargham A, Haber SN and Laruelle M (2003) “Imaging Human Mesolimbic Dopamine Transmission With Positron Emission Tomography. Part II: Amphetamine-Induced Dopamine Release in the Functional Subdivisions of the Striatum” *J. Cerebral Blood Flow and Metabolism* 23: 285-300

Maurice N, Tkcatch T, Meisler M, Sprunger LK and Surmeier DJ (2001) “D1/D5 Dopamine Receptor Activation Differentially Modulates Rapidly Inactivating and Persistent Sodium Currents in Prefrontal Cortex Pyramidal Neurons” *J. Neurosci.* 21(7): 2268-2277

McIntyre CC, Savasta M, Walter BL and Vitek JL (2004) “How does deep brain stimulation work? Present understanding and future directions” *J. Clin. Neurophysiol*. 21(1): 40-49

Meye FJ and Adan RAH (2013) “Feeling about food: the ventral tegmental area in food reward and emotional eating” *Trends Pharm. Sci*. doi: 10.1016/j.tips.2013.11.003

Millar J, Stamford JA, Kruk ZL, Wightman RM. (1984) “Electrochemical, pharmacological and electrophysiological evidence of rapid dopamine release and removal in the rat caudate nucleus following electrical stimulation of the median forebrain bundle” *Eur J Pharmacol* 109:341-348.

Mones RJ, Elizan TS and Siegel GJ (1971) “Analysis of L-dopa induced dyskinesias in 51 patients with Parkinsonism” *J. Neurol. Neurosurg. Psychiat*. 34: 668-673

Moreira AJC, Valadas RT and de Oliveira Duarte AM (1996) “Performance of infrared transmission systems under ambient light interference” *Optoelectronics, IEEE Proc.* 143(6): 339-346

Mundorf ML and Wightman RM (2002) “Amperometry and Cyclic Voltammetry with Carbon Fiber Microelectrodes at Single Cells” *Current Protocols in Neurosci*. Supp 18: 6.14.1-6.14.22

Nader MA, Czoty PW, Gould RW and Riddick NV (2008) “Positron emission tomography imaging studies of dopamine receptors in primate models of drug addiction” *Phil. Trans. R. Soc. B.* 363: 3223-3232

Narendran R, Frankle WG, Mason NS, Rabiner EA, Gunn RN, Searle GE, Vora S, Litschqe M, Kendro S, Cooper TB, Mathis CA and Laruelle M (2009) “Positron emission tomography imaging of amphetamine-induced dopamine release in the human cortex: a comparative evaluation of the high affinity dopamine D2/3 radiotracers [11C]FLB 457 and [11C]fallypride” *Synapse* 63(6): 447-461

Neve KA, Seamans JK and Tratham-Davidson H (2004) “Dopamine receptor signaling” *J. Receptors and Signal Transduction* 24(3): 165-205

Nirenberg MJ and Waters C (2006) “Compulsive eating and weight gain related to dopamine agonist use” *Movement Disorders* 21(4): 524-529

Norregaard L and Gether U (2001) “The monoamine neurotransmitter transporters: structure, conformation changes and molecular gating” *Curr. Opin. Drug Discov. Devel.* 4(5): 591-601

Paredes RG and Ågmo A (2004) “Has dopamine a physiological role in the control of sexual behavior? A critical review of the evidence” *Progress in Neurbiology* 73: 179-226

Pascual-Leone A, Valls-Solé J, Brasil-Neto JP, Cammarota A, Grafman J and Hallet M (1994) “Akinesia in Parkinson’s disease II. Effects of subthreshold transcranial motor cortex stimulation” *Neurology* 44(5): 892-898

Phelps ME (2006) “PET: Physics, instrumentation and scanners” Springer Sciences

Phillips PEM and Wightman RM (2003) “Critical guidelines for validation of the selectivity of in-vivo chemical microsensors” *Trends Anal. Chem*. 22(9): 509-514

Porrino LJ, Burns RS, Crane AM, Palombo E, Kopin IJ and Sokoloff L (1987) “Local cerebral metabolic effects of L-dopa therapy in 1-methyl-4-phenyl-1,2,3,6-tetrahydropyridine-induced parkinsonism in monkeys” *PNAS* 84(16): 5995-5999

Radhakishun FS, van Ree JM and Westerink BHC (1988) “Scheduled eating increases dopamine release in the nucleus accumbens of food-deprived rats as assessed with online brain dialysis” *Neurosci. Let.* 85(3): 351-356

Ritz MC, Lamb RJ, Goldberg SR and Kuhar MJ (1987) “Cocaine receptors on dopamine transporters are related to self-administration of cocaine” *Science* 237(4819): 1219-23

Roham M, Daberkow DP, Ramsson ES, Covey DP, Pakdeeronachit S, Garris PA and Mohseni P (2008) “A wireless IC for wide-range neurochemical monitoring using amperometry and fast-scan cyclic voltammetry” *IEEE Trans. Biomed. Circuits and Sys*. 2(1): 3-9

Roham M, Covey DP, Daberkow DP, Ramsson ES, Howard CD, Heidenreich BA, Garris PA and Mohseni P (2009) “A wireless IC for time-share chemical and electrical neural recording” *IEEE J. Solid State Phys*. 44(12): 3645-3658

Roham M, Covey DP, Daberkow DP, Ramsson ES, Howard CD, Garris PA and Mohseni P (2010) “A Miniaturized Device for FSCV Monitoring of Dopamine in an Ambulatory Subject” *Conf Proc IEEE Eng Med Biol Soc*. 2010: 5322-5325

Roitman MF, Stuber GD, Phillips PEM, Wightman RM and Carelli RM (2004) "Dopamine Operates as a Subsecond Modulator of Food Seeking" *J. Neurosci.* 24(6): 1265-1271

Rossetti ZL, Hmaidan Y, Gessa GL (1992) "Marked inhibition of mesolimbic dopamine release: a common feature of ethanol, morphine, cocaine and amphetamine abstinence in rats" *Eur. J. Pharm.* 221(2-3): 227-234

Roze E, Cahill E, Martin E, Bonnet C, Vanhoutte P, Betuing S, and Caboche J (2011) "Huntington's disease and striatal signaling" *Frontiers in Neuroanat.* 5: 1-16

Schiffman SN, Lledo PM and Vincent JD (1995) "Dopamine D1 receptor modulates the voltage-gated sodium current in rat striatal neurons through a protein kinase A" *J. Physiol.* 483(1): 95-107

Shon YM, Chang SY, Tye SJ, Kimble CJ, Bennet KE, Blaha CD and Lee KH (2010) "Comonitoring of adenosine and dopamine using the Wireless Instantaneous Neurotransmitter Concentration System: proof of principle" *J. Neurosurg.* 112(3): 539-548

Siegel GJ, Agranoff BW, Albers RW, Fisher SK and Uhler MD *Basic Neurochemistry: Molecular, Cellular and Medical Aspects. 6th edition* Philadelphia: Lippincott-Raven, 1999

Small DM, Jones-Gotman M and Dagher A (2003) "Feeding-induced dopamine release in dorsal striatum correlates with meal pleasantness ratings in healthy human volunteers" *NeuroImage* 19: 1709-1715

Smith Y, Bevan MD, Shink E and Bolam JP (1998) "Microcircuitry of the Direct and Indirect Pathways of the Basal Ganglia" *Neuroscience* 86(2): 353-387

Surmeier DJ, Eberwine J, Wilson CJ, Cao Y, Stefani A and Kitai ST (1992) "Dopamine receptor subtypes colocalize in rat striatonigral neurons" *Proc. Natl. Acad. Sci. of USA* 89(21): 10178-10182

Sutton RB, Davletov BA, Berghuis AM, Südhof TC and Sprang SR (1995) "Structure of the first C2 domain of synaptotagmin I: a novel Ca2+/phospholipid binding fold" *Cell* 80(6): 929-938

Terman JE and Rubin D (2004) "High Frequency Stimulation of the Subthalamic Nucleus Eliminates Pathological Thalamic Rhythmicity in a Computational Model" *J. Comp. Neurosci*. 16: 211-235

Trantham-Davidson H, Kröner S and Seamans JK (2008) “Dopamine Modulation of Prefrontal Cortex Interneurons Occurs Independently of DARPP-32” *Cerebral Cortex* 18: 951-958

Ungerstedt U (1968) “6-hydroxydopamine induced degeneration of central monoamine neurons” *Eur. J. Pharm.* 5: 107-110

Ungerstedt U (1991) “Microdialysis---principles and applications for studies in animals and man” *J. Internal Med.* 230: 365-373

Vaska P, Woody CL, Schlyer DJ, Shokouhi S, Stoll SP, Pratte JF, O’Connor P, Junnarkar SS, Rescia S, Yu B, Purschke M, Kandasamy A, Villaneuva A, Kriplani A, Radeka V, Volkow N, Lecomte R and Fontaine R (2003) “RatCAP: Miniaturized Head-Mounted PET for Conscious Rodent Brain Imaging” Brookhaven National Laboratory, Upton, NY

Volkow ND, Wang GJ, Maynard L, Jayne M, Fowler JS, Zhu W, Logan J, Gatley SJ, Ding YS, Wong C and Pappas N (2003) “Brain dopamine is associated with eating behaviors in humans” *Intl. J. Eating Disorders* 33(2): 136-142

Wang GJ, Geliebter A, Volkow ND, Telang FW, Logan J, Jayne MC, Galanti K, Selig PA, Han H, Zhu W, Wong CT, Fowler JS (2011) “Enhanced striatal dopamine release during food stimulation in binge eating disorder” *Obesity* (Silver Spring) 19(8):1601-8

Wang GJ, Volkow ND, Logan J, Pappas NR, Wong CT, Zhu W, Netusll N, Fowler JS (2001) “Brain dopamine and obesity” *The Lancet* 357(9253):354-7

Wightman RM, Jankowski JA, Kennedy RT, Kawagoe KT, Schroeder TJ, Leszczyszyn DJ, Near JA, Diliberto EJ Jr. and Viveros OH (1991) “Temporally resolved catecholamine spikes correspond to single vesicle release from individual chromaffin cells” *Proc. Natl. Acad. Sci.* 88: 10754-8

Winkelmüller W and Nitsch FM (1975) “Quantitative Registration of Motor Disorders following Bilateral Lesions of Substantia Nigra in the Rat” *Appl. Neurophysiol.* 38: 291-301

Wong DF, Wagner HN, Tune LE, Dannals RF, Pearlson GD, Links JM, Tamminga CA, Broussolle EP, Ravert HT and Wilson AA (1986) “Positron emission tomography reveals elevated D2 dopamine receptors in drug-naïve schizophrenics” *Science* 234(4783): 1558-63

Wood KM and Hashemi P (2013) “Fast-scan cyclic voltammetry analysis of dynamic serotonin reponses to acute escitalopram” *ACS Chem. Neurosci*. 4(5): 715-20

Zachek MK, Hermans A, Wightman RM and McCarty GS (2008) “Electrochemical detection: Comparing gold and carbon fiber microelectrodes using background subtracted fast scan cyclic voltammetry” *J. Electroanal. Chem*. 614: 113-120